

**NOVEL STRATEGIES TO IMPROVE VIRAL GENE TARGETING AND  
THERAPEUTIC LIVER REPOPULATION *IN VIVO*.**

**By**

**Nicole Kristen Paulk**

**A DISSERTATION**

**Presented to the Department of Cell and Developmental Biology**

**and the Oregon Health & Science University**

**School of Medicine**

**in partial fulfillment of**

**the requirements for the degree of**

**Doctor of Philosophy**

**March 2012**

**Copyright 2012 Nicole K. Paulk**

**School of Medicine**

**Oregon Health & Science University**

**CERTIFICATE OF APPROVAL**

---

This is to certify that the PhD dissertation of  
Nicole K. Paulk  
has been approved

\_\_\_\_\_  
Mentor/Advisor

\_\_\_\_\_  
Member

\_\_\_\_\_  
Member

\_\_\_\_\_  
Member

## TABLE OF CONTENTS

INDEX OF FIGURES.....	iv
INDEX OF TABLES.....	vi
LIST OF ABBREVIATIONS.....	vii
ACKNOWLEDGEMENTS.....	xiv
ABSTRACT.....	xvii

### **CHAPTER 1: Introduction**

A historical perspective on gene therapy.....	2
Wild-type AAV.....	3
Recombinant AAV as a gene therapy vector.....	5
Differences between AAV-mediated gene addition and gene repair.....	5
Clinical trials with AAV.....	9
Liver biology, architecture and function.....	10
The tyrosine catabolic pathway.....	12
Hereditary tyrosinemia type I as a model genetic disease.....	13
Abnormal biochemistry of HTI.....	15
Pathology of HTI.....	16
Treatment of HTI.....	18
Somatic mosaicism in HTI.....	18
The various <i>Fah</i> null mouse models and their applications.....	20
Gene therapy for liver diseases like HTI.....	22

**CHAPTER 2: AAV Gene Targeting Corrects a Mouse Model of Hereditary Tyrosinemia Type I *In Vivo***

Abstract.....24  
Introduction.....25  
Materials and Methods.....28  
Results.....34  
Figures.....40  
Tables.....46  
Discussion.....47

**CHAPTER 3: AAV-mediated Gene Targeting is Significantly Enhanced by Transient Inhibition of NHEJ or the Proteasome *In Vivo***

Abstract.....50  
Introduction.....51  
Materials and Methods.....54  
Results.....60  
Figures.....65  
Tables.....70  
Discussion.....72

## **CHAPTER 4**

### **Small Molecule Inhibitor of FAH Enzyme Allows for Selection of Genetically Resistant Donor Hepatocytes in Wild-type Settings *In Vivo***

Abstract.....	76
Introduction.....	77
Materials and Methods.....	81
Results.....	86
Figures.....	90
Tables.....	94
Discussion.....	96

## **CHAPTER 5**

### **Conclusions and Further Directions**

Current challenges in AAV-mediated gene repair.....	100
Promising pre-clinical work with AAV for liver diseases.....	107
Final thoughts.....	108

REFERENCES.....	109
-----------------	-----

BIOGRAPHY.....	131
----------------	-----

## INDEX OF FIGURES

- 1-1: Transcriptional map of the wild-type AAV genome
- 1-2: Biology of wild-type and recombinant AAV
- 1-3: Genome structure of AAV gene addition and gene repair vectors
- 1-4: Microscopic liver architecture
- 1-5: Metabolic zonation within each hepatic lobule
- 1-6: Tyrosine catabolic pathway
- 1-7: Timeline of liver repopulation
- 1-8: *Fah*<sup>5981SB</sup> mouse mutation
- 1-9: *Fah*<sup>exon5</sup> mouse mutation
- 2-1: AAV vector design and genomic organization of murine *Fah*
- 2-2: Liver immunohistology and whole mount staining for FAH
- 2-3: RT-PCR for *Fah* mRNA
- 2-4: Time course of AAV-mediated gene repair in neonates
- 2-5: Dose response of AAV-mediated gene repair in neonates
- 2-6: AAV-mediated gene repair is feasible in adult liver
- 3-1: Transient NHEJ or proteasome inhibition enhances gene targeting
- 3-2: Liver immunohistochemistry
- 3-3: Sexually dimorphic responses to AAV and vanillin
- 3-4: NHEJ inhibition is responsible for gene targeting increases
- 3-5: AAV-mediated gene repair with vanillin analogs
- 4-1: FAH enzyme assay confirms CEHPOBA function both *in vitro* and *in vivo*

4-2: Gene expression similarities between tyrosinemic mice and CEHPOBA-treated wild-type mice

4-3: Treatment duration illustrates the kinetics of liver repopulation

4-4: Liver immunohistochemistry

5-1: Current model of AAV cell entry and intracellular trafficking

5-2: Potential mechanisms for AAV-mediated gene targeting

5-3: AAV targeting strand bias

## INDEX OF TABLES

1-1: Summary of clinical trials using AAV gene transfer

2-1: *hAAT* copy numbers in recipient mice

3-1: Serological measures of functional correction

3-2: *eGFP* copy numbers in recipient mice

4-1: Effects of CEHPOBA treatment on liver gene expression

4-2: Biochemical measures of functional correction and injury

5-1: Successful liver-directed AAV gene addition models

## LIST OF ABBREVIATIONS

AADC	Aromatic-L-amino-acid decarboxylase
AAP	Assembly-activating protein
AAV	Adeno-associated virus
<i>Actb</i>	$\beta$ -actin
Ad	Adenovirus
Afp	$\alpha$ -fetoprotein
AGA	$\alpha$ -galactosidase A
Aku	Alkaptonuria
ALT	Alanine aminotransferase
ApoE	Apolipoprotein-E
<i>Ass1</i>	Argininosuccinate synthase 1
AST	Aspartate aminotransferase
ATM	Ataxia telangiectasia mutated
ATR	Ataxia telangiectasia and Rad3 related protein
BD	Bile duct
Bili	Bilirubin
Bort	Bortezomib
bp	Base pair
C	Celsius
cAMP	cyclic adenosine monophosphate
CAV	Caveolar endocytosis

CBS	Cystathionine $\beta$ -synthase
CCP	Clathrin-mediated endocytosis
cDNA	Complementary DNA
CEHPOBA	4-[(2-carboxyethyl)-hydroxyphosphinyl]-3-oxobutyrate
CFTR	Cystic fibrosis transmembrane regulator
Chr	Chromosome
CLN2	Tripeptidyl-peptidase I
DAPI	4,6-diamidino-2-phenylindole
<i>Ddit3</i>	DNA-damage-inducible transcript 3
dGE	Diploid genome equivalent
DMNB	4,5-dimethoxy-2-nitrobenzaldehyde
DNA	Deoxyribonucleic acid
dpi	Dots per inch
DSB	Double strand break
EE	Early endosome
eGFP	Enhanced green fluorescent protein
ENU	<i>N</i> -ethyl- <i>N</i> -nitrosourea
ER	Endoplasmic reticulum
Ex	Example
F	Forward
FAA	Fumarylacetoacetate
FAH	Fumarylacetoacetate hydrolase
FDA	Food and drug administration

FDR	False discovery rate
FLT1	Vascular endothelial growth factor-1
GAA	Acid $\alpha$ -glucosidase
GAD	Glutamic acid decarboxylase
GAPDH	Glyceraldehyde 3-phosphate dehydrogenase
G6Pase	Glucose-6-phosphatase
GC	Glucocerebrosidase
GSD-Ia	Glycogen storage disease type Ia
Gsta1	Glutathione S-transferase alpha 1
GUSB	$\beta$ -glucuronidase
H&E	Hematoxylin and eosin
HA	Hepatic artery
hAAT	Human $\alpha$ -1 antitrypsin
HCC	Hepatocellular carcinoma
HEPES	4-(2-hydroxyethyl)-1-piperazineethanesulfonic acid
hFIX	Human factor 9
HGD	Homogentisate 1,2-dioxygenase
HPD	4-hydroxyphenylpyruvate dioxygenase
HR	Homologous recombination
HSV	Herpes simplex virus
HTI	Hereditary tyrosinemia type I
IL-1	Interleukin-1
III2rg	Interleukin 2 receptor gamma

IP	Intraperitoneal
ITR	Inverted terminal repeat
iu	Infectious units
IUDA	iduronidase
IV	Intravenous
kb	Kilobase
kDa	Kilo-dalton
kg	Kilogram
Ki	Inhibition constant
Km	Substrate concentration that leads to half-maximal velocity
LacZ	$\beta$ -galactosidase
LD-PCR	Long distance PCR
LDL	Low-density lipoprotein
LDLR	LDL receptor
LE	Late endosome
LPL	Lipoprotein lipase
LSP	Liver specific promoter
MAA	Maleylacetoacetate
MAI	Maleylacetoacetate isomerase
mg	Milligram
MGMT	Methylguanine methyltransferase
MMR	Mismatch repair
mo	Month

MPS	Mucopolysaccharidosis
mRNA	Messenger RNA
MVM	Minute virus of mice
n	number of animals
nm	Nanometer
NHEJ	Non-homologous end joining
No	Nucleolus
NOD	Non-obese diabetic
NP	Nucleoplasm
NPC	Nuclear pore complex
<i>Nqo-1</i>	NAD(P)H dehydrogenase quinone 1
NSG	NOD SCID gamma
NTBC	2-(2-nitro-4-trifluoro-methylbenzol)-1,3-cyclohexanedione
O6-BG	O6-benzylguanine
ORF	Open reading frame
OTC	Ornithine transcarbamylase
P	Post-natal day
PBS	Phosphate-buffered saline
PCCA	Propionyl CoA carboxylase
<i>Pck1</i>	Phosphoenolpyruvate carboxykinase 1
PCR	Polymerase chain reaction
PEG	Polyethylene glycol
PK	Protein kinase

PKU	Phenylketonuria
PLA2	Phospholipase A2
PNRE	Perinuclear recycling endosome
PV	Portal vein
R	Reverse
rAAV	Recombinant AAV
rev	Reviewed
RMA	Robust multi-array averaging
RNA	Ribonucleic acid
RPE65	Retinal pigment epithelium-specific protein 65-kDA
RSV	Rous sarcoma virus
RT	Reverse transcriptase
SA	Succinylacetone
SAA	Succinylacetoacetate
SCID	Severe compromised immune deficiency
SD	Standard deviation
SERCA2a	Sarcoplasmic reticulum calcium ATPase 2a
sFLT01	Modified soluble Flt1 receptor
shRNA	Short hairpin RNA
SMX-TMP	Sulfamethoxazole-Trimethoprim
sTx	Serial transplantation
TAT	Tyrosine aminotransferase
TGN	Trans-Golgi network

TNFR-Fc	Tumor necrosis factor receptor-immunoglobulin Fc fragment
U/L	Units per liter
UDP	Uridine diphosphate
UGT1A1	UDP glucuronosyltransferase 1 family polypeptide A1
US	United states
v	version
Van	Vanillin
vg	Vector genome
VP	Viral protein
wk	week
wt/vol	Weight per volume

## ACKNOWLEDGEMENTS

Of mice and mates, those who helped me most. Without the use of mice for the pre-clinical animal modeling described herein, not one iota of data from my thesis could have been produced. Although not the norm, I wanted to thank them first and foremost. Similarly, with an *in vivo*-based project like mine that used thousands upon thousands of mice, I was utterly dependent on the help of countless technicians in the lab to help with the unending array of mouse work. Without the help of Eric Benedetti, Bryan Jensen, Laura Eaton, Laura Marquez-Loza, Jessie Coleman, Annelise Haft and Kathryn Schubert I would have never finished my PhD. Technicians are the hidden success of every *in vivo* project.

I was lucky enough to be a part of countless collaborative projects both within OHSU and at other universities. Several people have helped me the most and have been helping me since I was just a technician in the lab: Milton Finegold, Angela Major and Cristina Nordstrom of Texas Children's University, who have been my pathological and serological eyes and ears since the beginning; Mark Kay, Terry Storm and Leszek Liszowski of Stanford University, who have assisted in nearly every aspect of viral production and discussion for the last 6 years; James Gallagher, Jonathan Jarvis, Andrew Preston and Adam Taylor from the University of Liverpool who stuck with me on the alkaptonuria and ochronosis work to see that project through to publication.

Several other individuals have helped me in various aspects of collaboration or technical support: Aurelie Synder from OHSU for microscopy support; Cara Poage, Carolyn Gendron and Chris Corless from OHSU for histology support; Fred Alt and Yuko Fujiwara from Harvard University for the *Ku70<sup>+/-</sup>* mice; Xavier Montagutelli from the Pasteur Institute of Paris for the *Hgd<sup>+/-</sup>* mice; William Fleming from OHSU for the NSG mice, Devorah Goldman from OHSU for retro-orbital injections; Phillip Connell and Hillary Logan from the University of Chicago for work on the RAD51 inhibitor; Ko Mitani of the Saitama Medical University of Japan for work on the *Fah* adenoviral correction vector; Peter Glazer, Faisal Reya and Denise Hegan from Yale University for the work on the triplex-forming oligonucleotide against *Fah*; Eric Washburn of the OHSU Vollum Viral Core for tireless viral troubleshooting; Barry Stoddard and Summer Thyme from the University of Washington for engineering the custom *Fah* homing endonuclease; Cary Harding and Shelley Winn from OHSU for the pAAV-LSP-eGFP vector backbone; Lev Fedorov from OHSU for mouse rederivations; Susan Olson and Amy Hanlon-Newell from OHSU for cytogenetic analysis; Leslie Smith of OHSU for showing me how FISH is *really* done; Carl Pelz of OHSU for performing the biostatistical microarray analysis; Jude Samulski and Xiao Xiao of the University of North Carolina for countless discussions and vectors for the spAAV project; Gregory Clarke from OHSU for the urinalysis measurements; Phillip Streeter from OHSU for secretly funding my kidney antibody work; Dale Braden from OHSU for countless hours helping me with the paperwork bureaucracy for my F31 NRSA fellowship; and finally Leslie

Lublink of OHSU for basically doing everything under the sun and being the best administrative assistant anyone could ever possibly hope for.

And last, but never least, Markus. Oh Markus, how oh how can I ever thank you. We've put each other through the ringer. I really can't imagine another person on earth, much less here at OHSU, who could have possibly managed to keep up with me during this graduate school business, but you did it with flair. I won't bother to list all the knowledge you've imparted upon me because the list would be longer than my thesis. You are one for the record books Markus Grompe. You will never be forgotten.

## ABSTRACT

Many inborn errors of metabolism are caused by deficiencies in hepatic enzymes, thereby making whole orthotopic liver transplantation an effective therapy for these conditions. However, few patients benefit from or even undergo this procedure due to the limited availability of donor organs, the high cost and significant morbidity and mortality associated with the procedure, as well as the long-term requirement for immune suppression. Most pediatric metabolic diseases are caused by a specific loss-of-function in only hepatocytes with otherwise normal liver anatomical structure. This is in contrast to many adult liver disorders treated with whole liver transplant where severe anatomical abnormalities have accumulated that obstruct proper liver function. Thus, many pediatric patients with metabolic disease have little need for whole organ transplant and would benefit from restoration of enzymatic function through gene therapeutic approaches or hepatocyte replacement via cell transplantation.

My thesis attempts to address both of these potential therapeutic strategies. In Chapter 2, I provide the first proof-of-principle data establishing that recombinant adeno-associated viral (rAAV) vectors are capable of functional correction of a metabolic liver disease *in vivo* through a gene targeting approach. This work was the first to demonstrate the stability of gene targeting in both neonatal and adult mice using two different pseudotyped rAAV serotypes,

rAAV2/2 and rAAV2/8. Furthermore, this work established the functional time course for correction using both serotypes of rAAV at a range of viral doses.

In Chapter 3, I expand upon my established rAAV gene targeting paradigm from Chapter 2 and demonstrate increased gene targeting capabilities through transient use of the pharmacologics vanillin or bortezomib. The natural product vanillin acts as a potent inhibitor of the undesired repair pathway non-homologous end-joining (NHEJ) by inhibiting the protein kinase DNA-PK. Bortezomib is a proteasomal inhibitor that prevents AAV capsid degradation. Broadly, this study was the first to show the potential clinical benefit of inhibiting a non-desired DNA repair pathway for increasing AAV-mediated gene targeting with an animal model of any disease in a clinically relevant manner. More specifically, this work was the first to show the benefits of transient NHEJ inhibition with vanillin at improving AAV mediated gene targeting for an *in vivo* mouse model of hereditary tyrosinemia type I (HTI) to near therapeutic levels.

In Chapter 4, I describe the use of a small molecule agent to transiently apply positive selection for transplanted hepatocytes. Most liver diseases lack the advantage of positive selection, thus the ability to transiently apply positive selection for correction of liver disorders would represent a major advance. The small molecule 4-[(2-carboxyethyl)-hydroxyphosphinyl]-3-oxobutyrate (CEHPOBA) was tested both *in vitro* and *in vivo* for its ability to inhibit target pathways. As proof of principle, we attempted to positively select hepatocytes

genetically resistant to CEHPOBA by transplanting into wild-type recipients along with CEHPOBA treatment. Time course analyses with 3-5 week courses of CEHPOBA following transplantation showed a linear relationship between treatment length and degree of repopulation. Compared to controls, CEHPOBA-treated recipients had 10-100 fold increases in liver repopulation. This work established that selective repopulation in a non-selective wild-type liver through transplant of genetically resistant hepatocytes and daily administration of the pharmacological inhibitor CEHPOBA could provide transient selection to donor hepatocytes *in vivo*. Based on these findings, it is thought that the combination of transient shRNA knockdown of upstream enzymatic targets in donor cells, hepatocyte transplantation and drug treatment with CEHPOBA could constitute a new path for future therapeutic liver repopulation.

# **CHAPTER 1**

## **Introduction**

### ***A historical perspective on gene therapy***

Public health studies have shown the increasing significance of monogenic diseases to the total health care burden for both US and foreign nations [1-3]. Individual and societal costs imposed by treatment of these disorders have prompted a search for curative therapies, focusing on correcting genetic defects. Gene therapy is a promising means to permanently cure many genetic diseases. Collectively, there are 15,500 known genetic diseases, affecting over 13 million Americans [4, 5]. The burden of genetic disease is daunting, as up to 70% of all admissions to children's hospitals [3] and 10% of admissions to adult hospitals [6] are due to genetic disease. Even now, many of the oldest and most common inherited disorders—cystic fibrosis, sickle cell anemia, etc.—lack any real treatment beyond mere supportive care. When the first clinical trials for gene therapy began back in the 1980's, it was predicted that gene therapeutic approaches would become a clinical reality in just a few years. Yet 20 years of setbacks and failures caused many to lose hope in the technique as stem cell technologies were predicted to become the new miracle cure. However, those researchers who saw the potential, despite the setbacks, barreled through the technical hurdles and gene therapy is now finally entering what many believe will be its golden era. Successful clinical trials with various vectors for an array of diseases (rev. in [7]), as well as promising pre-clinical work in numerous animal models for many other diseases (rev. in [7]), has helped to ease the skepticism towards gene therapy by other scientific fields and it is now considered a respected scientific discipline.

### **Wild-type AAV**

Adeno-associated virus (AAV) is a single-stranded DNA virus of the family *Parvoviridae* and genus *Dependovirus* [8]. Nine naturally occurring subtypes (AAV1-9) have been found where humans are the animal reservoir. Although 50-96% of the population is seropositive for classic wild-type AAV (AAV2) [9, 10], no known human pathology is attributed to any subtype of the virus. Like the name suggests, AAVs require a helper virus—typically adenovirus or herpesvirus—to provide necessary protein factors for replication, as AAV is naturally replication-defective [8]. AAV lacks an envelope, has icosahedral capsid symmetry, and contains a 4.7-kb single-stranded DNA genome flanked by two 145-bp inverted terminal repeats (ITRs) which fold into a characteristic hairpin shape. The viral genome is simple, containing only two genes, *cap* and *rep*, which through use of alternative splicing and start codons, generates eight proteins with overlapping sequences (**Fig. 1-1**) [11]. The viral *cap* gene codes for 3 structural proteins (VP1, VP2, VP3) that assemble at a ratio of 1:1:18 to form each 60-mer capsid at ~25-nm in diameter, as well as a small non-structural protein (AAP) which plays a role in nucleolar capsid assembly [12]. The *rep* gene codes for two large (Rep78, Rep68) and two small (Rep52, Rep40) non-structural proteins that together perform an array of ITR-dependent functions ranging from viral replication, viral assembly, transcriptional regulation and site-specific integration into host chromosomes (in humans at site AAVS1 on chromosome 19 [13]). If integrated, AAV will persist in a dormant latent form until stimulated to reactivate following

host infection with helper virus at which time a lytic cycle will ensue that can infect both dividing and non-dividing cells [8].

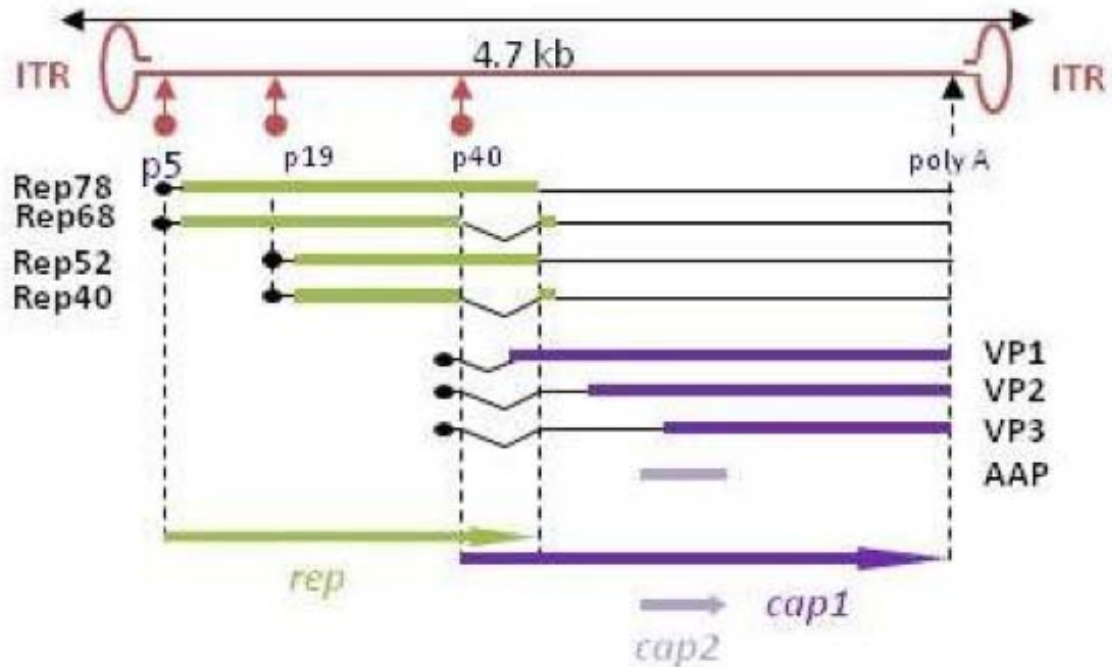


**Figure 1-1: Transcriptional map of the wild-type AAV genome**

AAV has a single-stranded 4.7-Kb DNA genome flanked by a pair of palindromic inverted terminal repeats (ITRs). The genome contains two open reading frames (ORFs) that direct the synthesis of several major RNA species, from three different transcription promoters (P5, P19 and P40) and alternative splicing signals. The **rep** ORF encodes four regulatory proteins that are involved in AAV DNA replication, gene expression and packaging. The **cap** ORF encodes four viral proteins, VP1, VP2 and VP3 that constitute the capsid, and one additional small protein, AAP that is involved in nucleolar capsid assembly [12]. Image reproduced with permission from [14].

### ***Recombinant AAV as a gene therapy vector***

Being naturally replication-defective and nonpathogenic to humans, AAV represents an ideal vector for use in humans and has spurred over 30 years of research into recombinant AAV (rAAV) technology. Nearly all rAAV research to date is based on work with AAV2/2 [15] (serotype 2 genomic ITR sequence, and serotype 2 viral capsid sequence) (**Fig. 1-2a**). In this manner, the viral *rep* and *cap* genes are removed and provided in *trans* during virus production. They are replaced with some form of gene delivery insert or transgene (**Fig. 1-2b**).

### ***Differences between AAV-mediated gene addition and gene repair***

AAV is the gold standard of safety in viral gene therapy, and research remains focused on gene addition strategies using full-length cDNA cassettes encoding the wild-type variation of the mutated gene of interest [16] (**Figure 1-3a**). Despite recent advances (**Table 1-1**), AAV gene addition approaches are limited by transient and unregulated expression [17], highly random integrations [18], and increased mutagenesis risks [19]. Few protein-coding genes have open reading frames small enough to fit within the low packaging capacity of AAV (~4.7-kb), thus there are few genetic diseases for which this type of gene therapy is applicable.

A decade after the advent of site-directed mutagenesis [20], it was shown that AAV could introduce specific targeted mutations in human cells at low frequency [21]. Since this discovery, numerous *in vitro* studies [22, 23] have

shown AAV vectors capable of correcting various types of mutations (insertions, deletions and substitutions) in a mechanism now known as gene repair (**Figure 1-3b**). Single-stranded AAV genomes modulate gene repair by integrating site-specifically via homologous recombination and targeting only the disease-causing mutation for replacement with wild-type sequence [24]. In stark contrast to gene addition, therapies by gene repair allow restoration of normal expression levels within the context of all endogenous regulatory elements [25]. AAV vectors engineered in this way have the ability to target multiple different genomic loci and largely prevent insertional mutagenesis. In addition, gene repair vectors show both targeted and stable expression through integration, and have an increased number of applicable human diseases [26].

Gene repair with AAV would represent the ideal strategy for two classes of disease: i) those with complex etiology (example: dominant genetic disorders); or ii) those with complex regulation (example: developmental diseases involving transcription factors). In all diseases, gene repair would be best suited to correct point mutation-based disorders that need only one or few nucleotides corrected to restore normal gene expression. This is essential, as point mutations are the most frequent genetic abnormality and source of acquired genetic disease [27].

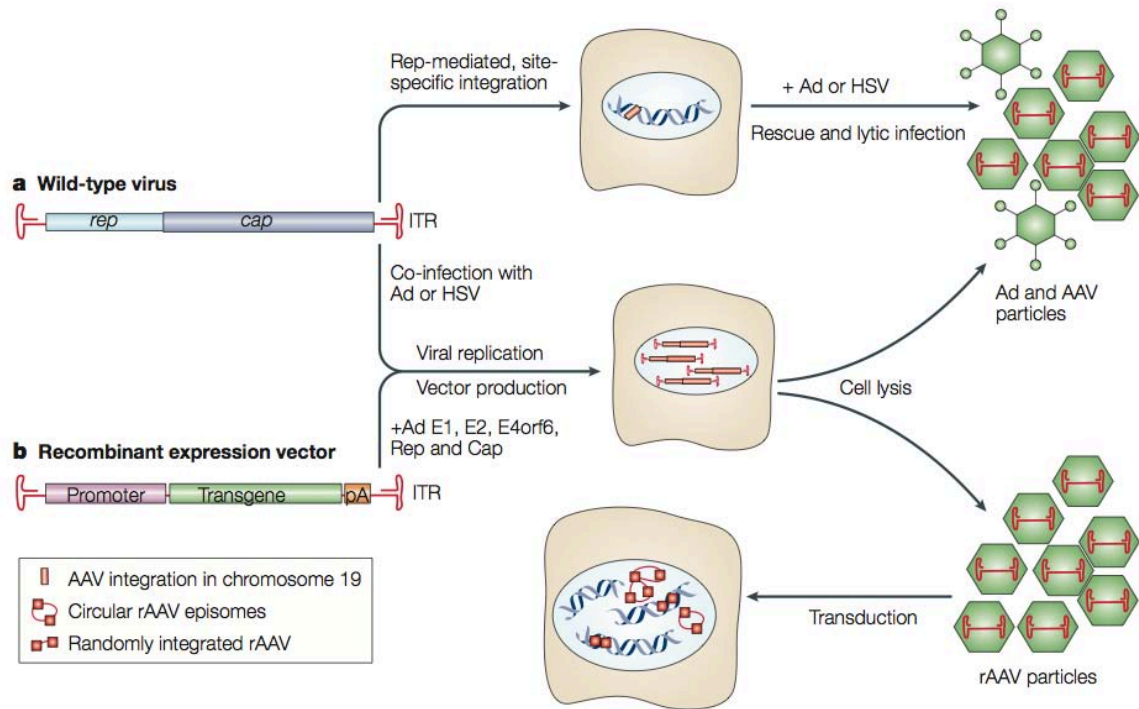


**Figure 1-2: Biology of wild-type and recombinant AAV**

**(a)** Structure of wild-type AAV. AAV can integrate into human chromosome 19 and persist latently. Co- or super-infection with adenovirus (Ad) or herpes simplex virus (HSV), which provide essential replication factors, will rescue the integrated pro-virus and produce a lytic infection.

**(b)** Structure of a generic recombinant AAV vector. The viral genome is replaced with an expression cassette of interest. To produce rAAV, *Rep* and *Cap* genes as well as helper virus elements (Ad E1, E2 and E4orf6), must be provided in *trans*. Image reproduced with permission from [28].

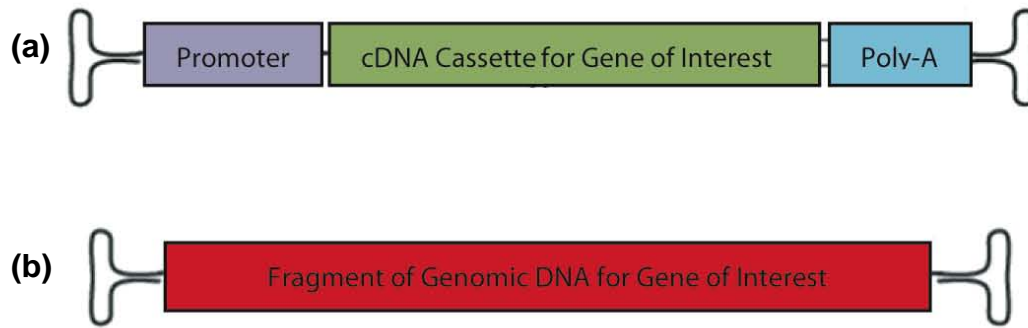


**Figure 1-3: Genome structure of AAV gene addition and gene repair vectors**

**(a)** Layout of an AAV gene addition construct containing elements required for episomal gene expression. A cDNA cassette driven by heterologous promoter and enhancer sequences is used to drive gene expression of a wild-type version of the mutated disease gene. This vector *is not* capable of correcting the gene of interest; it merely supplements the cell with an extra wild-type copy of the gene. The non-functional genomic copy remains.

**(b)** Layout of an AAV gene repair construct containing a fragment of the gene of interest centered on the nucleotide needed for correction. Long homology arms both 3' and 5' to the repair nucleotide are present. This vector *is* capable of correcting the gene of interest. The gene repair paradigm differs in that patient genomes are manipulated *in vivo* using site-specific recombination to correct underlying mutations. In this way, gene function is restored within the context of endogenous regulatory elements, thus eliminating problems with inadequate or inappropriate expression. Restored gene expression will only occur after successful chromosomal integration by homologous recombination.

## Clinical trials with AAV

Disease	Transgene product	Serotype	Route of administration	Clinical trial	ClinicalTrials.gov identifier
<i>AAV clinical trials for inherited diseases</i>					
$\alpha$ 1 antitrypsin deficiency	$\alpha$ 1 antitrypsin	AAV2	Intramuscular	Phase I/II	NCT00377416
		AAV1			NCT00430768
Batten's disease	CLN2	AAV2	Direct intracranial administration	Phase I	NCT00151216
		AAVrh10			NCT01161576
Canavan's disease	Aspartoacylase	AAV2	Direct intracranial administration	Phase I	NA
Cystic fibrosis	CFTR	AAV2	Direct instillation to maxillary sinus, bronchoscopy to right lower lobe, aerosol to whole lung	Phase I/II	NCT00004533
Haemophilia B	Factor IX	AAV2	Intramuscular	Phase I/II	NCT00076557
			Hepatic		NCT00515710
		AAV8	Intravenous	NCT00979238	
Leber's congenital amaurosis	RPE65	AAV2	Subretinal	Phase I/II	NCT00643747
					NCT00516477
					NCT00481546
LPL deficiency	LPL	AAV1	Intramuscular	Phase I/II	NCT01109498, NCT00891306
Pompe's disease	GAA	AAV1	Series of intradiaphragmatic injections	Phase I/II	NCT00976352
Muscular dystrophy: Duchenne	Microdystrophin	AAV1-AAV2 hybrid	Intramuscular	Phase I	NCT00428935
Muscular dystrophy: limb girdle	$\alpha$ -sarcoglycan	AAV1	Two to six separate injections into the selected muscle	Phase I	NCT00494195
<i>AAV clinical trials for acquired diseases</i>					
Severe heart failure	SERCA2a	AAV1	Antegrade epicardial coronary artery infusion	Phase I/II	NCT00454818
		AAV6			NCT00534703
Parkinson's disease	AADC	AAV2	Intracranial	Phase I/II	NCT00229736
	GAD				NCT00643890, NCT00195143, NCT01301573
	Neutrophin				NCT00252850, NCT00985517, NCT00400634
Age-related macular degeneration	sFLT01	AAV2	Intravitreal injection	Phase I	NCT01024998
Rheumatoid arthritis	TNFR-Fc	AAV2	Intra-articular	Phase I	NCT00617032, NCT00126724

**Table 1-1: Summary of clinical trials using AAV gene transfer**

Listed are the completed and ongoing clinical trials using AAV as a gene delivery vector. Table reproduced with permission from [7].

### ***Liver biology, architecture and function***

According to *Zakim & Boyer's Hepatology*, the definitive hepatic textbook, the liver is the largest organ in the abdominal cavity and the most complex. It is composed of an array of separate microscopic functional units known as hepatic acinii or lobules [29]. The liver parenchymal compartment consists of hepatocytes, while the non-parenchymal compartment is largely made up of Kupffer and biliary cells. The liver receives its dual blood supply from both the hepatic artery and portal vein. Small branches from each vessel enter each acinus at the portal triad. Pooled blood flows through sinusoids between plates of hepatocytes in order to exchange nutrients (**Fig. 1-4**). The hepatic vein carries efferent blood into the inferior vena cava and lymphatic vessels drain the liver.

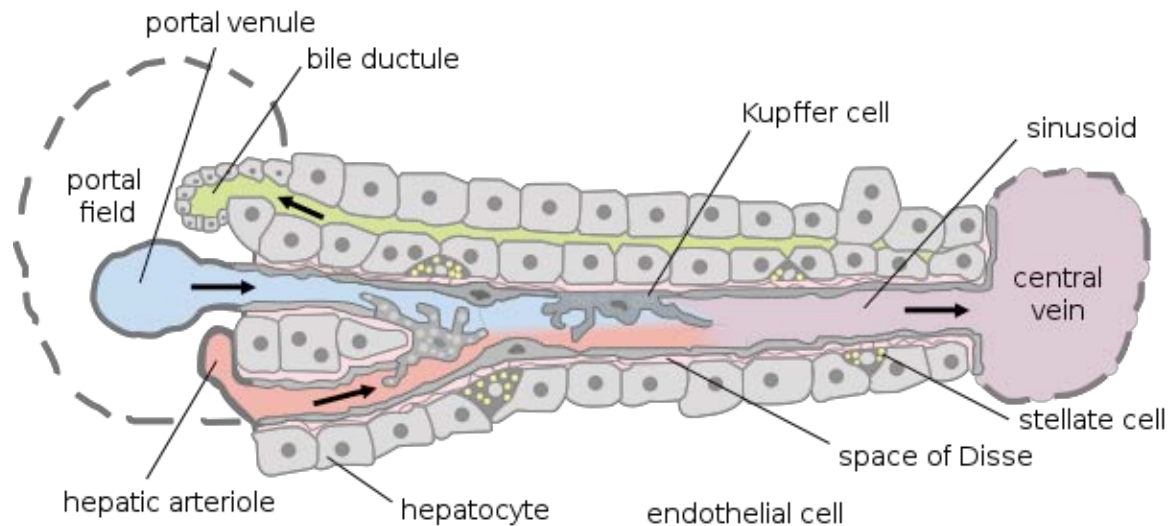


**Figure 1-4: Microscopic liver architecture**

The dual blood supply of the liver consists of portal vein and hepatic artery branches, which merge when entering the liver lobule at the portal field. Blood flows along the sinusoid and exits at the central vein. Diagram modified from [30].

Hepatocytes comprise the bulk of the liver and are responsible for the liver's central role in intermediary metabolism. These cells are involved in the formation and excretion of bile, regulation of carbohydrate homeostasis, lipid synthesis and secretion of plasma lipoproteins, control of cholesterol metabolism, and formation of urea, serum albumin, clotting factors, enzymes, and numerous proteins. Periportal and perivenous hepatocytes are distinguished by differences in function which run as gradients from one zone to the other (**Fig. 1-5**).

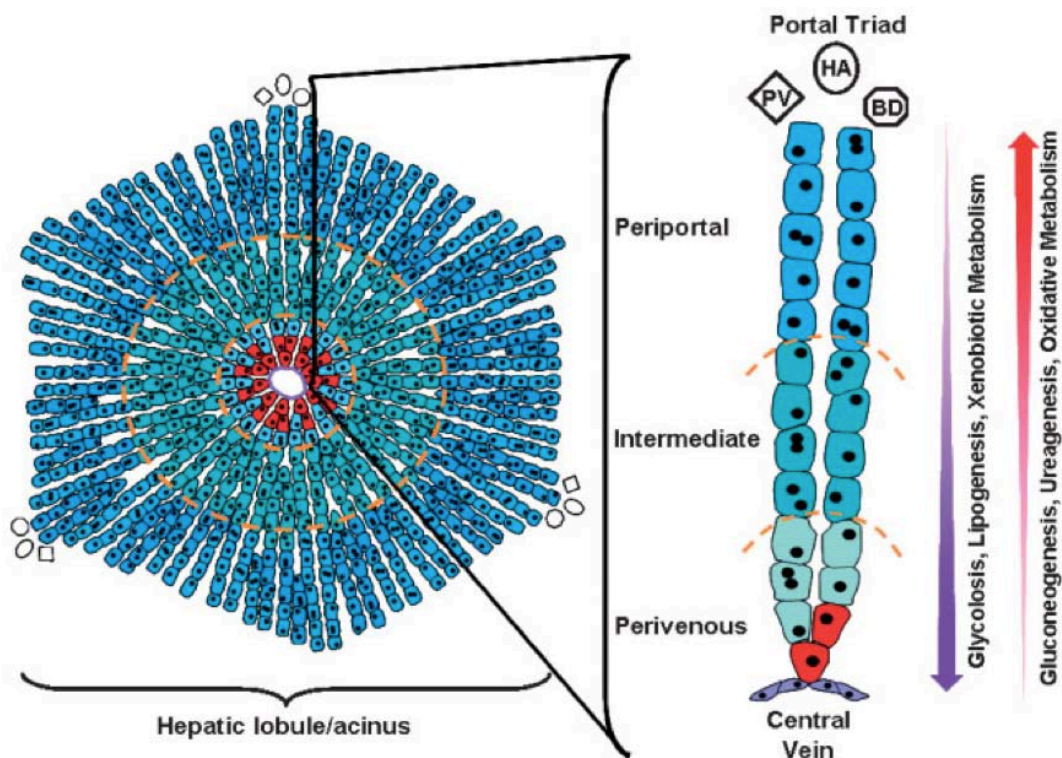


**Figure 1-5: Metabolic zonation within each hepatic lobule**

Along the portovenous axis, hepatocytes are divided into three zones: periportal, intermediate and perivenous. Gradients in metabolic pathways such as gluconeogenesis, glycolysis, xenobiotic metabolism, lipogenesis and ammonia metabolism are observed along this axis. PV = portal vein; HA = hepatic artery; BD = bile duct. Image reproduced with permission from [31].

The functional gradients within the liver arise because the activities of many rate-limiting enzymes for some pathways are higher and lower in different hepatic zones. Consequently, most major hepatocyte-driven functions exhibit differences in activity within the periportal and perivenous zones.

Kupffer cells line the hepatic sinusoids and act as filters to remove bacteria, toxins and other small foreign particles. They play an important role in immune processes that involve the liver by acting as liver macrophages. The numerous ductal epithelia of the liver carry bile—an essential component used for the digestion of food within the intestine—through the hepatic and cystic ducts towards the common bile duct, which opens into the small intestine.

### ***The tyrosine catabolic pathway***

Humans and mice share an identical tyrosine degradation pathway that is catalyzed in five sequential enzymatic reactions producing acetoacetate (ketogenic) and fumarate (glucogenic) as end products (**Fig. 1-6**) [32]. The complete pathway is only expressed in hepatocytes and renal proximal tubular cells. Human genetic diseases arising from enzymatic deficiency are known for four of the five pathway enzymes. My thesis work is predominantly focused on distal tyrosine degradation involving hereditary tyrosinemia type I (HTI).

### ***Hereditary tyrosinemia type I as a model genetic disease***

HTI is a genetic disease with an autosomal-recessive mode of inheritance that is caused by deficiency of fumarylacetoacetate hydrolase (FAH; Enzyme Commission 3.7.1.2), the terminal enzyme in the tyrosine catabolic pathway [32]. FAH is a homo-dimer of 46-kDa subunits that hydrolytically cleaves carbon-carbon bonds in both fumarylacetoacetate (FAA) and succinylacetoacetate (SAA) substrates. This is quite rare, as typical hydrolysis reactions involve amide and ester bonds, yet FAH catalyzes hydrolytic cleavage of stable carbon-carbon bonds [33]. The crystal structures of FAH and FAH complexed with fumarate and acetoacetate, have been determined [34].

HTI is characterized by accumulation of multiple abnormal compounds in both the blood and urine: tyrosine, methionine, tyrosine metabolites and succinylacetone [35]. Many such compounds and their breakdown products are toxic and result in liver and kidney failure characteristic of HTI in a cell-autonomous manner. Toxic metabolite accumulation can be blocked by 2-(2-nitro-4-trifluoromethylbenzoyl)-1,3-cyclohexanedione (NTBC) administration [36], a pharmacological inhibitor that blocks the pathway upstream of FAH (**Fig. 1-6**). NTBC acts as an indirect clinical intervention that provides palliative protection. HTI is an excellent model disease for testing both gene targeting and therapeutic liver repopulation therapies since several animal [37, 38] and fungal [39] models are defined. In addition, unique reagents like NTBC and FAH antibodies allow correction to be carefully controlled and quantified.

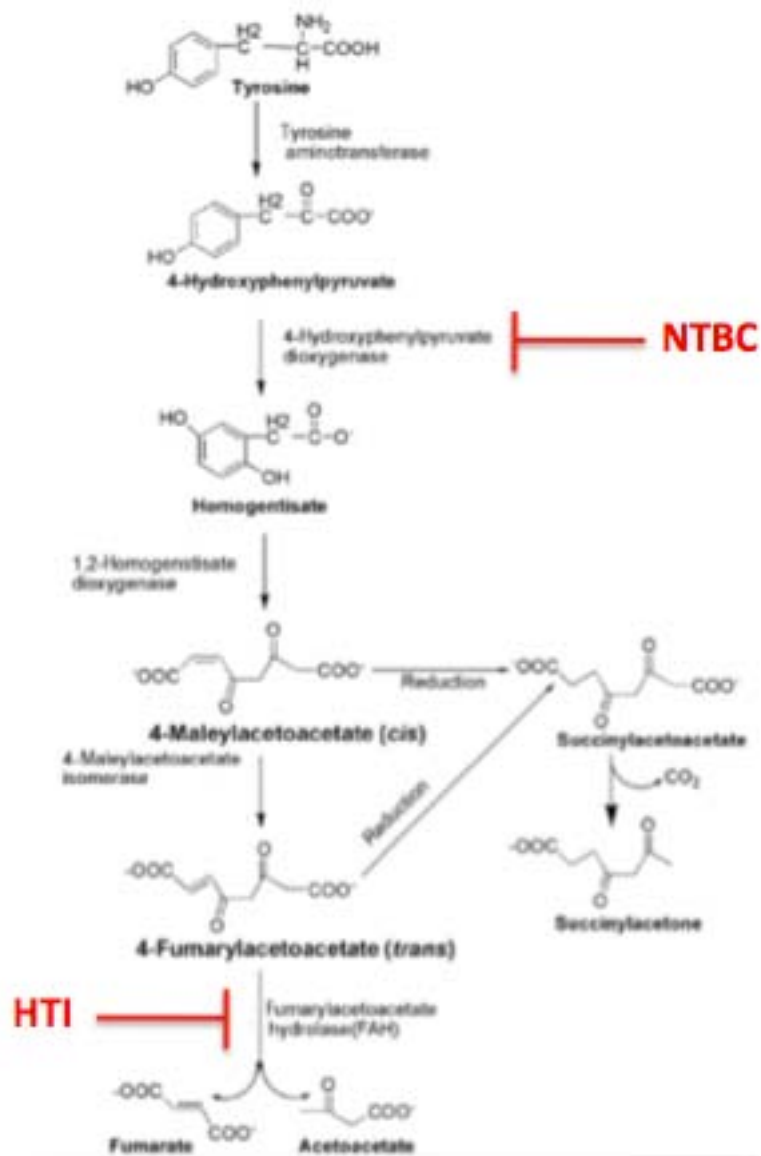


**Figure 1-6: Schematic of tyrosine catabolism**

Mutations in FAH lead to the toxic accumulation of numerous tyrosine pathway metabolites causing HTI-related damage. NTBC treatment blocks this accumulation upstream and is used in humans and mice alike to prevent and study hepatorenal damage.

## ***Abnormal Biochemistry of HTI***

### *Elevated blood tyrosine and tyrosine metabolites*

Both humans and mice with HTI display a markedly elevated blood tyrosine phenotype. Interestingly, the elevated tyrosine levels do not result from FAH deficiency and substrate accumulation as would be predicted, but rather from an indirect inhibition to steps upstream of FAH, namely tyrosine amino transferase (TAT) and hydroxyphenylpyruvate dioxygenase (HPD). Tyrosine accumulation is not itself a toxic hepatorenal event, but its accumulation can induce other unwanted side effects at distal sites such as the brain, skin and eyes [32]. In addition to tyrosine, tyrosine metabolites such as methionine and other acyl radicals of tyrosine will accumulate.

### *Elevated urine organic acids*

The FAH substrate FAA accumulates in HTI but is not seen in bodily fluids due to its rapid reduction to succinylacetoacetate (SAA) and succinylacetone (SA). Both metabolites can be found in blood and urine, and the presence of urine SA is the diagnostic indicator for HTI in the clinic. Although short-lived, FAA can cause extensive oxidative damage as it is a strong electrophile [40]. However, damage from FAA is local and cell autonomous, injuring only those hepatocytes and renal proximal tubules in which it is produced [41]. In addition, liver function tests in HTI display a characteristic increase in transaminases (ALT, AST), total bilirubin and  $\alpha$ -fetoprotein (AFP).

## ***Pathology of HTI***

### *Disregulated gene expression*

HTI patients and *Fah*<sup>-/-</sup> mice have a characteristic gene expression profile in the absence of NTBC therapy [42]. Notably, *Fah* expression is absent, cAMP-inducible genes (*Tat* [43], *Pck1* [44]) are down-regulated along with urea cycle enzymes (*Ass1*, *Otc*), whereas prominent up-regulation is seen in genes for DNA damage (*Ddit3*), oxidative damage (*Nqo-1*), and liver proliferation (*Afp*). These disregulated genes alter the biochemistry of several hepatic processes like gluconeogenesis, protein synthesis and the detoxification of ammonia in response to the oxidative stress induced by FAH loss.

### *Differential apoptotic response*

Accumulation of FAA in both hepatocytes and renal proximal tubules will differ in acute and chronic time frames. Acute FAA accumulation will induce rapid apoptosis in both cell types [45, 46]. Despite the fact that intracellular glutathione levels can quench the oxidative damage from FAA and protect the cell, an upper threshold of glutathione protection can be reached such that apoptosis still occurs [47]. The apoptotic effects of FAA have been confirmed both *in vitro* [45] and *in vivo* [48] to be induced by oxidative stress in the acute window of FAH loss. Chronically, a much different phenotype presents in both patients and mice. In patients, serum transaminase levels like AST, which indicate the level of hepatocyte loss, are lower than would be expected given the amount of liver failure seen [49]. Similarly, in surviving *Fah*<sup>-/-</sup> mice we see a resistance to

apoptosis with time and a decrease in hepatocellular cycling [48]. Thus, it appears that hepatocytes are only acutely sensitive to FAA accumulation and oxidative damage, but compensate with time by altering their gene expression to become resistant to further apoptosis as a survival mechanism [35].

### *Renal dysfunction*

As the only other cell type that expresses the full tyrosine pathway, renal proximal tubule cells are also affected by FAH deficiency. Acute FAA accumulation in the proximal tubules of the kidney parenchyma causes a cell autonomous injury and apoptotic response [46], while chronic injury leads to apoptotic resistance [50], similar to that seen in hepatocytes. Tyrosinemic kidneys are doubly affected by circulating SA which can trigger a renal Fanconi syndrome [51] characterized by failure to reabsorb crucial electrolytes (sodium, potassium, bicarbonate).

### *Hepatocellular carcinoma*

Human HTI patients are at high risk of acquiring hepatocellular carcinoma (HCC) later in life, particularly if they went untreated for longer than 6 months prior to being diagnosed [52]. Similarly, many *Fah*<sup>-/-</sup> mice will eventually develop liver tumors if their tyrosinemia was not adequately managed. Although the direct cause of HCC in HTI has yet to be determined, FAA likely mediates it. FAA is known to be a potent mutagen both *in vitro* [53] and *in vivo* [54] by an as yet undetermined mechanism. FAA has been shown to induce an array of mutations

including predominately genomic rearrangements, but also point mutations and small insertions/deletions. It is thought that FAA alkylates DNA directly, but it is also possible that damage is afflicted indirectly by impairing proteins that maintain genomic stability.

### ***Treatment of HTI***

Historically, the only treatment available for HTI patients was dietary restriction of tyrosine and phenylalanine [55] to prevent flux through the pathway, but this did not prevent disease progression. Liver transplantation has been used successfully in several HTI patients [56-59], however few patients undergo this procedure due to the limited availability of donor organs, the high cost and significant morbidity and mortality associated with the procedure, as well as the long-term requirement for immune suppression [60]. The current standard of care involves combination dietary restriction therapy, as well as treatment with the inhibitor NTBC. NTBC is an FDA-approved [61] inhibitor of HPD, an enzyme upstream of FAH in the tyrosine catabolic pathway, for protection from hepatotoxic FAA and MAA accumulation in HTI patients [62]. Although patients have dramatically improved liver function on NTBC treatment, the restrictive diet is needed to prevent corneal ulcers from elevated tyrosine.

### ***Somatic mosaicism in HTI***

FAH+ cells have a strong selective advantage in an HTI liver that can be exploited in both patients and animal models *in vivo* [63]. Many patients with HTI

have a somatic mosaic liver consisting of both FAH+ and FAH- hepatic tissue. The FAH+ nodules are generated by somatic reversion of the disease causing inherited mutation [64] followed by clonal selection of reverted hepatocytes (**Figure 1-7**). As few as 1,000 FAH+ hepatocytes will repopulate an *Fah*<sup>-/-</sup> liver to >90% in 2-3 months [63]. This observation has led to studies on the possibility of therapeutic liver repopulation. Indeed, several mouse models of HTI exist and have been used for an array of cell therapies [65-68], viral gene therapies [63, 69-71], and non-viral gene therapies [72, 73] to correct the tyrosinemia.

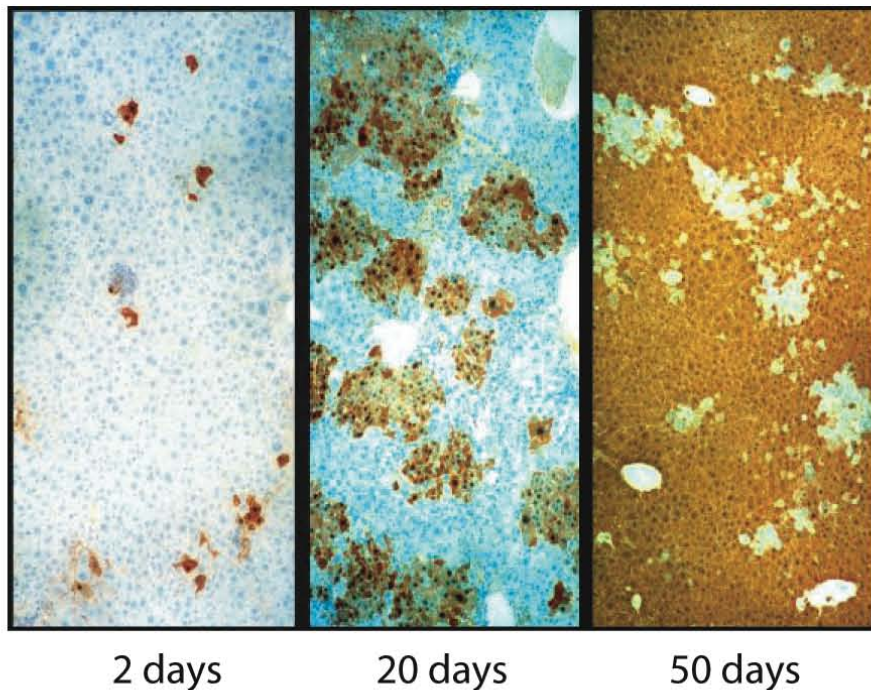


**Figure 1-7: Timeline of liver repopulation**

FAH null liver (**blue**) showing clonal expansion of FAH+ (**brown**) hepatocytes with time post-treatment under selective pressure off NTBC.

### **The various *Fah* null mouse models and their applications**

The *Fah*<sup>5961SB</sup>/*Fah*<sup>5961SB</sup> mouse (BALB/cRI background), herein referred to as *Fah*<sup>-/-</sup>, models HTI by bearing a single ENU-induced point mutation in the final nucleotide of exon 8 within the *Fah* gene [74] (**Figure 1-8**). This point mutation creates a premature downstream stop codon and leads to formation of truncated, unstable FAH protein that is degraded [38]. I backcrossed this *Fah*<sup>-/-</sup> mouse ten generations onto a C57BL/6J background. *Fah*<sup>-/-</sup> mice die as neonates from liver failure if NTBC is not continually administered in the drinking water [36]. NTBC treatment rescues the phenotype and completely prevents acute hepatocellular and renal injury. Discontinuation of NTBC in adult *Fah*<sup>-/-</sup> mice phenocopies acute human HTI. The mice develop liver and renal disease within 10-days, which progresses to hepatic failure and death within 6 to 8-wks [42]. Suboptimal NTBC treatment provides a model of chronic HTI with low-grade liver damage and development of HCC after 3 to 4-mo. The *Fah*<sup>-/-</sup> mouse was used in the gene repair studies (Chapters 2 and 3) as it is point-mutation-based and fully recapitulates the disease on an accelerated timescale.

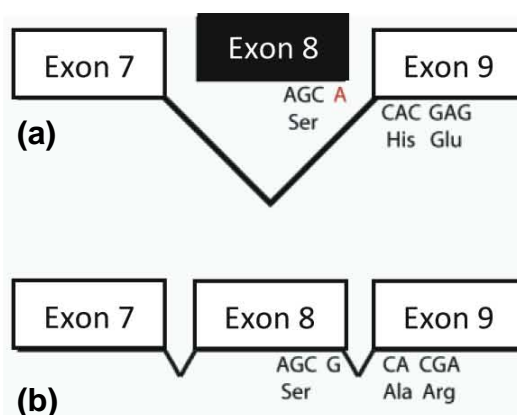


**Figure 1-8: *Fah*<sup>5961SB</sup> mouse mutation**

(a) A single G → A transversion (red) leads to *Fah* exon 8 splice errors and eventual FAH protein loss.

(b) Normal *Fah* splice pattern seen in wildtype mice.

In addition to the *Fah*<sup>5961SB</sup> mouse, another FAH null mouse, *Fah*<sup>Δexon5</sup>/*Fah*<sup>Δexon5</sup> (129S7/SvEvBrd background), herein referred to as *Fah*<sup>Δexon5</sup>, models HTI through Neo-cassette insertion within exon 5 of the *Fah* gene (Figure 1-9). This cassette disrupts exon 5, creating a frameshift and null allele [37]. The mice were backcrossed ten generations onto a C57BL/6J background. The *Fah*<sup>Δexon5</sup> and *Fah*<sup>5961SB</sup> mice are identical in phenotype. The *Fah*<sup>Δexon5</sup> mouse was used in the therapeutic liver repopulation studies (Chapter 4) and fully recapitulates the disease on an accelerated timescale.

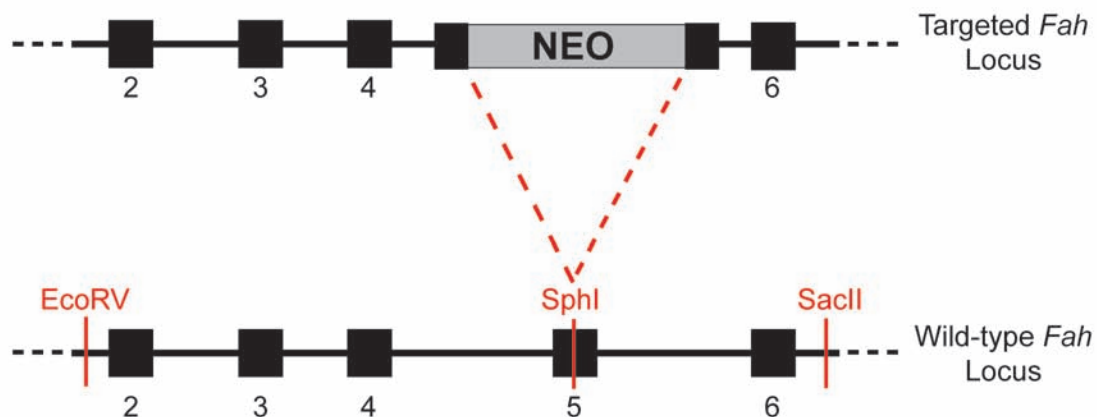


**Figure 1-9: *Fah*<sup>Δexon5</sup> mouse mutation**

The *Fah* gene was disrupted with a replacement vector containing a **Neo** expression cassette cloned into a unique **SphI** site within exon 5 of *Fah*. After linearizing the targeting plasmid (which contained 5-kb of homology 5' and 1.5-kb of homology 3'), the vector was electroporated into mouse ES cells. Targeted clones were injected into C57BL/6J blastocysts and germ-line chimeras were generated. Heterozygotes were crossed to get homozygous *Fah*<sup>Δexon5</sup> mutants.

### ***Gene therapy for liver diseases like HTI***

When attempting to treat a disease like HTI, or any other metabolic liver disease, by gene therapeutic approaches, one of the most important issues to address is the necessary level of liver correction (i.e. percentage of hepatocytes) needed to achieve positive therapeutic outcomes. This percentage will typically be low in non-cell autonomous diseases (ex. Crigler-Najjar [75], hemophilia A [76] and B [77]), and high in cell autonomous diseases (ex. ornithine transcarbamylase deficiency [78]). One exception to this rule is when a disease, like HTI, displays positive selection for corrected cells [63]. Although disorders characterized by selection for gene-corrected cells are rare, there are other examples of this phenomenon: Fanconi's anemia [79], the copper storage disorder Wilson's disease [80], adenosine deaminase deficiency [81], many bile-acid transporter defects [82], Bloom syndrome [83], and junctional epidermolysis bullosa [84]. Patients with diseases arising from point mutations are the most appropriate recipients for gene targeting therapies as historically point mutations have been the most frequent genetic abnormality and source of acquired genetic disease [27].

## CHAPTER 2

### **Adeno-Associated Virus Gene Repair Corrects a Mouse Model of Hereditary Tyrosinemia *In Vivo***

## ABSTRACT

AAV vectors are ideal for performing gene repair due to their ability to target multiple different genomic loci, low immunogenicity, capability to achieve targeted and stable expression through integration, and low mutagenic and oncogenic potential. However, many struggles for gene repair therapies remain. Most notable is the low frequency of correction *in vivo*. To date, this frequency is too low to be of therapeutic value for any disease. To address this, a point mutation based mouse model of the metabolic disease HTI was used to test whether targeted AAV integration by homologous recombination could achieve high-level stable gene repair *in vivo*. Both neonatal and adult mice were treated with recombinant AAV serotypes 2 and 8 carrying wild-type genomic sequence for repairing the mutated *Fah* gene. Hepatic gene repair was quantified by immunohistochemistry and supported with RT-PCR and serology for functional correction parameters. Successful gene repair was observed with both serotypes but was more efficient with rAAV2/8. Correction frequencies of up to 0.1% were achieved and highly reproducible within typical dose ranges. In this model, repaired hepatocytes have a selective growth advantage and are thus able to proliferate to efficiently repopulate mutant livers and cure the underlying metabolic disease.

## INTRODUCTION

Gene therapy is a promising means to cure many monogenic diseases. However, traditional gene therapies are best suited to treat diseases of deficient or absent gene products rather than those diseases caused by aberrantly functioning proteins. Even now, gene therapy efforts remain focused on gene addition strategies using full-length cDNA cassettes for the mutated gene of interest, driven by promoter and enhancer sequences [16]. Despite many advances, gene addition approaches with rAAV are limited by transient and unregulated expression [85, 86], highly random integrations [18], and increased mutagenic and oncogenic risks [19]. Not all protein-coding genes have open reading frames small enough to fit within the low coding capacity of rAAV (4.7-kb) [87], thus, this type of gene therapy is not applicable for all disorders.

Gene repair offers a solution to these drawbacks, where patient genomes are manipulated *in vivo* using site-specific recombination to actually correct the underlying mutation. Contrary to more widely used gene addition paradigms, gene repair restores gene function within the context of all endogenous regulatory elements, thereby eliminating potential problems with inadequate or inappropriate expression. Different vehicles have been utilized for performing gene repair including single-strand oligonucleotides [88-90], triplex-forming oligonucleotides [91], RNA-DNA hybrids [92, 93], and rAAV [21, 25]. Of these, rAAV has emerged as the most promising. Numerous *in vitro* studies have shown

rAAV capable of correcting various types of mutations (insertions, deletions, substitutions) by vector-mediated homologous recombination [22, 23]. AAV vectors engineered to perform gene repair have the ability to target multiple different genomic loci, show both targeted and stable expression through integration, and have an increased number of applicable human diseases [26]. Single-stranded rAAV genomes modulate gene repair by integrating site-specifically via homologous recombination and targeting only the disease-causing mutation for replacement with wild-type sequence [24]. Gene repair is best suited to correct point mutation based diseases that need only one or few nucleotides corrected to restore normal gene expression. This is important, as point mutations are the most frequent genetic abnormality and source of acquired genetic disease [27].

To demonstrate targeted hepatic gene repair *in vivo* for a clinically pertinent disease gene, a HTI mouse model was used. HTI is a fatal genetic disease caused by deficiency of FAH, the terminal enzyme in the tyrosine catabolic pathway [32]. When a FAH deficiency exists, toxic metabolites such as FAA accumulate in hepatocytes and renal proximal tubules causing death in a cell-autonomous manner [35]. Toxic metabolite accumulation can be blocked by NTBC administration, a pharmacological inhibitor that blocks the pathway upstream of FAH [36]. The *Fah*<sup>-/-</sup> mouse is ideal to study gene repair, because it is point mutation based and fully recapitulates the human disease on an accelerated time scale [38]. Strong positive selection for FAH<sup>+</sup> cells in the HTI

mouse liver has been demonstrated [63] and was exploited for *in vivo* selection of corrected hepatocytes following gene repair. In this system, when rAAV vectors containing genomic *Fah* sequence (hereafter referred to as AAV-*Fah*) are administered to *Fah*<sup>-/-</sup> mice, only corrected FAH+ hepatocytes that have undergone integration by homologous recombination can survive and repopulate the liver. The outcome is formation of corrected FAH+ nodules and loss of unintegrated episomal vector genomes. In both neonatal and adult mice treated with rAAV-*Fah*, gene repair restored proper gene and protein expression and cured the underlying HTI phenotype. These results demonstrate proof-of-principle that an appropriate monogenic liver disease can be corrected by AAV-mediated gene repair *in vivo*.

## MATERIALS AND METHODS

### ***Mouse Strains and Animal Husbandry***

The *Fah*<sup>-/-</sup> mouse models HTI by bearing a single ENU-induced point mutation in the final nucleotide of exon 8 within the *Fah* gene [38]. This point mutation creates a premature downstream stop codon and exon 8 loss, ultimately leading to formation of truncated, unstable FAH protein that is degraded [74]. *Fah*<sup>-/-</sup> mice die as neonates from acute liver failure if NTBC is not continually administered in the drinking water [42]. NTBC treatment at 4-mg/L rescues the phenotype and prevents acute hepatocellular and renal injury. Discontinuation of NTBC provides an accurate model of HTI. Mice develop liver and renal disease within 10 days, which progresses to full end-stage liver disease and death within 6 to 8-wks. The mice have been backcrossed ten generations onto a C57BL/J6 background. The Institutional Animal Care and Use Committee of Oregon Health and Science University approved all mouse procedures.

### ***Plasmid Vectors***

*Mus musculus* bacterial artificial chromosome clone RP23-121N17 from chromosome 7 was used as a template for the 4.5-kb LD-PCR amplification of sequence homologous to the region centered on the point mutation in exon 8 of murine *Fah* (RefSeq NM\_010176, chr7: 84461356-84481935). Primer sequences: Forward primer introducing NotI: 5'-GCGGCCGCTTCCCAGGGTTTTTGTGGTT-3'; Reverse primer: 5'-AGCCCCCACTGACAGCTACAGCT-3'.

The PCR resulted in a 4.5-kb product with an introduced 5'-*NotI* restriction site that allowed cloning into an AAV plasmid backbone as previously described [94] to generate rAAV-*Fah*. The rAAV-*Fah* vector was pseudotyped with either a serotype 2 or 8 capsid to produce rAAV2/2-*Fah* and rAAV2/8-*Fah*. Control vector rAAV2/8-LSP-*eGFP* encodes enhanced-GFP and is driven by the liver specific promoter (LSP) that contains sequence from the thyroxine hormone-binding globulin gene promoter, two copies of the  $\alpha$ 1-microglobulin/bikunin enhancer sequence, and a  $\beta$ -globin intron [77]. Control vectors rAAV2/2-RSV-*hAAT* and rAAV2/8-RSV-*hAAT* encode human  $\alpha$ 1 anti-trypsin and are driven by the Rous sarcoma virus long terminal repeat (RSV) promoter [95].

### ***Sequencing***

DNA sequencing was performed with an ABI-Prism 3130xl Genetic Analyzer at the Vollum Sequencing Core (Portland, OR). DNA sequences were aligned with MacVector software v.11.1.2 (MacVector, Inc., Cary, NC).

### ***Neonatal Vector Administration***

For time course studies, *Fah*<sup>-/-</sup> neonates at post-natal day two (P2) were administered  $1-2 \times 10^{11}$  vg of either rAAV2/2-*Fah* or rAAV2/8-*Fah* (in 10- $\mu$ l volume) by intravenous (IV) superficial temporal injection [96]. Littermate controls were similarly injected with  $1-2 \times 10^{11}$  vg of an irrelevant serotype-matched control vector, either rAAV2/2-RSV-*hAAT* [95] or rAAV2/8-LSP-*eGFP* [97]. All mice were maintained on NTBC throughout. Livers were harvested at 1, 2, or 4-wks post-

treatment. For dose-response studies, P2 *Fah*<sup>-/-</sup> neonates were administered one of four doses ranging from  $3 \times 10^8$  to  $3 \times 10^{11}$  vg (in 10- $\mu$ l volume) of each serotype by IV superficial temporal vein injection. All mice were maintained on NTBC throughout. Livers were harvested 2-wks post-treatment. For stable integration studies, P2 *Fah*<sup>-/-</sup> neonates were administered rAAV2/2-*Fah* at  $1 \times 10^{11}$  vg (in 10- $\mu$ l volume) by IV superficial temporal vein injection. Littermate controls were similarly injected with isotonic NaCl solution. Mice were maintained on NTBC until weaning and then withdrawn to select for corrected hepatocytes. Eleven weeks post-treatment, a two-thirds partial hepatectomy was performed to induce liver regeneration [98]. Livers were harvested >12 weeks post-surgery. For random integration studies, P2 *Fah*<sup>-/-</sup> neonates were co-administered  $4 \times 10^{10}$  vg of both rAAV2/8-*Fah* and rAAV2/8-RSV-*hAAT* (in 20- $\mu$ l volume) by IV superficial temporal vein injection. Mice were maintained on NTBC until weaning and then withdrawn to select for corrected hepatocytes. Serum for liver function tests and liver tissue were collected at harvest.

### ***Adult Vector Administration***

Adult *Fah*<sup>-/-</sup> mice (age 8-12 weeks) were administered  $1 \times 10^{11}$  vg of rAAV2/8-*Fah* (in 100- $\mu$ l volume) by IV lateral tail vein injection. Age-matched littermate controls were similarly injected with isotonic NaCl solution. Mice were placed on NTBC as needed. Serum and liver tissue were harvested >12 weeks after treatment.

### ***Liver Immunohistochemistry***

In both adult and neonatal mice, a minimum of three liver sections from varying depths and randomly selected liver lobes were analyzed for the number of FAH+ nodules. As nodules represent the clonal expansion of a single corrected hepatocyte, nodule frequency was corrected for nodule size. Briefly, the surface area of each liver section was measured by scanning the glass slide with a size standard using an Epson Perfection V700 scanner at 400-dpi resolution. Adobe Photoshop 7.0 software was then used to select and count pixels of each liver section. Pixel counts were then converted to numbers of hepatocytes based on the diameter of a mouse hepatocyte (~25 microns). Correction factors were then applied to frequencies of FAH+ nodules in a section containing (x) hepatocytes based on the following assumptions, as described previously [68]: 1) hepatocyte nodules are spherical; 2) in a given sample all nodules are the same size; 3) the number of hepatocytes in the largest clone represents the middle of that nodule. Immunohistochemical fixation and staining protocols for FAH and H&E were completed as described [68]. Two separate, blinded investigators performed quantitation. Microscopy was performed on a Zeiss AxioScope A-1 microscope (Zeiss, Thornwood, NY) using SPOT Insight Software v.3.4 (SPOT Imaging Solutions, Sterling Heights, MI). Blood for serology was collected by cardiac puncture and biochemical assays were completed as described [42].

### ***Statistical Analysis***

Statistics were conducted with GraphPad Prism software v.4.0 (GraphPad, San Diego, CA). Experimental differences were evaluated by student two-tailed *t*-test assuming equal variance. *P* values <0.05 were considered statistically significant.

### ***Recombinant AAV Production***

Standard transfection and viral isolation protocols described previously [99] were used with the following modifications. Unpurified virus was sedimented and resuspended in benzonase buffer for freezing at -80°C. After three freeze-thaw cycles in a dry ice/ethanol bath, the suspension was benzonase-treated (EMD Chemicals, San Diego, CA). Virus was pelleted and precipitated with 1M CaCl<sub>2</sub>, followed by 40% PEG-8000 treatment and resuspension in a sodium/HEPES buffer and rotated overnight at 4°C. Afterwards, purification by sequential cesium chloride density centrifugation was done as described [100] with the following modifications. Peak fractions from both gradients were determined by optical refractometry. Positive final fractions were dialyzed against PBS lacking Ca<sup>2+</sup> or MgCl<sub>2</sub> (Gibco, Grand Island, NY) and supplemented with 5% (wt/vol) D-sorbitol (Sigma, St. Louis, MI). Vector titering was performed by dot blot [101].

### ***Transplantation***

For serial transplantations, the liver of each corrected donor mouse was perfused as described [102], and 3x10<sup>5</sup> random hepatocytes were transplanted into four recipients, each by intrasplenic injection as described [103].

### ***Fah* Quantitative Reverse Transcription PCR**

Total RNA was isolated from randomly dissected liver tissue with an RNeasy Mini kit. cDNA was produced with a Superscript III First-Strand Synthesis kit (Invitrogen, Carlsbad, CA). PCR was performed on an iCycler (Bio-Rad, Hercules, CA). The RT reaction was subjected to two-step PCR amplification with 100-ng cDNA under the following conditions: 1 cycle 95°C 3-min, followed by 45 cycles of 95°C 15-sec and 68°C 50-sec. All samples were subjected to +/- RT controls and results were normalized to *Gapdh* expression. Primers: *Fah* F: 5'-AGAACTTACTGTCTG CCAGCCAAG-3'; *Fah* R: 5'-GAGGACCATCCCGAAA ATGTG-3'; *Gapdh* F: 5'-CC ACCCCAGCAAGGACACTG-3'; *Gapdh* R: 5'-GCTC CCTAGGCCCTCCTGT-3'.

### ***hAAT* Copy Number Quantitative PCR**

Total DNA was isolated from randomly dissected liver tissue with a MasterPure DNA Purification kit (Epicentre, Madison, WI). PCR was performed on an iQ5 Multicolor Real-Time PCR (Bio-Rad, Hercules, CA), using iQ5 Standard Edition Software v.2.0. Genomic DNA (10-ng) was subjected to two-step amplification under the following conditions: 1 cycle 95°C 3-min, followed by 45 cycles of 95°C 15-sec and 68°C 40-sec. Dilutions of *hAAT* plasmid into mouse genomic DNA were used to generate copy number standards. Results were normalized to *Gapdh* expression. Primer sequences: *hAAT* F: 5'-TCCTGGGTCAACTGGGCA TC-3'; *hAAT* R: 5'-CAGGGGTGCCTCCTCTGTGA-3'; *Gapdh* F: 5'-CCACCCCA GCAAGGACACTG-3'; *Gapdh* R: 5'-GCTCCCTAGGCCCTCCTGT-3'.

## RESULTS

### ***Target vector design***

In *Fah*<sup>-/-</sup> mice, a single point mutation (G-to-A transversion) at the terminal nucleotide of *Fah* exon 8 leads to mis-splicing and exon 8 deletion from the mRNA. Several important criteria derived from the literature [26] were considered for the design of the gene repair vector structure (**Fig. 2-1a**) to correct the *Fah*<sup>-/-</sup> point mutation. First, the vector should not contain elements needed for driving gene expression such as promoters, enhancers, or cDNA expression cassettes. Second, the fidelity and length of homology should be maximized with the packaging capacity of AAV (~4.7-kb) being the limit. Third, the position of the nucleotide targeted for repair should be at the center of the homology. A 4.5-kb PCR product homologous to murine *Fah* was cloned into an AAV plasmid backbone and verified by DNA sequencing. Recombinant AAV-*Fah* of serotypes 2 and 8 were produced and administered to *Fah*<sup>-/-</sup> mice as neonates or adults. Correction of the point mutation by homologous recombination (**Fig. 2-1b**) leads to normal *Fah* gene and protein expression.

### ***AAV-Fah mediates stable gene repair***

The evaluation of homologous recombination as a strategy for gene repair has traditionally relied on detecting alterations in reporter sequences rather than correcting a disease phenotype. Given the selective advantage of FAH<sup>+</sup> hepatocytes in the HTI liver, *Fah*<sup>-/-</sup> mice can be used to study the clinical

significance of AAV-mediated gene repair by homologous recombination. Four P2 *Fah*<sup>-/-</sup> neonates were intravenously injected with  $1 \times 10^{11}$  vg of rAAV2/2-*Fah* and kept on NTBC until weaning, followed by NTBC withdrawal to select for corrected hepatocytes. Two control groups were injected with isotonic NaCl solution. Control group I (n = 3) did not receive a course of NTBC post-weaning, continued to lose weight and died. Control group II (n = 2) did receive one course of NTBC post-weaning but failed to maintain a healthy weight and died. AAV-treated mice began to stabilize in weight 8-wks post-treatment, suggesting the onset of sufficient liver function. At age 11-wks, a two-thirds partial hepatectomy was performed to induce liver regeneration and subsequent episomal AAV loss. Continued clinical improvement following partial hepatectomy strongly suggested stable gene repair at the *Fah* locus. Immunohistochemistry for FAH showed >50% FAH+ hepatocytes in section overviews (**Fig. 2-2**). The numbers of detectable liver nodules ranged from 21-47 per 50-mm<sup>2</sup> section in treated mice and were never detected in controls. Nodules represent the clonal expansion of a single corrected hepatocyte, thus nodule frequency must be corrected for nodule size. For this experiment, the correction factor was estimated to be fourteen. After correction, the initial gene repair frequency ranged from 1/6,300 to 1/11,600 hepatocytes and was within the expected range from previous experiments where selection with NTBC did not apply.

To demonstrate that FAH staining was not artifactual and that proper *Fah* gene expression had indeed been restored, *Fah* RT-PCR was performed on RNA

from treated livers. The presence of correctly spliced mRNA was demonstrated in all treated mice (**Fig. 2-3**). To further demonstrate the stability of correction,  $3 \times 10^5$  random hepatocytes from each corrected mouse were serially transplanted into four secondary adult *Fah*<sup>-/-</sup> recipients. Serial transplantation is another means to induce hepatocyte turnover and eliminate episomal AAV genomes. Serial transplant recipients had successful engraftment and displayed clinical improvement, whereas untransplanted controls showed continuous weight loss and died. FAH immunohistochemistry from livers of serial transplant recipients had extensive hepatocellular FAH staining (**Fig. 2-2**), further demonstrating stability of the gene repair.

#### ***Time course comparison of rAAV2/8-Fah and rAAV2/2-Fah***

AAV8 is the preferred serotype for liver transduction because of its strong hepatic tropism, rapid capsid disassembly and genome release. In contrast, although AAV2 has been shown to transduce liver, it is characterized by slow capsid disassembly and genome release. To address the question whether rAAV serotypes 8 and 2 have different gene repair dynamics *in vivo*, P2 *Fah*<sup>-/-</sup> neonates were administered  $1-2 \times 10^{11}$  vg of rAAV2/8-*Fah* or rAAV2/2-*Fah* and analyzed 1, 2, or 4-wks post-treatment for the presence of FAH+ hepatocytes (**Fig. 2-4**). In rAAV2/8-*Fah* treated mice, the highest numbers of FAH+ hepatocytes seen were detected within the first week post-treatment. Correction frequencies declined with time and stabilized after 4-wks. In contrast, rAAV2/2-*Fah* treated mice had little detectable FAH expression within the first seven days,

supporting the fact that rAAV2/2 uncoats more slowly than rAAV2/8 [104]. Week two showed an increase in FAH expression that remained stable until week four. No FAH+ hepatocytes were detected at any time point in control mice injected with serotype-matched irrelevant control vectors rAAV2/8-LSP-*eGFP* or rAAV2/2-RSV-*hAAT* at equivalent doses. These results conclusively demonstrate that emergence of FAH+ hepatocytes were neither due to spontaneous reversion, nor gene repair stimulated non-specifically by mere AAV transduction.

### ***Gene repair in response to different vector doses***

To examine dose responses, P2 *Fah*<sup>-/-</sup> neonates were injected with four rAAV-*Fah* concentrations ranging from  $3 \times 10^8$  to  $3 \times 10^{11}$  vg for each serotype and kept on NTBC until harvest at weaning to prevent metabolic selection of FAH+ cells. In general, rAAV2/8-*Fah* displayed a linear dose response over the range of doses administered where the highest doses administered produced the greatest gene repair (**Fig. 2-5**). The difference in repair frequencies between the highest dose and all other doses administered was significant. In contrast, rAAV2/2-*Fah* had no significant change in repair frequency over the entire range of doses administered. It is unknown why rAAV2/2 displayed such a response. Overall, results indicate that rAAV2/8-mediated gene repair is superior to that with rAAV2/2.

### ***AAV-mediated gene repair is feasible in quiescent liver***

The adult liver has considerably less cellular turnover than neonatal liver undergoing rapid growth and proliferation. Thus, gene repair frequencies are predicted to be lower in adults as homologous recombination is most prevalent during mitotic S-phase. rAAV2/8 was chosen to test the feasibility of gene repair in the nearly quiescent adult liver as it had now been demonstrated to be both faster and more efficient at gene repair than rAAV2/2. Adult *Fah*<sup>-/-</sup> mice (8 to 12-wks old) were injected with  $1 \times 10^{11}$  vg of rAAV2/8-*Fah*, whereas age-matched littermate controls were injected with isotonic NaCl. Mice were withdrawn from NTBC to allow selection of corrected hepatocytes. Serum for liver function tests and liver tissue were harvested >12 weeks post-treatment. Mice treated with rAAV2/8-*Fah* showed clinical improvement and repopulation with FAH+ hepatocytes (**Fig. 2-6a**), whereas all mice in the control group had to be euthanized and showed no hepatic repopulation. Surprisingly, the initial correction frequency of FAH+ nodules was comparable to that seen with neonatal administration. The clonal expansion of corrected hepatocytes was able to reverse the tyrosinemic phenotype and was highly reproducible. Liver function tests for AST and bilirubin demonstrated near complete correction when compared to controls (**Fig. 2-6b**).

### ***Frequency of random integration***

Although phenotypic reversion of *Fah*<sup>-/-</sup> mice suggests successful site-specific gene repair, random integration could also occur. To assess random integration

frequencies, P2 *Fah*<sup>-/-</sup> neonates were co-injected with 4x10<sup>10</sup> vg of rAAV2/8-*Fah* and an irrelevant serotype-matched control vector rAAV2/8-RSV-*hAAT*. Post-weaning, mice were subjected to NTBC withdrawal to select for corrected hepatocytes. To ensure no episomes remained, 5x10<sup>5</sup> random hepatocytes were then serially transplanted into eight secondary *Fah*<sup>-/-</sup> recipients. After >12 weeks off NTBC, serum and liver tissue were collected at harvest. Quantitative PCR was used to determine *Fah* and *hAAT* copy numbers in each mouse (**Table 2-1**). The frequency of randomly integrated *hAAT* ranged from 0 (undetectable) to 0.058 per diploid genome equivalent (dGE) and averaged 0.018/dGE. Only half the hepatocytes in repopulated livers were donor-derived, thus frequencies were corrected by a factor of two, resulting in an average random integration frequency of 0.88% in corrected hepatocytes. This number is similar to multiple estimates of random integration of rAAV2/8 from the literature [94, 105]. Liver function tests in serially transplanted mice demonstrated near complete reconstitution by normalization of AST and bilirubin levels. Differences in serum AST and bilirubin levels were significant ( $p < 0.05$ ). In addition, in neonatal follow-ups 16-wks post-treatment, no tumors were observed (n = 15, data not shown).

## FIGURES

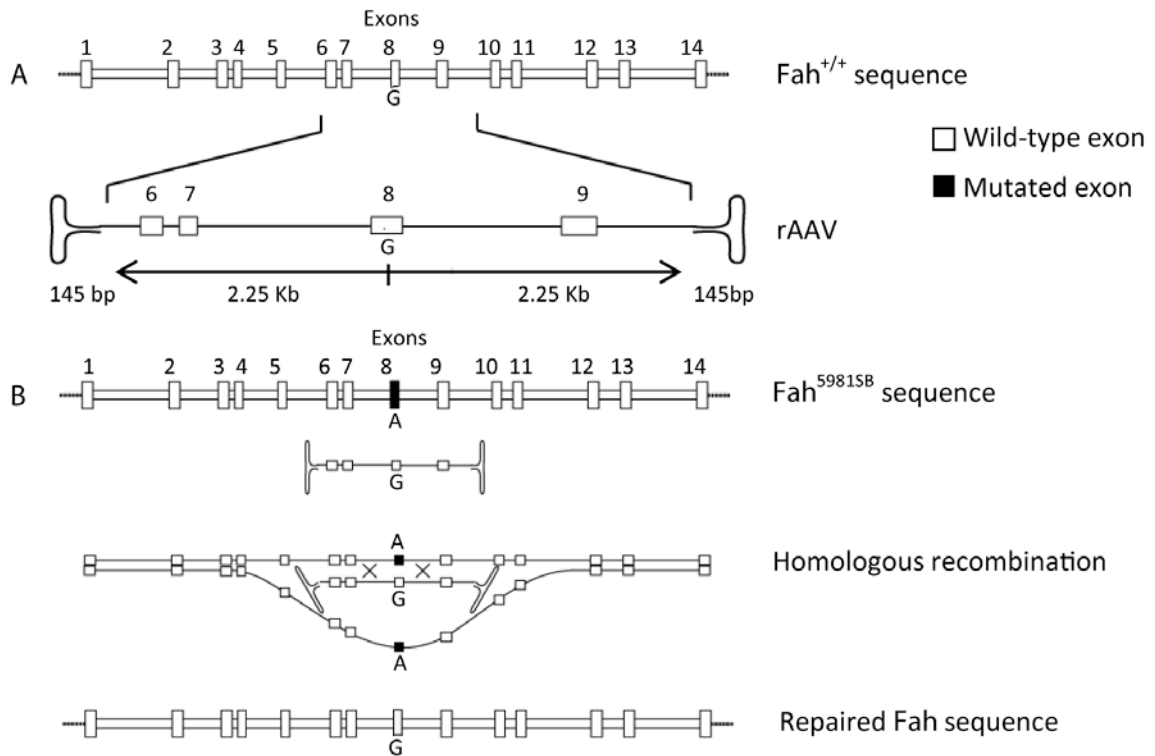


**Figure 2-1: AAV vector design and genomic organization of murine *Fah***

(a) A 4.5-kb gDNA fragment homologous to murine *Fah* was cloned into an AAV plasmid backbone and verified with sequencing. The position of the nucleotide needed to perform repair was centered within two 2.25-kb homology arms.

(b) Mechanism of AAV-mediated homologous recombination. Wild-type *Fah* has a guanine as the terminal nucleotide of exon 8. In  $Fah^{-/-}$  mice, a G-to-A transversion occurs at this position leading to mis-splicing and exon-8 deletion. Gene repair by AAV-mediated homologous recombination corrects the point mutation and restores proper *Fah* gene expression.

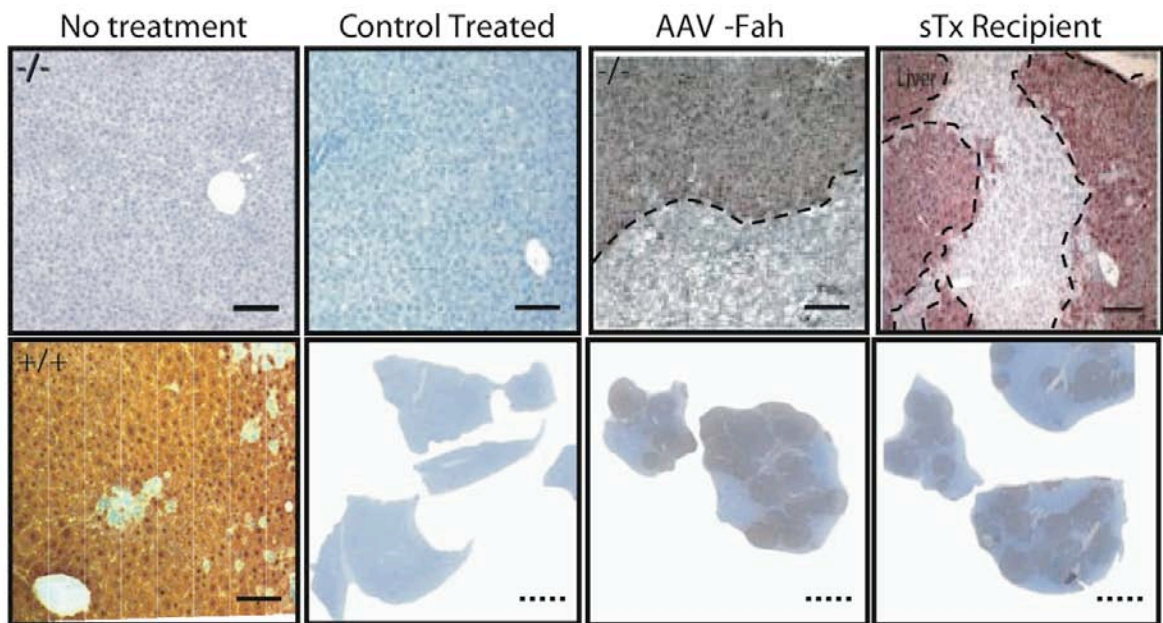


**Figure 2-2: Liver immunohistochemistry and whole-mount staining for FAH**

*Top row:* from left to right, FAH immunohistochemical staining on liver sections from an untreated *Fah*<sup>-/-</sup> mouse; mock-injected *Fah*<sup>-/-</sup> mouse; *Fah*<sup>-/-</sup> mouse treated with rAAV2/8-*Fah*; and *Fah*<sup>-/-</sup> mouse after serial transplantation (sTx) with corrected hepatocytes.

*Bottom row:* from left to right, FAH immunohistochemical staining on liver sections from an untreated (*Fah*<sup>+/+</sup>) wild-type mouse, mock-injected *Fah*<sup>-/-</sup> mouse, *Fah*<sup>-/-</sup> mouse treated with rAAV2/2-*Fah*, *Fah*<sup>-/-</sup> mouse treated with rAAV2/8-*Fah*. Scale bars: solid = 100 μm; dotted = 1 mm.

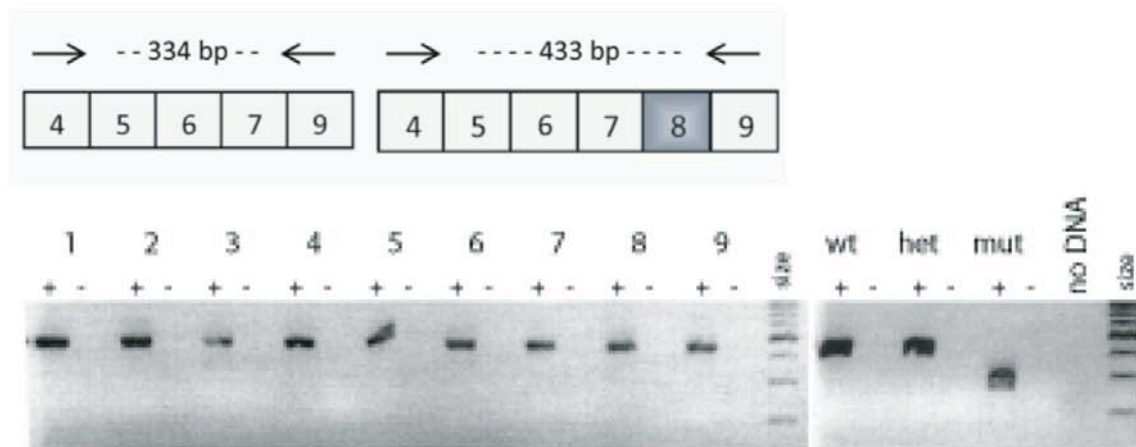


**Figure 2-3: RT-PCR for *Fah* mRNA**

*Top panel:* mutant *Fah* mRNA lacks exon 8 and produces a shorter 334-bp PCR product, whereas wild-type *Fah* mRNA produces a 433-bp PCR product.

*Bottom panel:* gel analysis of nine experimental samples at the left and controls at the right. The +/- indicates whether reverse transcriptase was used. Samples 1-3 are from AAV-treated neonatal mice, samples 4-5 are from AAV-treated adults, and samples 6-9 are from serial transplant recipients.

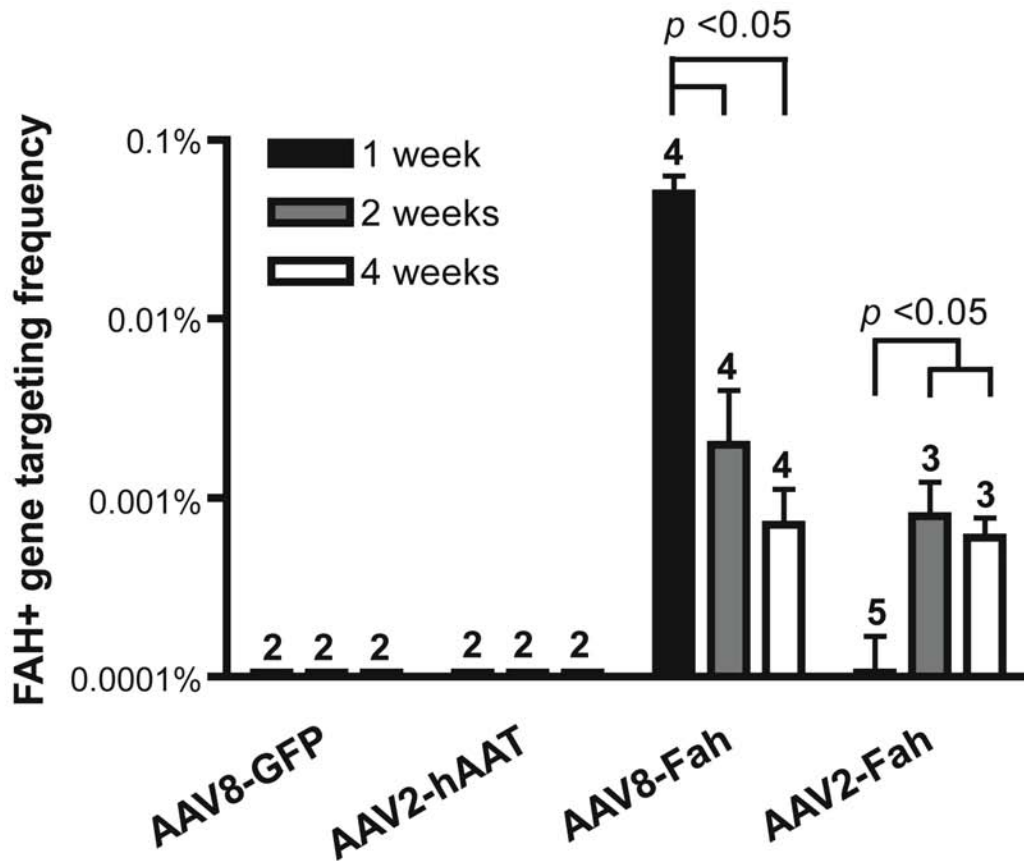


**Figure 2-4: Time-course of AAV-mediated gene repair in neonates**

Vectors are noted below each set and were administered at  $1-2 \times 10^{11}$  vg.

Frequencies were quantified by counting single FAH+ clones per x hepatocytes

(1/x) from neonates harvested 1, 2, or 4-wks post-treatment. Mean  $\pm$  SD are

shown, with the number of independent animals analyzed above each bar. Black

= 1-wk post-treatment; gray = 2-wks post-treatment; white = 4-wks post-

treatment.

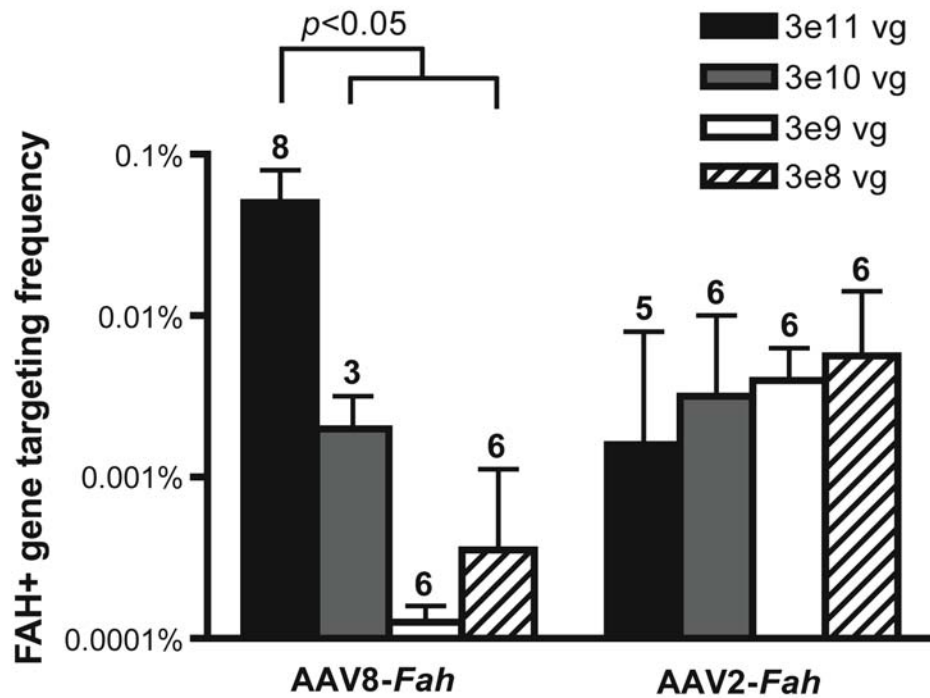


**Figure 2-5: Dose response of AAV-mediated gene repair in neonates**

Vectors administered are noted below each data set and were administered at  $3 \times 10^8$  to  $3 \times 10^{11}$  vg. Frequencies were quantified by counting single FAH+ clones per x hepatocytes ( $1/x$ ) from neonates harvested 3-wks post-treatment. Mean  $\pm$  SD are shown, with the number of independent animals analyzed above each bar. Black =  $3 \times 10^{11}$  vg; gray =  $3 \times 10^{10}$  vg; white =  $3 \times 10^9$  vg; diagonal lines =  $3 \times 10^8$  vg.

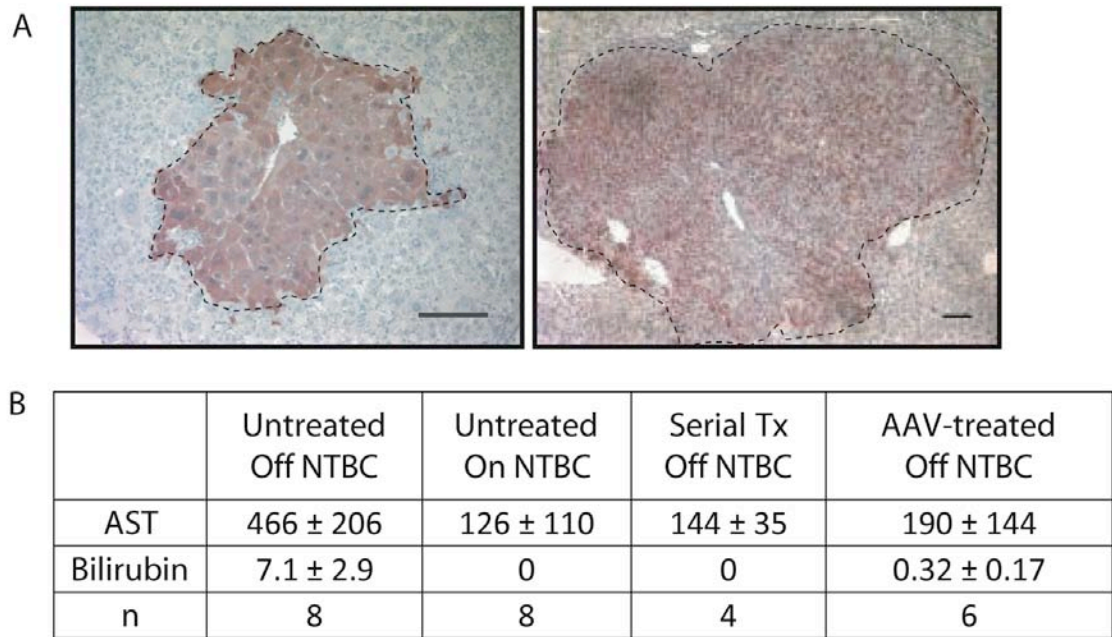


**Figure 2-6: AAV-mediated gene repair is feasible in adult liver**

(a) Liver sections stained for **FAH** from adult *Fah*<sup>-/-</sup> mice more than 12-wks post-treatment with rAAV2/8-*Fah*. Scale bars = 100- $\mu$ m.

(b) Liver function test results for AST (U/l) and bilirubin (mg/dL). Mean  $\pm$  SD are shown from untreated *Fah*<sup>-/-</sup> mice off or on NTBC, serially transplanted (Tx) *Fah*<sup>-/-</sup> mice off NTBC, and adult rAAV-treated *Fah*<sup>-/-</sup> mice off NTBC.

## TABLES

Donor	sTx Recipient	# copies/dGE	Average
<b>1</b>	1a	0.009	0.027
	1b	0.026	
	1c	0.002	
	1d	0.042	
	1e	0.058	
<b>2</b>	2a	0.002	0.001
	2b	0.001	
	2c	0.001	
<b>Total average</b>			0.018
<b>Random integration</b>			0.88%

**Table 2-1: *hAAT* copy numbers in recipient mice**

After neonatal co-injection of  $4 \times 10^{10}$  vg of rAAV2/8-*Fah* and rAAV2/8-RSV-*hAAT*, FAH+ hepatocytes were selected for and then serially transplanted to remove episomes. Data represent the number of copies of *hAAT* per diploid genome equivalent (dGE) in serial transplant (sTx) recipients. Roughly 50% of the hepatocytes in repopulated recipients were donor-derived at the time of harvest, so the frequency was corrected by a factor of 2 to give an estimated random integration frequency of 0.88%.

## DISCUSSION

AAV has emerged as the vector of choice for gene repair as its single-stranded nature facilitates correction by homologous recombination. Numerous studies have demonstrated successful rAAV-mediated gene repair to correct different mutation types *in vitro* [22, 23]. In doing so, these studies provided the essential validation and framework for all rAAV-mediated gene repair studies *in vivo*. Few publications exist demonstrating repair *in vivo* [106, 107], and they are hindered by the fact that they target clinically irrelevant marker mutations in exogenously provided transgenes like *GFP* or *LacZ*. One report has shown limited efficacy *in vivo* using a mouse model of the disease mucopolysaccharidosis type VII [25]. In that study, a single point mutation in the glucuronidase gene was corrected at frequencies of 0.001% to 0.01% using rAAV2/2 and rAAV2/6 at  $2-6 \times 10^{11}$  vg doses. Nonetheless, the low correction frequencies were not therapeutic in treated mice, because no selective advantage exists for corrected hepatocytes in that model. This study differs from our own in several ways. Our study is the first to demonstrate the stability of gene correction in both adult and neonatal mice. In addition to rAAV2/2, our study demonstrated greater correction using rAAV2/8, the most hepatotropic of all the naturally occurring AAV serotypes. Furthermore, correction frequencies of up to 0.1% as early as 3-wks post-treatment in adult mice were shown; rather than 0.01% in 12 to 24-wks post-treatment in the previous study. Finally, our work tested a range of rAAV doses from  $10^{11}$  down to  $10^8$  vg and was able to demonstrate correction at all doses administered.

Numerous struggles for rAAV-mediated gene repair remain. Most notable is the low frequency of correction *in vivo*. To date, this frequency is too low to be of therapeutic value for many diseases. However, our work demonstrates that rAAV-mediated gene repair has the capacity to be a viable therapeutic alternative in a suitable selection-based disease. In HTI, corrected hepatocytes have a selective growth advantage and can clonally expand to restore liver function, even if the initial gene repair efficiency is low. While this situation is an exception, there are several disorders in which selection has been shown, including Fanconi's anemia [79], the copper storage disorder Wilson's disease [80], many bile-acid transporter defects [82], and junctional epidermolysis bullosa [84]. If correction frequencies were increased 100-fold, they would become clinically relevant for a broad range of diseases. For example, it has been predicted that gene repair frequencies of 5% would have therapeutic benefit in patients with hemophilia A [76].

## CHAPTER 3

# **Adeno-Associated Virus-Mediated Gene Targeting is Significantly Enhanced by Transient Inhibition of Non-Homologous End Joining or the Proteasome *In Vivo***

## ABSTRACT

Recombinant adeno-associated virus (rAAV) vectors have clear potential for use in gene targeting but low correction efficiencies remain the primary drawback. One approach to enhancing efficiency is a block of undesired repair pathways like non-homologous end joining (NHEJ) to promote the use of homologous recombination. The natural product vanillin acts as a potent inhibitor of NHEJ by inhibiting DNA-PK. Using a homology containing rAAV vector, we previously demonstrated *in vivo* gene repair frequencies of up to 0.1% in a model of liver disease murine hereditary tyrosinemia type I. To increase targeting frequencies, we administered vanillin in combination with rAAV injection. Gene targeting frequencies increased up to 10-fold over AAV alone, approaching 1%. *Fah*<sup>-/-</sup> *Ku70*<sup>-/-</sup> double knockout mice also had increased gene repair frequencies, genetically confirming the beneficial effects of blocking NHEJ. A second strategy, transient proteasomal inhibition also increased gene targeting frequencies, but was not additive to NHEJ inhibition. This study establishes the benefit of transient NHEJ inhibition with vanillin, or proteasome blockage with bortezomib, for increasing hepatic gene targeting with rAAV. Functional metabolic correction of a clinically relevant disease model was demonstrated and provided evidence for the feasibility of gene targeting as a therapeutic strategy.

## INTRODUCTION

Adeno-associated virus (AAV) is one of the safest viral vectors for use in human gene therapy [108]. The field of AAV gene therapy research continues to be dominated by gene addition approaches using cDNA cassettes driven by heterologous promoter and enhancer sequences. Yet, drawbacks to this methodology abound including unregulated and transient episomal expression [85, 86], random integration [18], increased oncogenic risks [19], and the inability to treat genetically dominant disorders arising from misfolded or abnormally functioning proteins.

AAV-based gene targeting paradigms differ in that patient genomes are manipulated *in vivo* using site-specific recombination to correct underlying mutations. In this way, gene function is restored within the context of endogenous regulatory elements, thus eliminating problems with inadequate or inappropriate expression. AAV gene targeting vectors can correct different genomic loci, show both targeted and stable expression through integration, and cover a greater number of applicable human diseases [26]. Single-stranded AAV genomes utilize homologous recombination machinery to correct mutations through targeted site-specific integration [24].

Our lab has demonstrated the utility of rAAV for performing gene targeting in an ENU-generated point mutation mouse model of HTI [69], a fatal disease

arising from a breakdown in tyrosine catabolism at FAH. In both HTI patients and *Fah*<sup>-/-</sup> mice, hepatotoxic metabolites accumulate causing death in a cell-autonomous manner. Treatment with 2-(2-nitro-4-trifluoromethylbenzoyl)-1,3-cyclohexanedione (NTBC), an inhibitor that blocks upstream of FAH, prevents metabolite accumulation and rescues the phenotype [36]. FAH<sup>+</sup> cells have a strong selective advantage in the HTI mouse liver [63] that can be exploited for selection of repaired hepatocytes *in vivo*. One advantage of the *Fah* model for gene targeting studies is that the readout is functional phenotype restoration, not merely correction of an artificial reporter system with no bearing on physiology. When rAAV-*Fah* vectors are administered to *Fah*<sup>-/-</sup> mice, only corrected hepatocytes will survive and repopulate the liver. Our repair vectors contain a 4.5-kb genomic *Fah* fragment centered on the nucleotide needed for correction in the *Fah*<sup>-/-</sup> mouse. Hepatic correction frequencies of up to 0.1% were previously achieved with this model, a level that was sub-therapeutic without selection [69].

To improve upon earlier results and further increase correction to more therapeutic levels, we sought to transiently inhibit unwanted repair pathways such as NHEJ to promote the sole use of homologous recombination (HR) machinery. NHEJ is the primary pathway of double strand break (DSB) repair in post-embryonic human cells [109]. AAV vectors do not contain an endonuclease to create DNA DSB's and free chromosomal ends, thus naturally occurring breaks must be used when integrating. If NHEJ utilization were prevented, theoretically HR proteins should take over to repair the break with the

homologous rAAV repair template. Vanillin (3-methoxy-4-hydroxybenzaldehyde), a natural phytochemical, acts as a potent inhibitor of NHEJ by binding to and inhibiting DNA-PK [110]. Vanillin is highly selective for DNA-PK and has been shown to have no measurable effect on other steps of NHEJ or on various other unrelated protein kinases like ATM, ATR or PKC [110]. In addition, it was well tolerated at therapeutic dosing levels in a rat model of neuropathic pain [111].

Through work using proteasomal inhibitors, it was shown that the majority of AAV particles do not deliver their genomic payload to the nucleus [112]. Indeed, several labs have shown that proteasomal inhibitors are capable of enhancing AAV transduction both *in vitro* and *in vivo* [112-114], but the mechanism by which this occurs remains unknown. Several hypotheses have been put forward including that they increase AAV trafficking efficiency, block cytoplasmic or nuclear capsid degradation, indirectly improve genome stability, decrease T-cell activation/proliferation, or that they decrease capsid antigen presentation. The only proteasomal inhibitor currently approved for clinical use is bortezomib (Velcade™) and we therefore sought to uncover whether this compound would work alongside vanillin in our AAV gene targeting studies by improving AAV transduction.

## MATERIALS AND METHODS

### ***Mouse Strains and Animal Husbandry***

The ENU-generated  $Fah^{5961SB}/Fah^{5961SB}$  mouse (herein described as  $Fah^{-/-}$ ) models human HTI with a single point mutation in exon 8 of  $Fah$  [74]. Neonates die from acute liver failure if NTBC is not continually administered. NTBC treatment at 4-mg/L in the drinking water prevents hepatorenal injury and rescues the phenotype. NTBC withdrawal allows modeling of HTI as mice rapidly develop hepatorenal disease over the course of several weeks and die of end-stage liver disease in 6-8 weeks [42]. I backcrossed these mice ten generations onto a C57BL/6J background.  $Xrcc6^{tm1Fwa}/Xrcc6^{tm1Fwa}$  (129S6/SvEvTac background) mice (herein described as  $Ku70^{-/-}$  mice) were crossed with  $Fah^{-/-}$  mice [115] to establish  $Fah^{-/-}Ku70^{+/-}$  breeders. All mice described are maintained on irradiated high fat low protein mouse chow (Lab Diet, Brentwood, MO) *ad libitum* to decrease flux through the tyrosine pathway. The Institutional Animal Care & Use Committee of Oregon Health & Science University approved all mouse procedures.

### ***Plasmid Vectors and Recombinant AAV Production***

Plasmid construction and design strategy for rAAV2/8- $Fah$  were described previously [69]. Control vector rAAV2/8-LSP-eGFP encodes enhanced-GFP and is driven by the liver specific promoter (LSP) that contains sequence from the thyroxine hormone-binding globulin gene promoter, two copies of the  $\alpha 1$ -

microglobulin/bikunin enhancer sequence, and a  $\beta$ -globin intron [77]. Standard transfection and viral isolation protocols described previously [99], were used with the following modifications. Unpurified virus was sedimented and resuspended in benzonase buffer for freezing at  $-80^{\circ}\text{C}$ . After three freeze-thaw cycles in a dry ice/ethanol bath, the suspension was benzonase-treated (EMD Chemicals, San Diego, CA). Virus was pelleted and precipitated with 1M  $\text{CaCl}_2$ , followed by 40% PEG-8000 treatment and resuspension in a sodium/HEPES buffer and rotated overnight at  $4^{\circ}\text{C}$ . Afterwards, purification by sequential cesium chloride density centrifugation was performed as described [100] with the following modifications. Peak fractions from both gradients were determined by optical refractometry. Positive final fractions were extensively dialyzed against PBS lacking  $\text{Ca}^{2+}$  or  $\text{MgCl}_2$  and supplemented with 5% (wt/vol) D-sorbitol. Vector titering was performed by dot blot [101].

### ***Neonatal Vector Administration***

For comparative treatment studies, P1 *Fah*<sup>-/-</sup> neonates were injected with  $1 \times 10^{11}$  vg per mouse (in 10- $\mu\text{l}$  volume) of rAAV2/8-*Fah* by IV injection into the superficial temporal vein [96]. All mice were maintained on NTBC throughout. Livers were harvested at weaning, 21-days post-treatment. For random integration studies, P1 *Fah*<sup>-/-</sup> neonates were co-injected with  $4 \times 10^{10}$  vg/mouse of both rAAV2/8-*Fah* [69] and rAAV2/8-LSP-eGFP [77] (in 20- $\mu\text{l}$  volume) by IV injection into the superficial temporal vein. Neonates were treated with NTBC until weaning and then withdrawn from it to select for corrected hepatocytes. Serum and liver tissue

were collected after serial transplantation.

### ***Adult Vector Administration***

Adult *Fah*<sup>-/-</sup> mice (age 13+ weeks) were administered  $2 \times 10^{11}$  vg/mouse of rAAV2/8-*Fah* (in 100- $\mu$ l volume) by IV lateral tail vein injection. NTBC treatment was continued for 1-wk following vector administration during capsid uncoating, and then withdrawn for 3-wks up to 3-mo depending on the study. Liver tissue and serum were collected at the end of each experiment.

### ***Vanillin Administration***

For each experiment, a fresh vanillin (Alfa Aesar, Ward Hill, MA) stock solution of 10-mg/mL solubilized in dH<sub>2</sub>O was prepared, sterile filtered, and kept at 55°C to keep vanillin in solution. This solution was then administered at 100-mg/kg/day by IP injection for 7-days starting on the day of vector administration. Dose was chosen based on work in rats establishing well-tolerated dosing levels [111].

### ***Bortezomib Administration***

For each experiment, a fresh bortezomib (Melone Pharmaceutical, Edison, NJ) stock solution of 5-mg/mL solubilized in DMSO was prepared, sterile filtered and diluted in 0.9% sterile saline for co-administration with AAV at 0.5-mg/kg by IV tail vein injection (100- $\mu$ l total volume). Dose was chosen based on work in hemophilia mice that established well-tolerated levels that achieve inhibition [116].

### ***DMNB (4,5-dimethoxy-2-nitrobenzaldehyde) Administration***

For each experiment, a fresh DMNB (Sigma, Milwaukee, WI) stock solution of 10-mg/mL solubilized in DMSO was prepared, sterile filtered and diluted in 0.9% sterile saline. This solution was then administered at 100-mg/kg on days 2 and 5 after vector administration by IP injection.

### ***Transplantation***

For serial transplantations, livers of corrected donor mice were perfused as described [102] and  $4.5 \times 10^5$  random hepatocytes were transplanted into six recipients, each by intrasplenic injection as described [103].

### ***Liver Immunohistochemistry***

In all experimental mice, a minimum of four liver sections from varying depths and randomly selected liver lobes were analyzed for the number of FAH+ nodules. As nodules represent the clonal expansion of a single corrected hepatocyte, nodule frequency was corrected for nodule size. Briefly, the surface area of each liver section was measured by scanning the glass slide along with a size standard using an Epson Perfection V700 scanner at 400-dpi resolution. Adobe Photoshop 7.0 software was then used to select and count pixels of each liver section. Pixel counts were then converted to numbers of hepatocytes based on the diameter of a mouse hepatocyte (~25 microns). Correction factors were then applied to frequencies of FAH+ nodules in a section containing (x) hepatocytes based on the following assumptions, as described previously [68]: 1)

hepatocyte nodules are spherical; 2) in a given sample all nodules are approximately the same size; 3) the number of hepatocytes in the largest clone represents the middle of that nodule. Immunohistochemical staining protocols for FAH and H&E were completed as described [68]. Two separate, blinded investigators performed quantitation. Microscopy was performed on a DM IL LED microscope (Leica, Buffalo Grove, IL) using Leica LAS Image Analysis Software. Blood for serology was collected by terminal cardiac puncture and biochemical measurements were completed as described [42].

### ***Statistical Analysis***

Statistics were conducted with GraphPad Prism software v.4.0 (GraphPad, San Diego, CA). Experimental differences were evaluated by student two-tailed *t*-test assuming equal variance. *P* values <0.05 were considered statistically significant.

### ***eGFP Copy Number Quantitative PCR***

Total DNA was isolated from randomly dissected liver tissue with a MasterPure DNA Purification kit (Epicentre, Madison, WI). Genomic DNA (75-ng) was subjected to a two-step PCR amplification under the following conditions: 1 cycle 95°C 3-min; 45 cycles 95°C 15-sec and 68°C 40-sec. Primer sequences: *eGFP* F: 5'-ACTTCAAGATCCGCCACAAC-3'; *eGFP* R: 5'-GAACTCCAGCAGGACCA TGT-3'; *Actb* F: 5'-CCACCCCAGCAAGGACACTG-3'; *Actb* R: 5'-GCTCCCTAGG CCCCTCCTGT-3'. Dilutions of *eGFP* plasmid into mouse genomic DNA were used to generate copy number standards. Results were normalized to  $\beta$ -*actin*

expression. PCR was performed on an iQ5 Multicolor Real-Time PCR (Bio-Rad, Hercules, CA), using iQ5 Standard Edition Software, v.2.0.

## RESULTS

### ***Transient inhibition of NHEJ or the proteasome increases gene targeting***

To examine the effects of NHEJ and the proteasome on gene targeting, 13 week old *Fah*<sup>-/-</sup> adult mice were subjected to one of four treatments: AAV alone, AAV and vanillin, AAV and bortezomib, or AAV and both vanillin and bortezomib. rAAV2/8-*Fah* was given at a dose of  $2 \times 10^{11}$  vg/mouse by IV tail vein injection. Based on pharmacokinetic dosage data on vanillin in a model of neuropathic pain [111], we administered vanillin at 100-mg/kg/day by IP injection for 7-days starting on the day of vector administration. Using published dosages of bortezomib from promising studies in hemophilic mice [113], we co-injected bortezomib with rAAV at 0.5-mg/kg by IV tail vein injection. Mice were maintained on NTBC for 1-wk following vector administration and then it was withdrawn for 3-wks. Livers were harvested from mice and scored for FAH+ nodules (**Fig. 3-1**). Nodules represent the clonal expansion of a single corrected hepatocyte, thus nodule frequency was corrected for nodule size [68].

Figure 3-2 shows representative FAH immunohistochemistry from control (**Fig. 3-2a,b**) and treated mice (**Fig. 3-2c-f**). All co-treatment regimens had significantly higher gene targeting frequencies than AAV alone. H&E staining for histological correlates on control mice treated only with vanillin (**Fig. 3-2g**) or only with bortezomib (**Fig. 3-2h**) showed a lack of toxicity.

Given that bortezomib was no better at enhancing gene targeting than vanillin, we decided to focus exclusively on vanillin co-treatment for the duration of the studies. Of note, attempts to replicate the adult co-treatment studies in neonates were not possible, as bortezomib treatment was lethal during this developmental window no matter the dose administered (data not shown).

Attempts to further improve gene targeting with vanillin analogs were unfruitful. 4,5-dimethoxy-2-nitrobenzaldehyde (DMNB), a known vanillin analog and even more potent disruptor of DNA-PK [110], was unsuccessful at improving gene targeting at doses tested in a 2-day time course (**Fig. 3-5**), and was not well tolerated in mice. Both 5 and 7-day courses of DMNB proved lethal.

### ***Gene targeting frequencies are sexually dimorphic***

To examine effects of gender and age on gene targeting, P1 *Fah*<sup>-/-</sup> neonates and 13-wk *Fah*<sup>-/-</sup> adult mice of different sexes were treated with either rAAV or rAAV and vanillin. rAAV2/8-*Fah* was given at  $2 \times 10^{11}$  vg/mouse by IV tail vein injection to adults, and  $1 \times 10^{11}$  vg/mouse by IV facial vein to neonates. Vanillin was administered at 100-mg/kg/day by IP injection for 7-days starting on the day of vector administration. Neonates were maintained on NTBC until harvest. Adults were maintained on NTBC for 1-wk following vector administration and then it was withdrawn for 3-wks to allow for easier nodule quantification given the lower gene targeting in adults. Livers were harvested from mice and scored for FAH+ nodules (**Fig. 3-3**). In both ages of mice, males consistently showed significantly

higher gene targeting than female littermates when treated with AAV alone. It is not known whether this difference is due to a difference in transduction frequency between genders. In neonates, a significant difference was seen in both genders with vanillin co-treatment, compared to AAV alone. Even with co-treatment, male neonates had significantly more gene targeting than female littermates. This trend continued in adult mice, wherein males always showed significantly greater gene targeting than females, no matter the treatment cohort. Interestingly, although statistically adult females showed no significant difference between AAV treatment and AAV and vanillin combination therapy, there was still a trend towards increased gene targeting frequencies with vanillin.

### ***Toxicity profile of vanillin***

To investigate whether the significant increases in gene targeting with vanillin treatment were the result of NHEJ inhibition or simply a toxic response to vanillin causing hepatocellular turnover, we performed *in vivo* toxicity studies on mice treated only with vanillin. *Fah*<sup>-/-</sup> adult mice were treated with vanillin alone at 100-mg/kg/day by IP injection for 7-days. Mice were maintained on NTBC during the experiment to mimic the experimental conditions used during vector combination therapy studies. Livers were immediately harvested after the final day of vanillin treatment and examined for signs of injury by immunohistochemistry and serology. Results by H&E showed only a slight loss of hepatic glycogen retention but no signs of injury (**Fig. 3-2g**). Serology to examine potential hepatic toxicity showed normal bilirubin and transaminase levels (**Table 3-1**), further

demonstrating the safety and non-toxic attributes of vanillin.

### ***Genetic mutations in Ku70 mimic chemical affects of vanillin***

After examining the tolerability of vanillin, we sought non-pharmacologic validation to confirm the effects of NHEJ inhibition. *Ku70*<sup>-/-</sup> mice, which genetically lack the ability to perform NHEJ through loss of functional *Ku70*, were bred with *Fah*<sup>-/-</sup> mice to create double mutants. P1 *Fah*<sup>-/-</sup>*Ku70*<sup>-/-</sup> neonates were treated with 1x10<sup>11</sup> vg/mouse of rAAV2/8-*Fah* by IV facial vein and compared to identically treated *Fah*<sup>-/-</sup>*Ku70*<sup>+/+</sup> and *Fah*<sup>-/-</sup>*Ku70*<sup>+/-</sup> littermates. If NHEJ loss was truly responsible for the increase in gene targeting seen with vanillin co-treatment, then AAV treatment alone in mice genetically incapable of NHEJ should show similar gene correction frequencies by immunohistochemistry (**Fig. 3-2j-l**). As hypothesized, *Fah*<sup>-/-</sup>*Ku70*<sup>+/+</sup> and *Fah*<sup>-/-</sup>*Ku70*<sup>+/-</sup> neonates treated with AAV (**Fig. 3-2j,k**) had normal levels (~0.1%) of gene correction (**Fig. 3-4**). Only the *Fah*<sup>-/-</sup>*Ku70*<sup>-/-</sup> littermates had significantly higher gene correction frequencies at the levels seen in *Fah*<sup>-/-</sup> mice treated with AAV and vanillin (~1%) (**Fig. 3-2l**).

### ***Random integration frequencies are unaffected by NHEJ inhibition***

Although phenotypic reversion suggested successful site-specific gene targeting, random integration of AAV genomes could also occur. Current data in the field are conflicting as to whether inhibition of NHEJ would worsen [117] or improve [118] random integration frequencies. As the majority of post-embryonic DNA damage is repaired by NHEJ, it is plausible that a transient block to NHEJ would

decrease the frequency of random integration. To assess whether random integration frequencies change with vanillin treatment, P1 *Fah*<sup>-/-</sup> neonates were co-injected with 4x10<sup>10</sup> vg/mouse of both rAAV2/8-*Fah* and rAAV2/8-LSP-*eGFP* (non-selectable serotype-matched control vector). Concomitantly, neonates were treated by IP injection with vanillin at 100-mg/kg for 7-days following viral administration. Post-weaning, mice were subjected to NTBC withdrawal to select for corrected hepatocytes. To ensure no episomes remained and to select for integrants, 5x10<sup>5</sup> random hepatocytes were then serially transplanted into six secondary *Fah*<sup>-/-</sup> recipients as described [65]. After >12 weeks off NTBC, serum and liver tissue of the secondary transplant recipients were collected.

Liver function tests for bilirubin and transaminases demonstrated complete correction in all treatment cohorts when compared to untreated controls off NTBC (**Table 3-1**). Liver FAH immunohistochemistry illustrated the extensive repopulation in serial transplant recipients (**Fig. 3-2i**). Q-PCR was used to determine *eGFP* copy numbers in each of these highly repopulated mice (**Table 3-2**). The average copy number of irrelevant vector corrected for repopulation efficiency indicated that ~0.8% of gene targeted hepatocytes also had a random rAAV2/8-LSP-*eGFP* integration event. This number was well within the range of reported random rAAV integration estimates from the literature between 0.1-1% [119, 120], and nearly identical to historical random integration frequencies with this vector alone (0.88%) [69]. As a result, it can be concluded that vanillin treatment did not increase or decrease AAV random integration frequencies.

## FIGURES

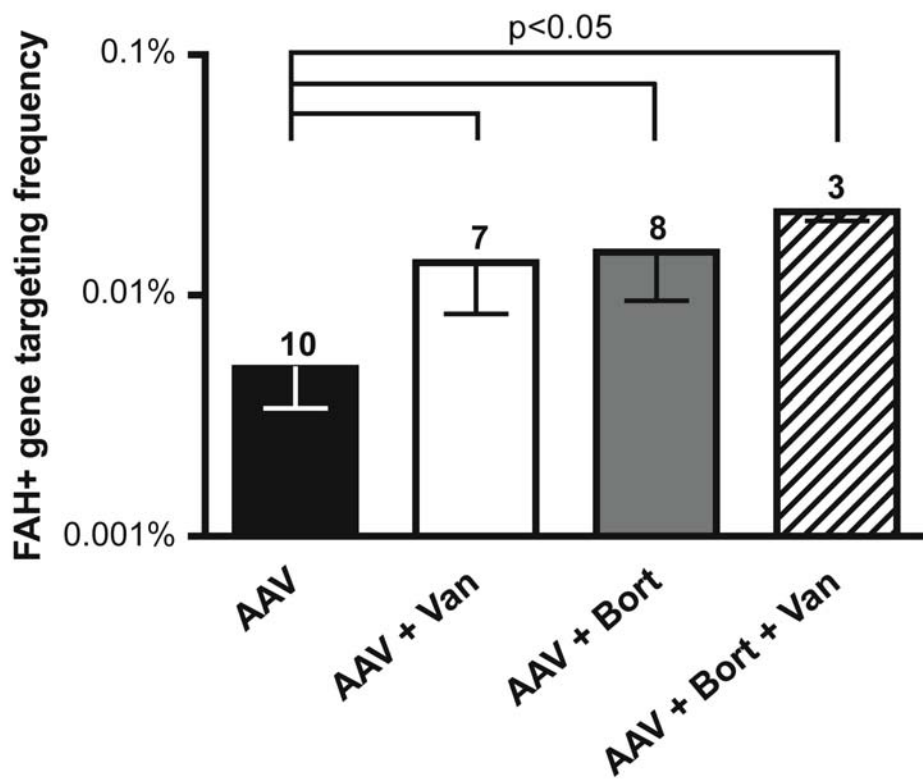


**Figure 3-1: Transient NHEJ or proteasome inhibition enhances gene repair**

Frequencies of corrected nodules were quantified by counting the number of FAH+ clones per x hepatocytes (1/x) from adult mice harvested 4-wks post-treatment. Mean and SD are shown, with the number of independent animals analyzed above each bar. Black = AAV, white = AAV + vanillin, gray = AAV + bortezomib, diagonal lines = AAV + bortezomib + vanillin.

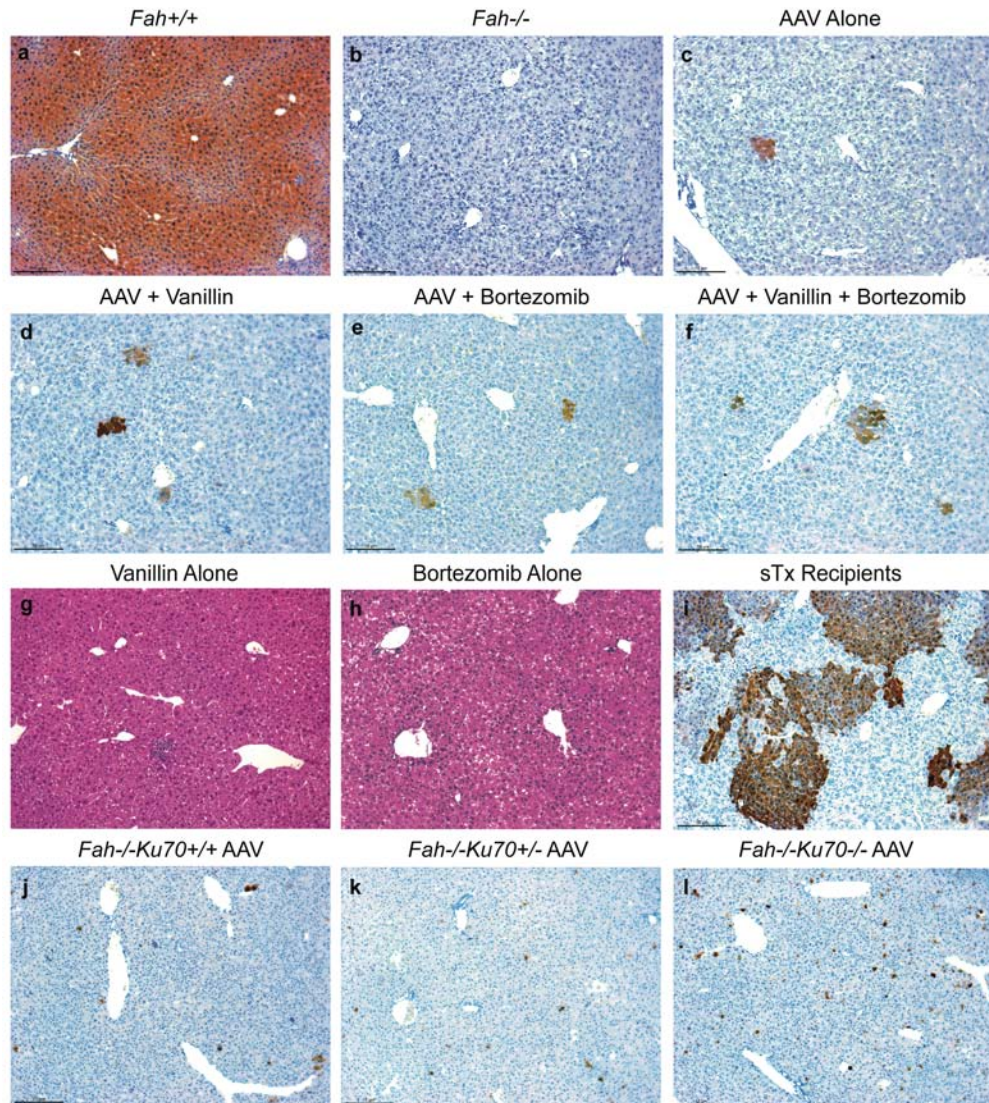


**Figure 3-2: Liver immunohistochemistry**

(a) **FAH+** stain on adult *Fah*<sup>+/+</sup>; (b) **FAH-** stain on adult *Fah*<sup>-/-</sup>; (c) FAH stain on adult *Fah*<sup>-/-</sup> treated with AAV, or (d) AAV + vanillin, or (e) AAV + bortezomib, or (f) AAV + vanillin + bortezomib; (g) H&E stain on adult *Fah*<sup>-/-</sup> treated with vanillin; (h) H&E stain on adult *Fah*<sup>-/-</sup> treated with bortezomib; (i) FAH stain on adult *Fah*<sup>-/-</sup> serial transplant recipient; (j) FAH stain on neonatal *Fah*<sup>-/-</sup>*Ku70*<sup>+/+</sup>, or (k) *Fah*<sup>-/-</sup>*Ku70*<sup>+/-</sup>, or (l) *Fah*<sup>-/-</sup>*Ku70*<sup>-/-</sup> treated with AAV. Scale bar = 10 microns.

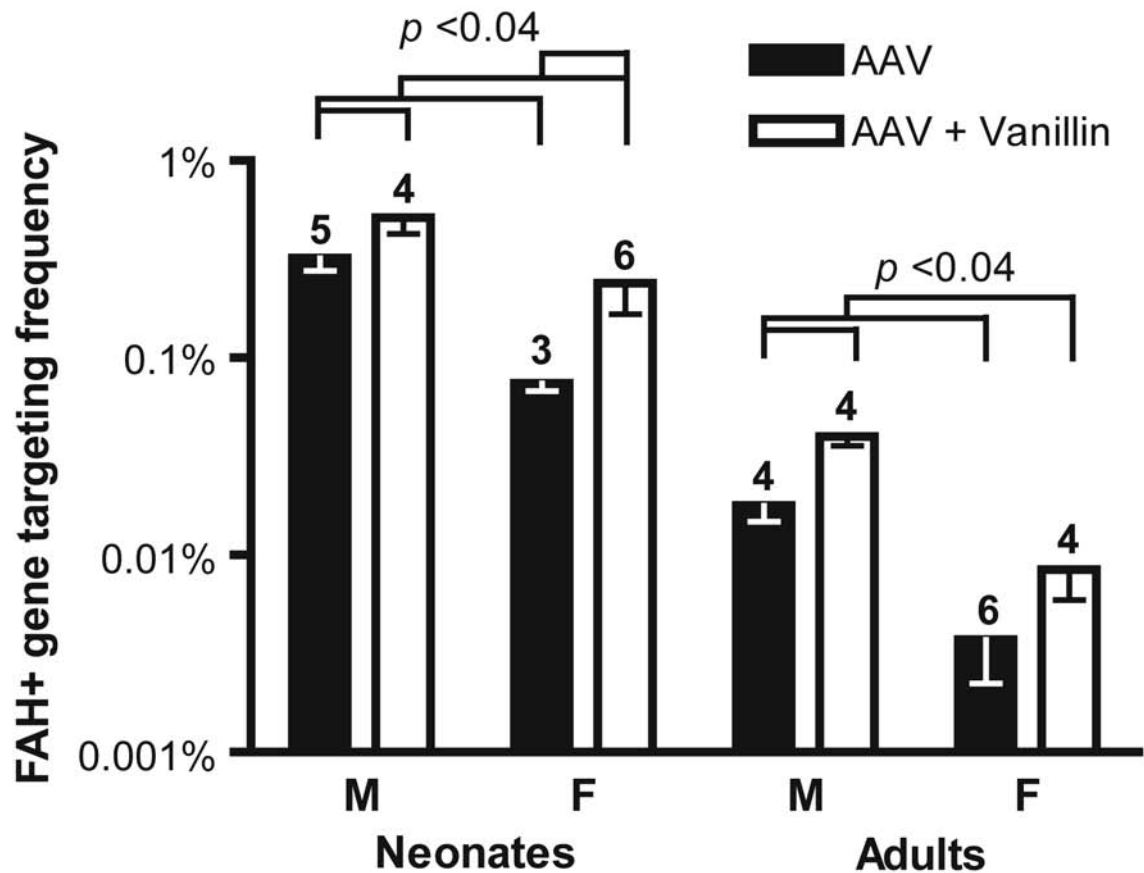


**Figure 3-3: Sexually dimorphic responses to AAV and vanillin**

Frequencies of corrected nodules were quantified by counting the number of FAH+ clones per  $x$  hepatocytes ( $1/x$ ) from neonates harvested at 3-wks and adults harvested 4-wks post-treatment. Mean and SD are shown, with the number of independent animals analyzed above each bar. Black = AAV, white = AAV + vanillin.

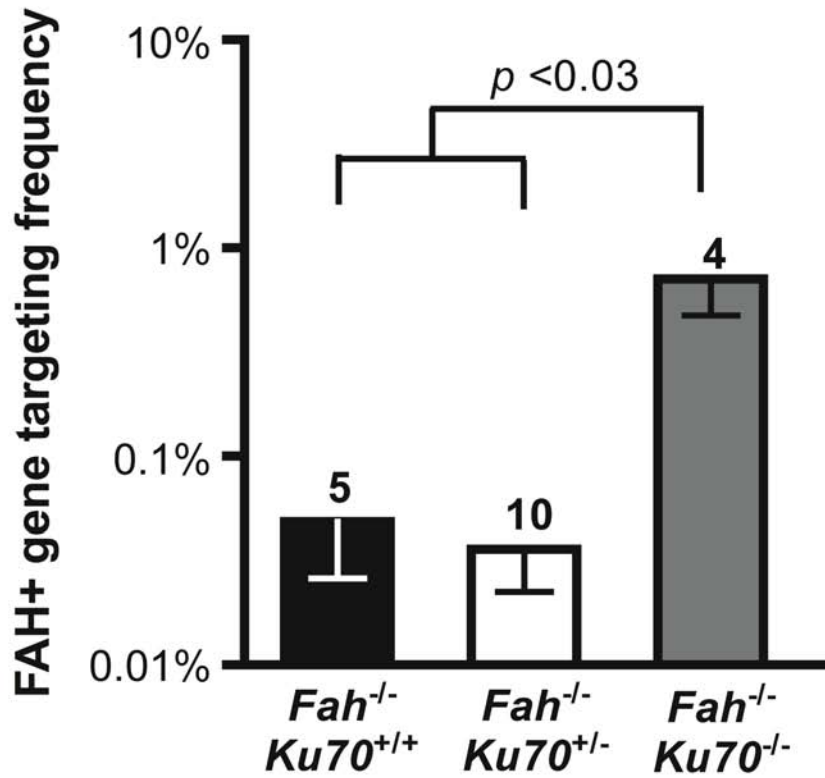


**Figure 3-4: NHEJ inhibition is responsible for increases in gene targeting**  
 Frequencies of corrected nodules were quantified by counting the number of FAH+ clones per x hepatocytes (1/x) from neonates harvested at 3-wks post-treatment. Mean and SD are shown, with the number of independent animals analyzed above each bar. Black = *Fah*<sup>-/-</sup> *Ku70*<sup>+/+</sup>, white = *Fah*<sup>-/-</sup> *Ku70*<sup>+/-</sup>, gray = *Fah*<sup>-/-</sup> *Ku70*<sup>-/-</sup>.

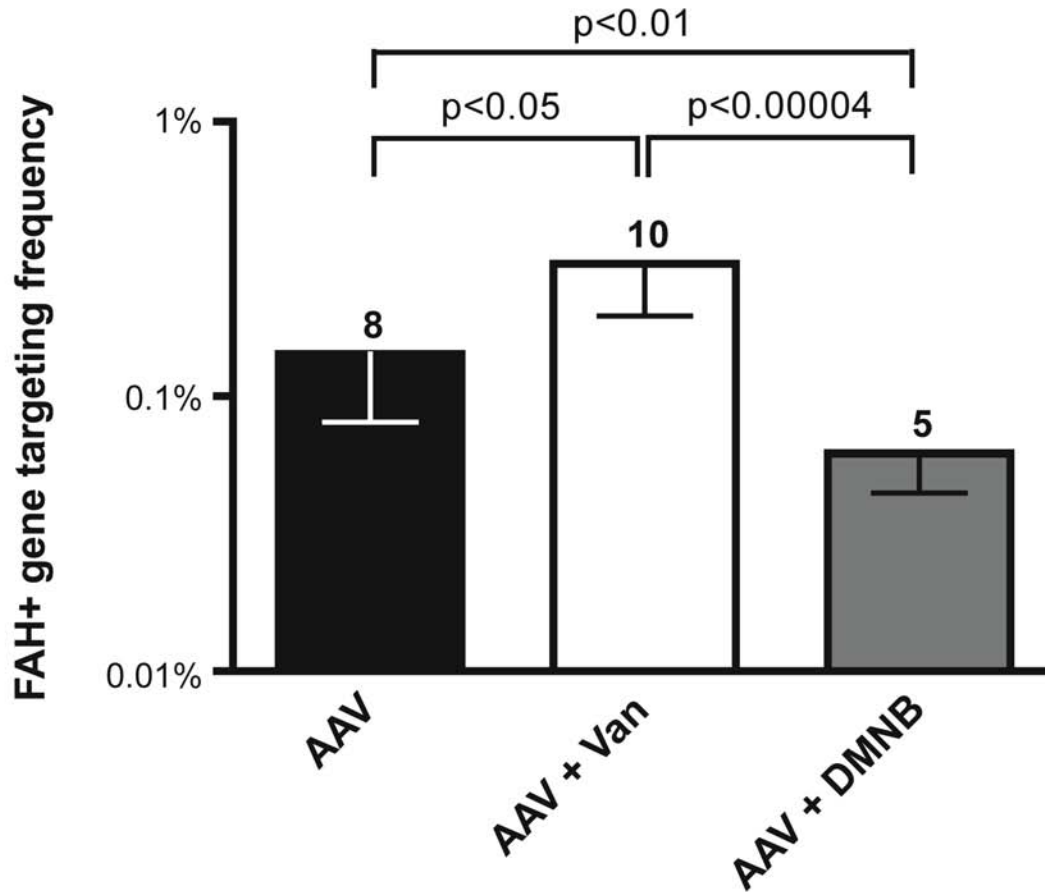


**Figure 3-5: Gene targeting with vanillin analogs**

Frequencies of corrected nodules were quantified by counting the number of FAH+ clones per x hepatocytes (1/x) from neonates harvested at 3-wks post-treatment. Mean and SD are shown, with the number of independent animals analyzed above each bar. Black = AAV, white = AAV + vanillin, gray = AAV + DMNB.

## TABLES

	<i>Fah</i> <sup>-/-</sup> off NTBC	<i>Fah</i> <sup>-/-</sup> on NTBC	Wild- type	<i>Fah</i> <sup>-/-</sup> Van	<i>Fah</i> <sup>-/-</sup> AAV	<i>Fah</i> <sup>-/-</sup> AAV + Van	sTx <i>Fah</i> <sup>-/-</sup> AAV + Van
<b>Bili</b>	3.4 ± 1.3	0.2 ± 0	0.0 ± 0.1	0.1 ± 0	0.1 ± 0	0.1 ± 0	0.2 ± 0.1
<b>AST</b>	353 ± 86	121 ± 47	91 ± 27	98 ± 26	86 ± 8	91 ± 32	116 ± 13
<b>ALT</b>	291 ± 51	59 ± 56	36 ± 5	38 ± 4	45 ± 1	53 ± 12	92 ± 10
<b>n</b>	6	5	5	3	3	7	6

**Table 3-1: Serological measures of functional correction**

From left to right, values represent mean ± SD from untreated *Fah*<sup>-/-</sup> mice off NTBC, untreated *Fah*<sup>-/-</sup> mice on NTBC, untreated wild-type mice, *Fah*<sup>-/-</sup> mice treated with vanillin alone for 7-days on NTBC, *Fah*<sup>-/-</sup> mice treated with AAV alone and selected for 3 months off NTBC, *Fah*<sup>-/-</sup> mice treated with AAV and vanillin and selected for 3 months off NTBC, and serially transplanted (sTx) *Fah*<sup>-/-</sup> mice selected for 3 months off NTBC, respectively. All values in white columns are significantly different from corresponding values in the gray column (p<0.05).

Donor	sTx Recipient	# copies/dGE	Average
1	1a	0.01	0.01
	1b	0.01	
	1c	0.01	
2	2a	0.00	0.006
	2b	0.01	
	2c	0.01	
<b>Total</b>			0.008
<b>Random integration</b>			0.008 = 0.8%

**Table 3-2: eGFP copy numbers in recipient mice**

After neonatal co-injection of  $1 \times 10^{10}$  vg of rAAV2/8-*Fah* and rAAV2/8-LSP-*eGFP* and 7-days of vanillin treatment, FAH+ hepatocytes were selected for and then serially transplanted to remove episomes. Data represent the number of copies of *eGFP* per diploid genome equivalent (dGE) in serial transplant (sTx) recipients. Roughly 50% of the hepatocytes in repopulated recipients were donor-derived at the time of harvest, so the frequency was corrected by a factor of 2 to give an estimated random integration frequency of 0.8%.

## DISCUSSION

In spite of advances made in gene therapy research, the disadvantages of traditional AAV gene addition methodologies remain: episomal expression will always be inherently unregulated, expression will be transient in cells that turn over, the risk of eventual transgene silencing will always be present, integration events will be random as they are not based on homology, random integration will produce increased mutagenic and oncogenic risks, and disorders caused by aberrantly functioning or misfolded proteins are untreatable by this approach. Our interest in AAV-mediated gene targeting stems from its ability to elegantly bypass these disadvantages through simple site-directed gene repair.

The precise nature of the interactions between NHEJ machinery and AAV are not clear and thus it was unknown whether inhibition of NHEJ would exacerbate [117] or improve [118] both random and targeted integration frequencies. We pursued both pharmacological and genetic approaches in various ages and genders of mice with a clinically relevant disease model to address the differences in the current literature. Our results show that transient NHEJ inhibition with vanillin both increased targeted AAV integration and had no effect on random AAV integration.

Our results with vanillin combination therapy are all the more promising when other attributes of vanillin are taken into consideration: vanillin is a known

anticarcinogen [121], antioxidant [122], anticlastogen [123], antimutagen [124], antimicrobial [125], analgesic [111], and has antineoplastic activity [126]. Moreover, vanillin is already an FDA-approved food additive, thus an off-label use for vanillin in gene therapy seems feasible.

In addition to transient NHEJ inhibition, transient proteasomal inhibition is a promising avenue in gene therapy research given the results seen in mouse and dog models of hemophilia treated with AAV and bortezomib [113]. Our data with bortezomib highlights its potential as a second parallel approach to vanillin treatment, wherein bortezomib combination therapy improved gene targeting frequencies in a safe and efficacious manner. Having already gained FDA approval for human multiple myeloma and mantle cell lymphoma studies, bortezomib combination therapies with AAV have potential for rapid approval and the added benefit of pre-existing toxicity studies in humans [127].

As in other fields, gene therapists are beginning to appreciate gender differences in response to AAV therapies [128-131]. For example, in hepatocytes there are more than 1,000 genes that are differentially expressed in males and females [132, 133]. However, no data exists to date for AAV gene targeting vectors in animal models of any disease where gender was controlled. Here we present the first data demonstrating that at neonatal and adult life stages, male mice displayed significantly more AAV-mediated gene targeting than their female counterparts. The detailed mechanisms responsible for gender differences in

AAV liver transduction are still unclear, but have at least been shown to involve androgen-dependant pathways [128]. The implications of our findings could affect the design and dosing strategies of future clinical trials.

Obstacles to AAV-mediated gene targeting remain. Notably, therapeutic levels of gene correction have proven elusive in disease models. However, our current work highlights the capacity of AAV-mediated gene targeting in a suitable selection-based disease. While disorders characterized by selection for gene-corrected cells are rare, there are other examples of this phenomenon: Fanconi's anemia [79], the copper storage disorder Wilson's disease [80], many bile-acid transporter defects [82], and junctional epidermolysis bullosa [84]. If correction frequencies achieved with vanillin were increased just 5-fold, they would become clinically relevant even for diseases that do not display a selective advantage. For example, it has been predicted that gene targeting frequencies of 5% would have therapeutic benefit for patients with hemophilia A [76], and 10% for phenylketonuria patients [134]. Patients with diseases arising from point mutations are the most appropriate recipients for gene targeting therapies. Historically, point mutations have been the most frequent genetic abnormality and source of acquired genetic disease [27]. This study establishes the utility of transient NHEJ inhibition with vanillin, or proteasome inhibition with bortezomib, for increasing hepatic gene targeting with AAV in neonatal and adult mice of both genders.

## CHAPTER 4

### **Small Molecule Inhibitor of FAH Enzyme Allows for Selection of Genetically Resistant Donor Hepatocytes in Wild-type Settings *In Vivo***

## ABSTRACT

FAH deficiency causes the genetic liver disease hereditary tyrosinemia type I (HTI). In this disease, healthy gene-corrected hepatocytes have a strong growth advantage and can completely repopulate the diseased liver. Unfortunately, most genetic liver diseases lack this advantage of positive selection in corrected cells. Therefore, the ability to transiently apply positive selection for correction of liver disorders would represent a major advance. To mimic the selective pressure of HTI in animals proficient in FAH activity, a small molecule inhibitor of FAH, 4-[(2-carboxyethyl)-hydroxyphosphinyl]-3-oxobutyrates (CEHPOBA) was developed. One-time and chronic *in vivo* administration effects were characterized. As proof of principle, we attempted to positively select genetically resistant hepatocytes transplanted into sex-mismatched wild-type recipients. Time course analyses with 3-5 weeks of CEHPOBA following transplantation showed a linear relationship between treatment length and degree of repopulation. Compared to controls, CEHPOBA-treated recipients had 10-100 fold increases in repopulation. Given daily, the FAH-inhibitor CEHPOBA was effective *in vivo* and mimicked genetic *Fah* deficiency. Conceivably, the combination of either shRNA knockdown or over-expression of the desired enzyme, as well as hepatocyte transplantation and drug treatment will constitute a new path for therapeutic liver repopulation.

## INTRODUCTION

Many inborn errors of metabolism are caused by deficiencies in hepatic enzymes, thereby making whole liver transplant an effective therapy for these conditions [135]. However, few patients benefit from or even undergo this procedure due to the limited availability of donor organs, the high cost and significant morbidity and mortality associated with the procedure, as well as the long-term requirement for immune suppression [60]. Most pediatric metabolic diseases are caused by a specific loss-of-function in only hepatocytes with otherwise normal liver anatomical structure. This is in contrast to many adult liver disorders treated with whole liver transplant (cirrhosis, fibrosis, portal hypertension, etc.) where severe anatomical abnormalities have accumulated that obstruct proper liver function. Thus, many pediatric patients with metabolic disease have little need for whole organ transplant and would greatly benefit from either restoration of enzymatic function through gene therapeutic approaches or hepatocyte replacement via cell transplantation.

Clinical hepatocyte transplantation has many advantages over that of the whole organ for patients [136, 137]: 1) the procedure is less invasive; 2) cells from a single donor liver could be used for multiple recipients; 3) human hepatocytes can be farmed in mice providing a constant reliable source of transplantable hepatocytes; 4) hepatocytes can be cryo-preserved with little loss in viability; and 5) cell suspensions may be less likely to induce an immune

response than whole organs. In addition, cell transplantation can be achieved using the patient's own cells, whereby the cells are removed from the body, genetically manipulated, and then transplanted back into the patient's liver.

Hepatocyte transplantation is easily studied in animal models, the most well established of which are mouse models of the metabolic disease hereditary tyrosinemia type I (HTI). HTI is a tyrosine catabolism disorder caused by deficiency of fumarylacetoacetate hydrolase (*Fah*), the terminal enzyme in the pathway, which causes progressive liver disease and renal tubular dysfunction. In both HTI patients and *Fah* null mice, hepatotoxins like fumarylacetoacetate (FAA) and subsequent metabolites accumulate causing death in a cell-autonomous manner. Treatment with 2-(2-nitro-4-trifluoromethylbenzoyl)-1,3-cyclohexanedione (NTBC), an inhibitor that blocks upstream of FAH, prevents metabolite accumulation and rescues the phenotype [36]. FAH<sup>+</sup> cells have a strong selective advantage in an HTI liver that can be exploited in both patients and animal models *in vivo* [63]. Indeed, many patients with HTI have a somatic mosaic liver consisting of both FAH<sup>+</sup> and FAH<sup>-</sup> hepatic tissue. The FAH<sup>+</sup> nodules are generated by somatic reversion of the disease-causing, inherited mutation followed by clonal selection of reverted hepatocytes [64]. This observation demonstrated the strong selective growth advantage of FAH<sup>+</sup> hepatocytes in this disease and led to studies on therapeutic liver repopulation in the mouse. Several mouse models of HTI exist and have been used for an array

of cell therapies [65-68], viral gene therapies [63, 69-71], and non-viral gene therapies [72, 73].

To study therapeutic liver repopulation outside the context of *Fah* null mice for use in metabolic selection studies during cell transplant, we generated a small molecule inhibitor of FAH, 4-[(2-carboxyethyl)-hydroxyphosphinyl]-3-oxobutyrate (CEHPOBA) [138]. The basic biochemistry of CEHPOBA including detailed chemical kinetics *in vitro* and pharmacokinetics *in vivo* were determined. CEHPOBA is a transition state analogue that works at nanomolar concentrations with favorable therapeutic kinetics (i.e. a long half-life that permits once daily administration). The  $K_m$  of FAH for FAA is 3.5  $\mu\text{M}$  and the  $K_i$  of CEHPOBA is 41 nM. In addition, the crystal structure of FAH with CEHPOBA bound to the enzyme active site was determined [139].

Here we show proof of principle, that selective repopulation in a non-selective wild-type liver through transplant of genetically resistant hepatocytes and daily administration of the pharmacological FAH inhibitor CEHPOBA provides transient selection to donor hepatocytes *in vivo*. *Hgd*<sup>-/-</sup> hepatocytes were used for transplantation as they are genetically protected from FAH deficiency due to their inability to convert tyrosine to FAA. Given the genetic resistance to CEHPOBA in donor hepatocytes, CEHPOBA treatment is predicted to make the recipient liver essentially null for FAH, providing a selective advantage to donor hepatocytes for engraftment and subsequent proliferation. Conceivably, the

combination of either transient shRNA knockdown of upstream enzymatic targets in donor cells, or over-expression of the desired enzyme, as well as hepatocyte transplantation and drug treatment with CEHPOBA could constitute a new path for future therapeutic liver repopulation.

## MATERIALS AND METHODS

### ***Mouse Strains and Animal Husbandry***

Mouse strains used were C57BL/6J (herein referred to as WT mice) available from Jackson Labs,  $Fah^{\Delta\text{exon5}}/Fah^{\Delta\text{exon5}}$  (herein referred to as  $Fah^{\Delta\text{exon5}}$  mice [37]) backcrossed ten generations onto a C57BL/6J background, and  $Hgd^{\text{aku}}/Hgd^{\text{aku}}$  (herein referred to as  $Hgd^{-/-}$  mice [140]) on a mixed 129/Sv.C57BL/6J.NB background. All mice described were maintained on irradiated high fat low protein mouse chow (Lab Diet, Brentwood, MO, Cat# Picolab 5LJ5) *ad libitum* to decrease flux through the tyrosine pathway.  $Fah^{-/-}$  mice are maintained on 4-mg/L NTBC water as described [65]. The Institutional Animal Care & Use Committee of Oregon Health & Science University approved all mouse procedures.

### ***CEHPOBA Administration***

All mice were given CEHPOBA at 1  $\mu\text{mole/g}$  of a 0.22M stock solution by IP injection. CEHPOBA stocks were solubilized in sterile water, pH 7.8, and stored at  $-80^{\circ}\text{C}$  until use. Detailed chemical synthesis and pharmacokinetic data were described previously [138].

### ***Hepatocyte Transplantation***

Two days prior to transplant, recipients were pre-treated with  $1 \times 10^9$  PFU of an adenovirus expressing urokinase to enhance initial cell engraftment as described

[67]. Donor hepatocytes were acquired from male *Hgd*<sup>-/-</sup> mice by collagenase liver perfusion as described [102], and  $4.5 \times 10^5$  hepatocytes were transplanted into female WT recipients by intrasplenic injection as described [103]. Pre- and post-surgical pharmacologics were administered as follows: ceftiofur (broad-spectrum cephalosporin antibiotic) was given at 4-mg/kg by IP injection immediately prior to surgery and for two days following surgery; anakinra (IL-1 receptor antagonist) was given at 75-mg/kg by intrasplenic injection with the cells at transplant and by IP injection two days post-surgery. CEHPOBA injections, if administered, began 3 days following transplant to allow mice to recover from surgery prior to selection. If mice receiving CEHPOBA lost >20% of their pre-transplant weight, treatment was suspended for 3-7-days to allow mice to recover before further selection began. Procedures for 2/3 partial hepatectomy were performed as described [98].

### ***FAH Enzyme Assay***

Livers of treated mice were harvested and snap frozen in liquid nitrogen until the assay was performed. Cytosolic liver homogenate was incubated with 250- $\mu$ M FAA substrate and the disappearance rate was measured spectrophotometrically at 330-nm as described [67]. Livers from untreated wild-type and *Fah* <sup>$\Delta$ exon5</sup> mice were used for positive and negative controls for the assay.

### ***Liver Immunohistochemistry***

In all experimental mice, a minimum of 2 liver sections from varying depths and randomly selected liver lobes were analyzed for Y-chromosome positivity and structural integrity by H&E. Mouse Y chromosome FISH was performed on 4- $\mu$ m paraffin sections using a Cy-3 labeled mouse Y-IDetect paint (ID Labs, Ontario, Canada) and counterstained with DAPI (Abbott Molecular, Des Plaines, IL). Deparaffinization of paraffin slides was performed using the Vysis Paraffin Pretreatment Reagent Kit II (Abbott Molecular) using the VP2000 Automated Processor (Abbott Molecular) according to manufacturer's instructions. After these treatments, hybridization, washing, and counterstaining were performed according to the FISH probe manufacturer's instructions. Fluorescence was visualized on a CytoVysion image capture system (Applied Imaging, San Jose, CA) with a Nikon E800 (Nikon, Melville, NY) microscope. 200 interphase nuclei per sample were scored for presence or absence of mouse chromosome Y. Immunohistochemical staining protocols for H&E were completed as described [141]. Microscopy was performed on a DM IL LED microscope (Leica, Buffalo Grove, IL) using Leica LAS Image Analysis Software.

### ***Biochemical Parameters***

Sterile urine was collected by cystocentesis at time of harvest. Quantitative urine amino acids were analyzed on a Waters ACQUITY UPLC using the Waters MassTrak™ Amino Acid Analysis System as described [142]. Quantitative measurements of the urine organic acids succinylacetone and homogentisic acid

were measured by trimethylsilyl derivatization followed by gas chromatography-mass spectrometry as described [143]. The lowest limit of detection for HGA was 40µg/mg creatinine. All urine parameters were normalized to creatinine excretion using the DetectX Urinary Creatinine Detection Kit Catalog #K002-H1 (Arbor Assays, Ann Arbor, MI). Blood for serology was collected by terminal cardiac puncture at time of harvest. Serum measurements of total bilirubin and transaminases were performed as described [42].

### ***Statistical Analysis***

Statistical analyses were conducted with GraphPad Prism software v.4.0 (GraphPad, San Diego, CA). Experimental differences were evaluated by student two-tailed *t*-test assuming equal variance. *P* values <0.05 were considered statistically significant.

### ***Y Chromosome q-PCR***

Total DNA was isolated from randomly dissected liver tissue with a MasterPure DNA Purification kit (Epicentre, Madison, WI). Genomic DNA (100-ng) was subjected to a two-step PCR amplification under the following conditions: 1 cycle 95°C 3-min; 45 cycles 95°C 15-sec and 68°C 40-sec. Primer sequences: Y-chr F: 5'-TCCTTGGGCTCTTCATTATTCTTAAC-3'; Y-chr R: 5'-GAGAACCACGTTGGTTTGAGATG-3'; *Actb* F: 5'-AGAGGGAAATCGTGCG TGAC-3'; *Actb* R: 5'-CAATAGTGATGACCTGGCCGT-3'. Dilutions of male gDNA into female gDNA were used to generate the standard curve. Results were normalized to *β-actin*

expression. PCR was performed on an iQ5 Multicolor Real-Time PCR (Bio-Rad, Hercules, CA), using iQ5 Standard Edition Software, v.2.0.

### ***Microarray Analysis***

The three treatment cohorts were analyzed: *Fah*<sup>Δexon5</sup> mice on NTBC for 2-wks, *Fah*<sup>Δexon5</sup> mice off NTBC for 2-wks, and wild-type mice treated with CEHPOBA daily for 2-wks. Labeled target cRNA was prepared from total RNA from two mice in each cohort using the AMC One Cycle cDNA IVT Amplification/Labeling Kit (Affymetrix, Santa Clara, CA). Labeled samples were hybridized overnight to a Mouse Genome 430 2.0 GeneChip Array (Affymetrix, Santa Clara, CA). Arrays were washed, scanned and median intensities of each element on the array were captured with Affymetrix GCOS software v.1.2. Quality control diagnostic plots were prepared for each array, and those failing to exhibit high-quality hybridizations were excluded [144]. Microarray assays were performed in the Affymetrix Microarray Core of the OHSU Gene Microarray Shared Resource. For statistical analysis, CEL files were processed with the RMA method [145] in the Affymetrix Bioconductor package [146]. Statistics were applied using False Discovery Rate (FDR) [147] adjusted p-values from an empirical Bayes [148] moderated t-test. The adjusted p-value (q-Val) threshold used was 0.01 and the fold change threshold used was 2.0 [149].

## RESULTS

### ***WT hepatocytes treated with CEHPOBA lose FAH enzyme activity in vitro***

Livers from wild-type mice were homogenized and analyzed for levels of FAH enzyme activity *in vitro* with or without CEHPOBA added to the homogenate at 600- $\mu$ M (**Fig. 4-1a**). The enzymatic assay tests for the reduction of 250- $\mu$ M of FAA by FAH at a wavelength of 330-nm over time. Untreated wild-type liver has full FAH enzyme activity, thus the FAA level decreased steadily with time. When CEHPOBA was added to the liver homogenate, FAH activity was reduced and prevented the metabolism of FAA causing the levels to remain steady.

### ***Single CEHPOBA injection leads to prolonged suppression of FAH enzyme activity in vivo***

Wild-type mice were administered a single dose of CEHPOBA by intraperitoneal (IP) injection and the livers harvested at various time points following treatment. CEHPOBA-treated livers were homogenized and assayed for FAH enzyme activity for up to 72-hr post-treatment (**Fig. 4-1b**). FAH enzyme activity dropped precipitously immediately after administration of CEHPOBA, but the maximum inhibitory effect was seen after 4-hr. Reduced FAH activity levels were maintained for at least 72-hr.

### ***Expression profiles in mice given CEHPOBA mimic $Fah^{-/-}$ mice off NTBC***

In order to confirm that CEHPOBA administration resulted in FAH inhibition and

affected hepatocytes in a similar fashion as genetic *Fah* deficiency, we performed microarray analysis on the livers of CEHPOBA-treated wild-type mice and compared the patterns to genetic *Fah*<sup>Δexon5</sup> mice. Three treatment cohorts of two mice each were assayed for differences in hepatic gene expression after 2-wks of treatment: *Fah*<sup>Δexon5</sup> mice off NTBC for 2-wks to induce tyrosinemia, *Fah*<sup>Δexon5</sup> mice kept on NTBC and thus protected from HTI-related damage, and wild-type mice given daily CEHPOBA injections for 2-wks. Livers were harvested from all six mice and the labeled cRNA was analyzed by microarray. We found that just 2-wks of CEHPOBA administration resulted in a gene expression pattern very similar to genetic *Fah* deficiency. Both CEHPOBA treatment and *Fah* deficiency resulted in massive changes to hepatic gene expression and there was considerable overlap (>80%) in the genes that were up- and down-regulated. Cluster analysis clearly indicated that wild-type mice treated with CEHPOBA were most similar in hepatic gene expression to tyrosinemic *Fah*<sup>Δexon5</sup> mice off NTBC (**Fig. 4-2a**). The heat map illustrates the level of similarity and difference between the three treatment cohorts (**Fig. 4-2b**).

HTI patients and *Fah* null mice have a characteristic gene expression profile off NTBC [42]. Notably, *Fah* expression is completely absent, cAMP-inducible genes (*Tat*, *Pck1*) are down-regulated along with urea cycle enzymes (*Ass1*, *Otc*), whereas up-regulation is seen in genes for DNA damage (*Ddit3*), oxidative damage (*Nqo-1*), and liver proliferation (*Afp*). Importantly, WT mice given a 2-wk course of CEHPOBA mimicked these gene expression profiles (**Table 4-1**). In

addition, p21 mRNA was highly up-regulated, and we know from other work that p21 is crucial for blocking hepatocyte cell division in *Fah*<sup>Δexon5</sup> mice [150] and thus essential for the growth advantage of transplanted cells. Generally speaking, the changes were somewhat smaller with CEHPOBA-treatment than NTBC withdrawal in *Fah*<sup>Δexon5</sup> mice.

***CEHPOBA selects for transplanted Hgd<sup>-/-</sup> hepatocytes in wild-type mice***

To test the principle of transient FAH deficiency with CEHPOBA to provide positive selection in a traditionally non-selective setting, the following *in vivo* experiment was devised. Female wild-type mice (*Fah*<sup>+/+</sup>) were transplanted with genetically resistant hepatocytes from a sex-mismatched *Hgd*<sup>-/-</sup> donor and given a 3-5 week course of daily CEHPOBA. Donor *Hgd*<sup>-/-</sup> hepatocytes are protected from FAH-deficiency and are positively selected *in vivo* [54] as they cannot convert tyrosine to FAA. Given the genetic resistance to CEHPOBA in donor hepatocytes, CEHPOBA treatment should make the recipient liver essentially null for FAH, providing a selective advantage to donor hepatocytes for engraftment and subsequent proliferation.

Results from the time course analyses with 3-5 week courses of CEHPOBA following transplantation, showed a linear relationship between time of treatment and degree of repopulation. Compared to controls receiving transplant alone, CEHPOBA-treated transplant recipients had 10- to 100-fold increases in the degree of repopulation (**Fig. 4-3**) as measured by percent Y-chromosome

positivity by Q-PCR.

Figure 4-4 shows representative Y chromosome FISH in control mice (female XX, male XY) (**Fig. 4-4a,b**), and transplant-treated (female XX) mice (**Fig. 4-4d,e**). Results indicated that a significant proportion of Y chromosomes could only be found in those transplant recipients who also received CEHPOBA treatment. H&E staining on treated mice (**Fig. 4-4c,f**) showed a lack of overall toxicity from CEHPOBA treatment in both liver and kidney. Serology and urinalysis to examine potential hepatorenal toxicity demonstrated that the engrafted hepatocytes were functional and that CEHPOBA treatment lacks short-term toxicity (**Table 4-2**). Untransplanted control mice treated with only daily CEHPOBA for 2-wks were unable to compensate for a 2/3 partial hepatectomy for >48-hr, indicating impaired cell proliferation (data not shown). Additionally, two control non-transplanted CEHPOBA-treated mice were monitored for 8-mo and no evidence of hepatocellular carcinoma was found (data not shown).

## FIGURES

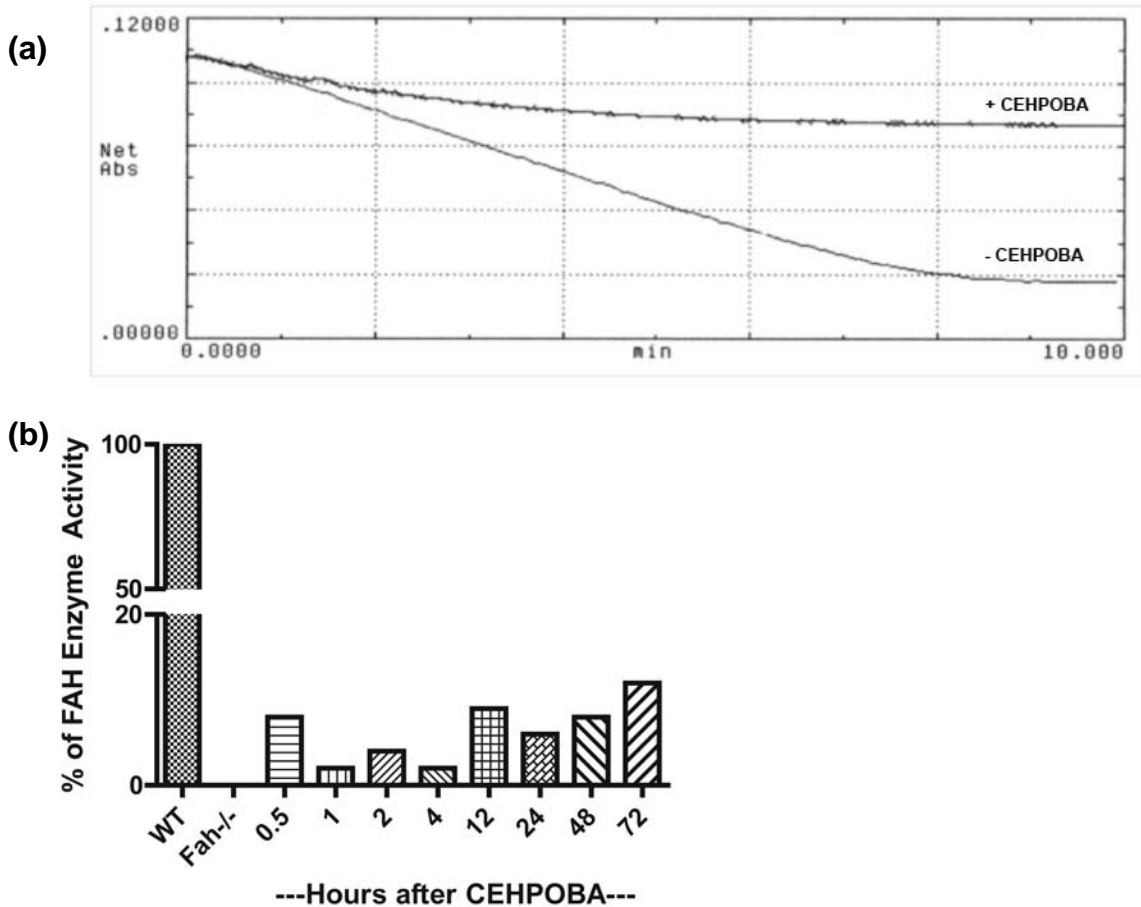


**Figure 4-1: FAH enzyme assay confirms CEHPOBA function**

(a) Livers from adult wild-type mice were homogenized and analyzed for levels of FAH enzyme activity with and without CEHPOBA *in vitro*. The enzymatic assay tests for the reduction of the substrate FAA over time.

(b) Wild-type mice were treated with a single injection of CEHPOBA at 1  $\mu$ mole/g and the liver was harvested at varying time points post-treatment and assayed for the percent of FAH activity remaining. Untreated WT and *Fah* <sup>$\Delta$ exon5</sup> mice were used as positive and negative controls, respectively.

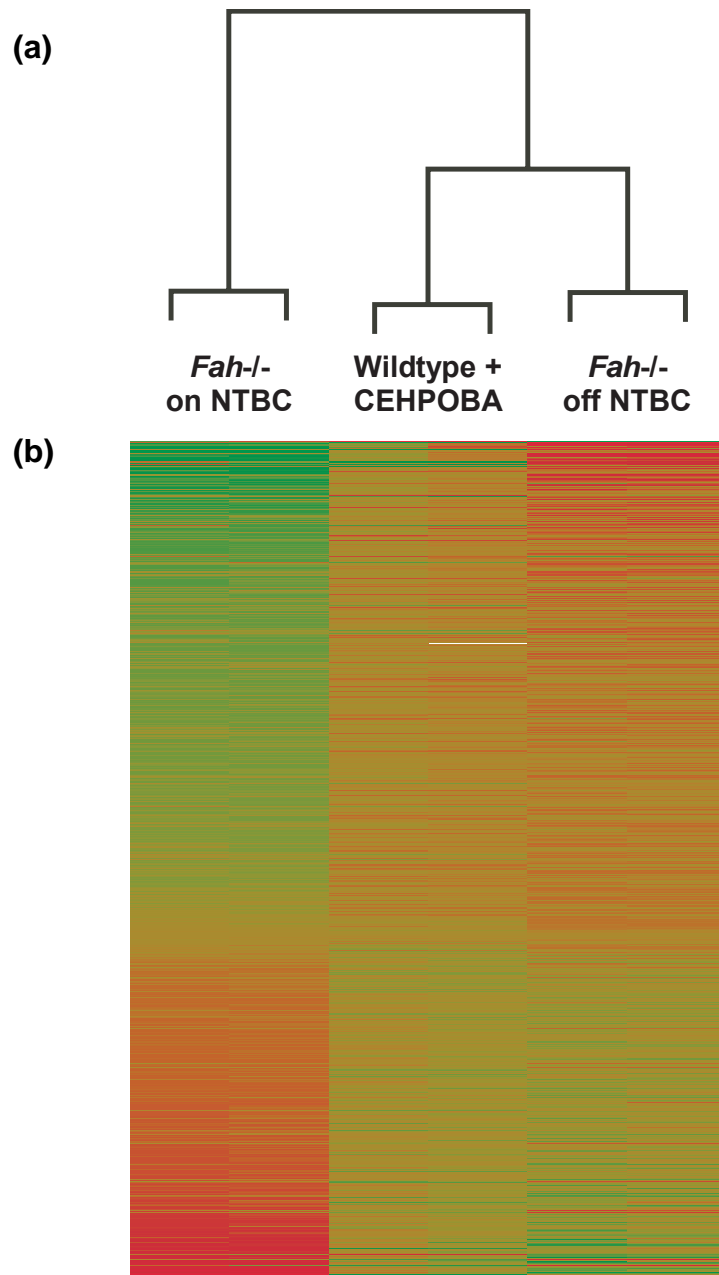


**Figure 4-2: Microarray gene expression data illustrate the similarities between tyrosinemic mice and CEHPOBA-treated wild-type mice**

(a) Microarray cluster analysis, and (b) heat map comparing cohorts of *Fah*<sup>Δ<sub>exon5</sub></sup> mice on NTBC, *Fah*<sup>Δ<sub>exon5</sub></sup> mice off NTBC, and wild-type mice treated with CEHPOBA daily, all for 2-wks. Green = up-regulated; red = down-regulated.

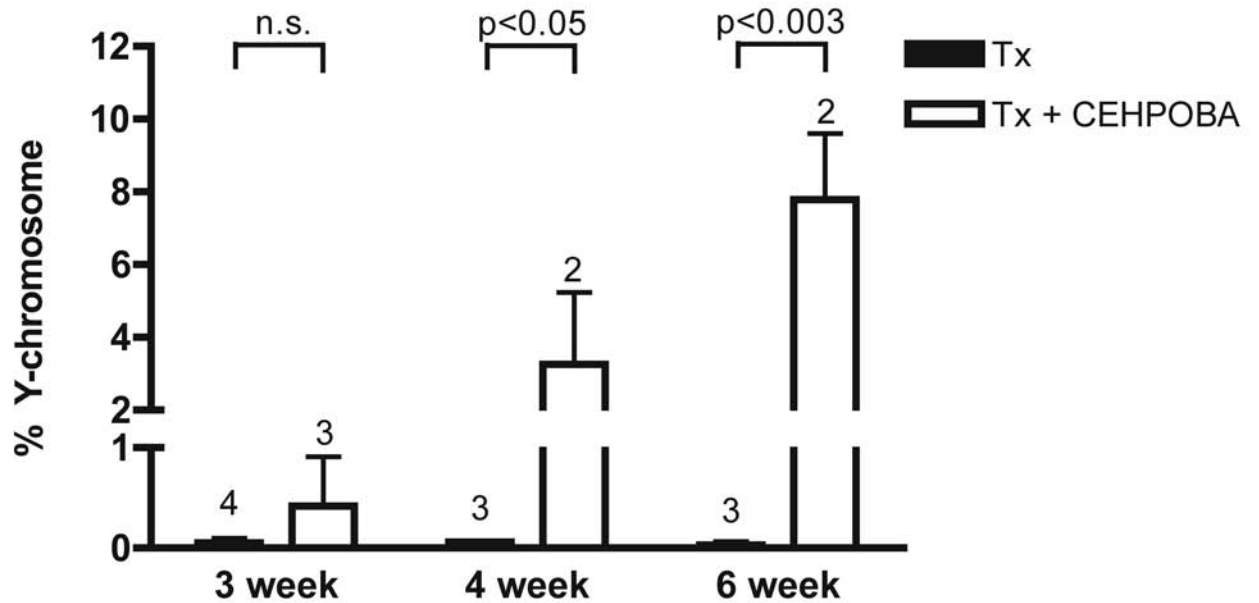


**Figure 4-3: Treatment duration illustrates the kinetics of liver repopulation**

Percent of Y-chromosome donor marker was quantified by qPCR from wild-type mice transplanted with *Hgd*<sup>-/-</sup> hepatocytes, or wild-type mice transplanted with *Hgd*<sup>-/-</sup> hepatocytes and administered a 3 to 5-wk course of CEHPOBA. Mean ± SD are shown, with the number of independent animals analyzed above each bar. Black = Tx alone, white = Tx + CEHPOBA.

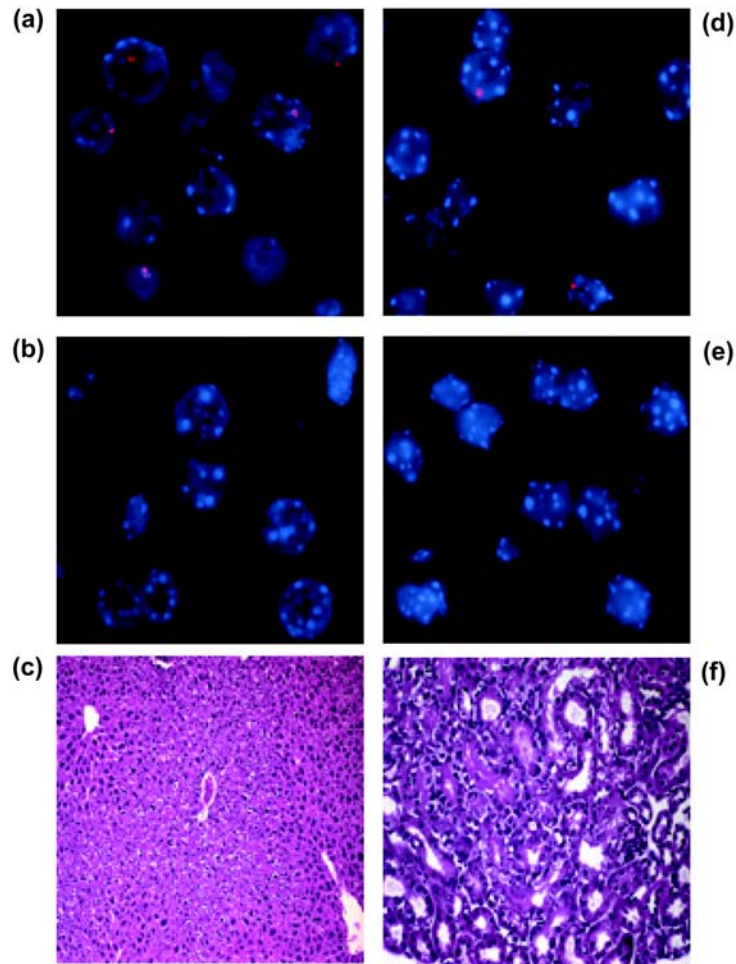


**Figure 4-4: Liver immunohistochemistry**

(a) Control Y-chr<sup>+</sup> stain from an untreated male wild-type mouse (DAPI, Y-Chr); (b) Control Y-chr<sup>-</sup> stain from an untreated female wild-type mouse; (c) H&E stain of liver from a female wild-type mouse transplanted with male *Hgd*<sup>-/-</sup> hepatocytes and treated with a 5-wk course of CEHPOBA; (d) Y-chr stain from a female wild-type mouse transplanted with male *Hgd*<sup>-/-</sup> hepatocytes and a 5-wk course of CEHPOBA; (e) Y-chr stain from a female wild-type mouse transplanted with male *Hgd*<sup>-/-</sup> hepatocytes; (f) H&E stain of kidney from a female wild-type mouse transplanted with male *Hgd*<sup>-/-</sup> hepatocytes and treated with a 5-wk course of CEHPOBA.

## TABLES

Gene	Mouse Abbrev	Up	Down
Fumarylacetoacetate hydrolase	<i>Fah</i>		2.58
Tyrosine aminotransferase	<i>Tat</i>		4.81
Hydroxyphenylpyruvic acid dioxygenase	<i>Hpd</i>		1.55
Phosphoenolpyruvate carboxykinase 1	<i>Pck1</i>		2.33
Ornithine transcarbamylase	<i>Otc</i>		1.7
Argininosuccinate synthetase 1	<i>Ass1</i>		2.18
DNA damage inducible transcript 3	<i>Ddit3</i>	1.22	
NADPH dehydrogenase, quinone 1	<i>Nqo-1</i>	2.16	
Alpha-fetoprotein	<i>Afp</i>	10.7	
Cyclin-dependent kinase inhibitor 1A (p21)	<i>Cdkn1a</i>	4.66	
Glutathione S-transferase alpha 1	<i>Gsta1</i>	1.91	

**Table 4-1: Effects of CEHPOBA treatment on liver gene expression**

Genes that are similarly expressed in both wild-type mice treated with CEHPOBA and *Fah*<sup>Δexon5</sup> mice off NTBC. Values represent fold change relative to *Fah*<sup>Δexon5</sup> mice on NTBC.

	Unit	<i>Fah</i> <sup>Δ<sub>exon5</sub></sup> off NTBC	<i>Fah</i> <sup>Δ<sub>exon5</sub></sup> on NTBC	WT Tx + 5-wks CEHPOBA
<b>Bilirubin</b>	mg/dL	3.1 ± 1.1	0.1 ± 0	0.3 ± 0.1
<b>AST</b>	U/l	308 ± 98	109 ± 52	99 ± 22
<b>ALT</b>	U/l	236 ± 88	65 ± 52	43 ± 0
<b>Tyrosine</b>	μmol/mmol	1112	97	6.3
<b>Methionine</b>	μmol/mmol	216	9.9	36.4
<b>Phenylalanine</b>	μmol/mmol	26.6	4	0
<b>Alanine</b>	μmol/mmol	161	18.8	18.2
<b>Lysine</b>	μmol/mmol	162	23.6	4.8
<b>Glycine</b>	μmol/mmol	475	61.6	0
<b>Histidine</b>	μmol/mmol	959	10	17.1
<b>Asparagine</b>	μmol/mmol	104	11.8	9.3
<b>Serine</b>	μmol/mmol	250	7.6	0.9
<b>Leucine</b>	μmol/mmol	35.1	4.2	4.0
<b>Isoleucine</b>	μmol/mmol	22.3	1.6	1.4
<b>Arginine</b>	μmol/mmol	103.7	0	111
<b>Glutamine</b>	μmol/mmol	2369	37	0
<b>Citrulline</b>	μmol/mmol	15.3	3.2	5.8
<b>Glutamic acid</b>	μmol/mmol	23.5	4.6	5.3
<b>Ornithine</b>	μmol/mmol	25.7	43.7	8
<b>Creatinine</b>	mg/dL	49.0	99.0	44.9
<b>Succinylacetone</b>	μg/mg	45.7	<2	<9
<b>Homogentisic acid</b>	μg/mg	0	0	0

**Table 4-2: Biochemical measures of functional correction and injury**

Values represent mean from untreated *Fah*<sup>Δ<sub>exon5</sub></sup> mice off NTBC (n = 4), untreated *Fah*<sup>Δ<sub>exon5</sub></sup> mice on NTBC (n = 3), wild-type mice transplanted with *Hgd*<sup>-/-</sup> hepatocytes and treated with CEHPOBA for 5-wks (n = 3). Tests performed on urine: all amino acids (μmol/mmol), succinylacetone (μg/mg) and homogentisic acid (μg/mg). SD values were not possible as urine was pooled from mice in each cohort to reach testable volumes. Results were normalized to creatinine excretion. Tests performed on serum: aspartate aminotransferase (AST), alanine aminotransferase (ALT), and bilirubin. SD values are shown.

## DISCUSSION

Several critical conditions must be met in order to make therapeutic liver repopulation for patients a clinical reality: 1) a viable source of healthy donor human hepatocytes for transplantation must be readily available; 2) a selective advantage must exist for the donor hepatocytes, whether through proliferation or survival; 3) host hepatocytes must be damaged or removed, either acutely or chronically, so that donor hepatocytes can grow and expand. Few metabolic liver diseases exist with naturally occurring positive selection, thus a broadly applicable protocol for inducing selection in donor cells that still allows for other normal hepatocellular functions to continue is needed. Traditional hepatocyte-specific conditioning regimens for host cells such as acetaminophen, galactosamine, carbon tetrachloride, hepatic irradiation, thioacetamide and *Amanita* mushroom poison are not ideal in that they all cause severe acute hepatic failure [151]. Successful liver repopulation takes weeks to months to achieve and patients simply cannot survive without hepatocellular function for this duration. Other more hepatocyte-specific conditioning regimens such as retrorsine, monocrotaline and other pyrrolizidine alkaloids are useful in that they maintain sufficient liver function during conditioning, yet the potent DNA-damage and hepatocarcinogenicity they cause is not appropriate for the clinic [152]. A safe, minimally invasive strategy to transiently apply positive selection for donor hepatocytes is needed.

Examples of successful selective repopulation have been achieved in both the hepatic and hematopoietic systems. A study by Mitchell *et al* in 2000 elegantly showed the ability to selectively repopulate an apolipoprotein-E (*ApoE*) deficient mouse liver using anti-apoptotic protection with transgenic Fas/CD95-resistant hepatocytes expressing APOE [153]. Daily injections of non-lethal doses of Jo2 antibody (a Fas agonist) provided a selective advantage for donor hepatocytes and resulted in normalization of the hypercholesterolemia and atherosclerosis in the mice. Similarly, the work of several groups has shown that genetic modifications to the DNA repair gene methylguanine methyltransferase (*Mgmt*) allows for genetic resistance to the chemotherapeutic O6-BG. The combined approach of transducing bone marrow with a O6-BG resistant MGMT variant by retrovirus and then treating the O6-BG sensitive tumor to inhibit its wild-type MGMT activity, showed increases in the therapeutic index in mouse tumor xenograft models [154].

Over a decade of work modeling liver repopulation in *Fah*<sup>Δexon5</sup> mice has shown two basic cellular phenomena critical to the unparalleled success of liver repopulation in this model: 1) cell autonomous accumulation of FAA induces cell cycle arrest in host, but not donor, hepatocytes; 2) hepatocytes lacking functional FAH activity are resistant to cell death. This system allows donor hepatocytes to selectively expand while host hepatocytes fail to cycle, yet the cell death resistance phenotype in host cells permits ongoing liver function, thus preventing acute liver failure and patient death. The promise in CEHPOBA treatment is that

now any patient, with any metabolic liver disease, can be given the therapeutic benefit of positive selection from the *Fah*<sup>Δexon5</sup> model system in a transient, safe and effective manner.

Most human HTI patients experience extended periods (weeks to years) without therapy prior to diagnosis. The effects of FAH deficiency are fully reversible if NTBC is started before 6 months of age [52]. Thus, short-term use of pharmacological FAH inhibitors like CEHPOBA has clinical potential. There are 4 enzymes upstream of FAH in tyrosine catabolism and deficiency of any of these (TAT, HPD, HGD, MAI) could prevent the accumulation of FAA. However, MAA can be isomerized to FAA, thus excluding MAI as a target for blocking the pathway. Strong genetic evidence exists to show that mutations in *Hpd* or *Hgd* completely block the accumulation of FAA in hepatocytes *in vivo* [54, 155]. In the clinic, shRNA-mediated targeting of *Hgd*, *Hpd* or *Tat*, all of which provide suitable protection from FAH deficiency, could be administered to donor hepatocytes prior to transplant.

## **CHAPTER 5**

### **Conclusions and Future Directions**

## ***Current challenges in AAV-mediated gene targeting***

### *Cellular interactions of AAV*

One of the predominant challenges to all AAV gene therapies is the lack of knowledge on intracellular AAV trafficking and nuclear transport in target cells. For example, efficient transduction of lung epithelial cells by AAV is dependent on the cell surface used for entry: apical entry results in 200-fold lower transduction than basolateral entry [156]. Yet this difference is not due to a lack of entry receptors on the apical surface, but rather from impaired trafficking after entry from the apical surface by an as yet undetermined mechanism. This is just one example. In nearly every cell, the detailed mechanisms controlling both intracellular and nuclear pathway choice are unknown. The most current models for AAV entry and intracellular trafficking highlight the known and unknown aspects of this complicated process (**Fig. 5-1**).

### *Serotype specific limitations*

Current serotypes have limited and unexplained differences in their tropism. For example, in the mouse liver, 10% of hepatocytes will be transduced by rAAV2/2 vectors, and 100% by rAAV2/8 vectors despite the fact that an equivalent amount of cell entry receptors are present for each serotype and that viral cell entry is not impaired [157-159]. The discrepancy occurs post-entry [104, 160], and has to do with gene expression difficulties from rAAV2/2, but not rAAV2/8 vectors. The variations in how different cells internalize and process different serotypes of AAV are unclear.

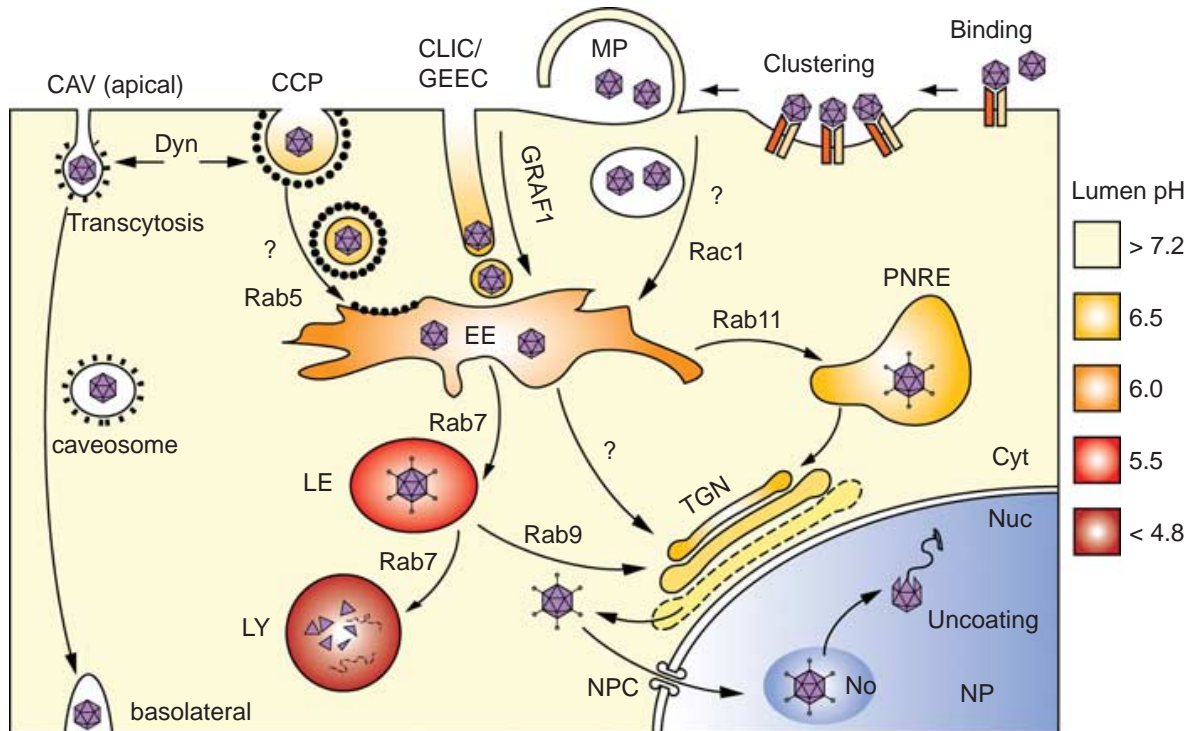


**Figure 5-1: Current model of AAV cell entry and intracellular trafficking**

Following binding to a receptor/co-receptor complex, rAAV enters the target cell through endocytosis via one or more of the following pathways: CLIC/GEEC endocytosis, clathrin-mediated endocytosis (CCP) or caveolar endocytosis (CAV). Viral particles are sorted toward the trans-Golgi network (TGN) along a retrograde transport pathway presumably involving trafficking via early endosomes (EEs), followed by late endosomes (LEs), perinuclear recycling endosomes (PNREs) or both. Capsid conformation changes and exposure of the phospholipase A2 (PLA2) domain (spikes) allows cytoplasmic release from the Golgi or the ER, and nuclear import via the NPC. After nuclear import, intact capsids accumulate in the nucleolus (No) before mobilization into the nucleoplasm (NP) and genome release by partial uncoating. Image reproduced with permission from [161].

### *Preexisting neutralizing antibodies*

AAV capsids are composed of an array of VP1, VP2 and VP3 proteins arranged with icosahedral symmetry. Viral capsid proteins elicit the formation of anti-capsid antibodies upon exposure. It is estimated that 50-96% of the human population is seropositive for AAV2/2 [9, 10] and contain preexisting neutralizing antibodies against this serotype. Even the rare patient who lacks preexisting neutralizing antibodies for an AAV will create them upon repeated vector administration [162]. Although serotype switching strategies work to escape AAV destruction by neutralizing antibodies, this requires that both serotypes effectively transduce the same target tissue. Current clinical trials mandate that patients be prescreened for preexisting neutralizing antibodies for that AAV serotype prior to trial entry.

### *T-cell response to AAV in human subjects*

Several human clinical trials with AAV gene therapy for hemophilia B have taught us much about the importance of the immune system--for both gene addition and gene targeting trials with AAV--despite the fact that AAV is not considered very immunogenic. In a 2006 dose escalation trial, hemophilia B patients were treated with rAAV2/2-hFIX at  $4 \times 10^{11}$ - $2 \times 10^{12}$  vp/kg and an unexpected cytotoxic CD8+ T-cell response against the AAV2 capsid was observed [163]. Although therapeutic levels of factor IX transgene expression were achieved, expression was lost during a self-limiting elevation in liver transaminase levels between weeks 4 and 8 post-treatment. It is thought that the cytotoxic T-cell response was based on the re-activation of memory T-cells that were acquired from prior exposure to

wild-type AAV. As stated earlier, nearly 50-96% of the human population is seropositive for AAV2/2 from prior infections acquired in childhood. Although AAV is naturally replication defective, it is plausible that the initial infection occurred in combination with a helper virus that would trigger activation of the innate immune system to generate CD8+ T-cells against both AAV and the helper virus [164, 165]. The preclinical animal modeling for this trial never used mice previously exposed to wild-type AAV and helper virus prior to treatment, thus explaining the failure to predict the cytotoxic T-cell response against rAAV2 capsid in the clinic.

In a second dose escalation hemophilia B trial completed in 2011, patients were treated with scAAV2/8-hFIX at  $2 \times 10^{11}$ - $2 \times 10^{12}$  vp/kg and a CD8+ T-cell response against the AAV8 capsid was observed [166]. Therapeutic levels of factor IX expression were achieved (2-14%), and although liver transaminase levels rose in several patients, a short treatment with glucocorticoids was enough to restore normal transaminase levels and destroy circulating capsid-specific T-cells in the peripheral blood prior to hepatocellular destruction. The authors of the study proposed that peripheral blood T-cells may be different from those in the liver or that levels of AAV8 capsid antigen presentation on MHC class I hepatocytes were insufficient to mount an effective clearance of transduced hepatocytes. These trials highlight the importance of pre-screening patients for capsid-specific neutralizing antibodies and memory CD8+ T-cells as well as constant transaminase monitoring during liver treatment.

Some immunological limitations for the broad clinical use of gene therapy are tissue specific in the amount and types of risk that can be tolerated in each organ during clinical trial. For example, both the liver and skeletal muscle can withstand a moderate level of immune-mediated damage and still function appropriately, whereas the brain and cardiac muscle have little to no ability to sustain immunological damage [7].

#### *Mechanism for gene targeting*

Despite the *in vivo* gene targeting success described in animal models of HTI [69] and mucopolysaccharidosis type VII [25], the mechanism of AAV gene correction is still unclear. It is unknown whether the AAV genome is truly integrating by gene crossover or simply acting as a template for repair by gene conversion (**Fig. 5-2**). In addition, there is no experimental evidence for how chromatin structure at the target locus may be influencing correction frequencies with AAV *in vivo*.

It has been proposed that AAV may exhibit a strand preference in gene targeting based on interesting results from another parvovirus, minute virus of mice (MVM) [18]. In these experiments, it was shown that although single polarity MVM vectors of either orientation (plus or minus) could target a mutated gene for repair, vectors that targeted the coding strand during transcription or the lagging strand during replication, showed significantly higher gene correction frequencies (Fig. 5-3). This strand bias was hypothesized to be due to processes that

preferentially expose one chromosomal strand and facilitate easier pairing between the vector and the host genome. Confirming these results in AAV vectors and elucidating the mechanism of targeting strand preference may help investigators to augment cellular conditions to better prepare vectors for successful targeting, or direct more informed AAV vector designs.

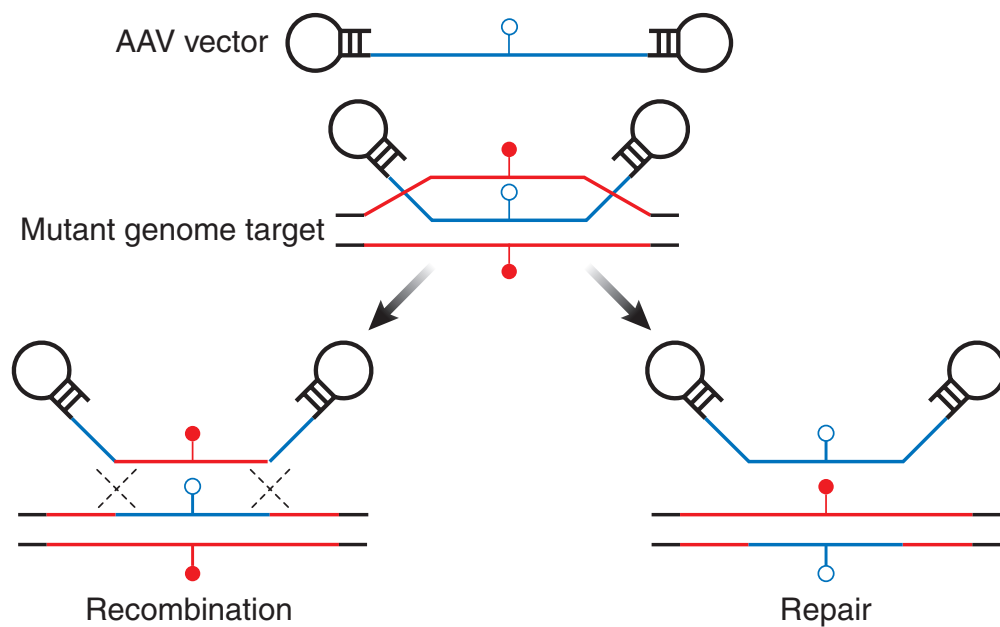


**Figure 5-2: Potential mechanisms for AAV-mediated gene targeting**

On the left, the recombination hypothesis is shown with the homologous pairing of **vector** and **genomic** sequence followed by two recombination events where the AAV vector receives the mutated gene sequence and the genomic sequence is corrected by integration of the viral sequence. On the right, the repair hypothesis is shown with the identical pairing situation occurring but the vector only acting as a template for repair but not integrating. The viral genome remains intact. Image reproduced with permission from [167].

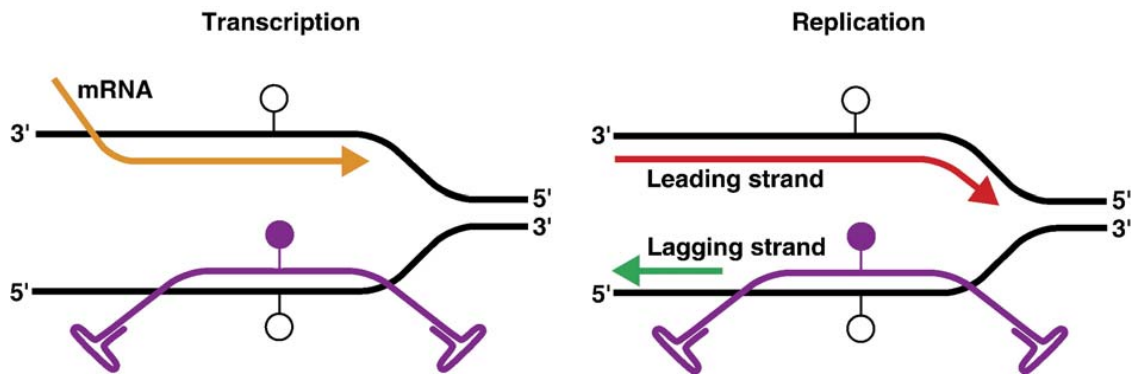


**Figure 5-3: AAV targeting strand bias**

(a) The AAV vector (**purple**) is shown pairing with the exposed chromosomal coding strand (**black**) during transcription, while mRNA (**orange**) occupies the template strand. The coding strand is favored as it is more accessible to pairing.

(b) The AAV vector (**purple**) is shown pairing with the chromosome at gaps generated during lagging strand DNA synthesis (**green**), while the continuous leading strand (**red**) occupies the other strand. The lagging strand is favored as it is more accessible to pairing. Image reproduced with permission from [26].

### **Promising pre-clinical work with AAV for liver diseases**

In addition to the first AAV gene targeting study demonstrating functional correction with murine models of HTI described in Chapters 2 and 3, numerous successes with AAV-mediated gene addition for various animal models of disease are emerging (**Table 5-1**).

<b>Disease</b>	<b>Model</b>	<b>Transgene product</b>	<b>Serotype used</b>	<b>Delivery method</b>	<b>Outcome</b>
Hunter syndrome	MPS II mice	Human iduronate sulphatase	AAV2	Tail vein	Restoration of skeleton abnormalities and locomotor defects of MPS II mice
Gaucher disease	D409V mice	Human GC	AAV8	Intravenous	Prevention and correction of the biochemical and pathological abnormalities
Crigler–Najjar syndrome	Gunn rats	UGT1A1	AAV1, AAV2, AAV6, AAV8	Intraportal	Improvements in serum bilirubin
GSD-Ia	GSD-Ia mice	cG6Pase	AAV8	Intravenous (retro-orbital sinus)	Phenotypical correction
OTC deficiency	OTC-deficient mice	Mouse OTC	AAV2, AAV7, AAV8, AAV9	Portal vein	Prolonged survival and urinary orotate correction
Homocystinuria	Cbs <sup>-/-</sup> mice	Human CBS	AAV2	Intraperitoneal	Elongation of lifespan
Haemophilia A	Haemophilia A mice	Human and canine factor VIII heavy and light chains	AAV2	Portal vein	Therapeutic to superphysiologic levels of active factor VIII were achieved in plasma
Haemophilia B	Haemophilia B dogs	Canine factor IX	AAV2	Portal vein	Sustained high-level factor IX expression
MPS VII	MPS VII mice	GUSB	AAV	Intravenous	Long-term expression of GUSB in multiple tissues and a reduction in lysosomal storage
MPS I	MPS I mice	IDUA	AAV2	Intrathecal	Dose response and reduction of storage vacuoles
Haemochromatosis	Hfe <sup>-/-</sup> mice	Mouse HFE	AAV8	Tail vein	Lower liver iron level and increases in hepcidin expression
α1 antitrypsin deficiency	Wild-type mice	Human α1 antitrypsin	AAV8	Portal vein	Dose response in serum α1 antitrypsin levels

**Table 5-1: Successful liver-directed AAV gene addition models**

Listed are the various pre-clinical animal models of liver-related disease where AAV gene addition therapy has shown promise. Table reproduced with permission from [7].

### ***Final thoughts***

My thesis has focused on novel strategies to improve both viral gene targeting with AAV and therapeutic liver repopulation *in vivo*. Although both strategies are still in the pre-clinical stage of experimentation, the successes shown herein highlight the potential for these strategies to have real clinical benefit in the coming years. Additional problems will need to be addressed for the switch from bench-to-bedside including: scalable manufacturing processes for AAV vectors that follow good manufacturing practices [168], standardized methods for purifying and titering AAV [169], as well as securing a viable source of healthy donor human hepatocytes for transplantation.

## REFERENCES

1. Baird, PA, Anderson, TW, Newcombe, HB, and Lowry, RB (1988). Genetic disorders in children and young adults: a population study. *Am J Hum Genet* **42**: 677-693.
2. Christianson, A, Howson, CP, and Modell, B (2006). Global report on birth defects--The hidden toll of dying and disabled children. pp. 1-84. March of Dimes.
3. McCandless, SE, Brunger, JW, and Cassidy, SB (2004). The burden of genetic disease on inpatient care in a children's hospital. *Am J Hum Genet* **74**: 121-127.
4. Naylor, J, and Benkendorf, J (1994). *Mendelian inheritance in man: A catalog of human genes and genetic disorders*, Johns Hopkins University Press.
5. Borgaonkar, D (1994). *Chromosomal Variation in Man: A Catalog of Chromosomal Variants and Anomalies* Wiley-Liss.
6. Emery, AEH, and Rimoin, DL (1990). *Principles and Practice of Medical Genetics*, Churchill Livingstone: New York.
7. Mingozzi, F, and High, KA (2011). Therapeutic in vivo gene transfer for genetic disease using AAV: progress and challenges. *Nat Rev Genet* **12**: 341-355.
8. Knipe, DM, and Howley, PM (2006). *Field's Virology*, Lippincott Williams & Wilkins: Philadelphia.

9. Erles, K, Sebokova, P, and Schlehofer, JR (1999). Update on the prevalence of serum antibodies (IgG and IgM) to adeno-associated virus (AAV). *J Med Virol* **59**: 406-411.
10. Moskalenko, M, *et al.* (2000). Epitope mapping of human anti-adeno-associated virus type 2 neutralizing antibodies: implications for gene therapy and virus structure. *J Virol* **74**: 1761-1766.
11. <http://hvd.ens-lyon.fr/teams/AAV> (2010). Map of the AAV Genome.
12. Sonntag, F, Schmidt, K, and Kleinschmidt, JA (2010). A viral assembly factor promotes AAV2 capsid formation in the nucleolus. *Proc Natl Acad Sci U S A* **107**: 10220-10225.
13. Samulski, RJ, *et al.* (1991). Targeted integration of adeno-associated virus (AAV) into human chromosome 19. *EMBO J* **10**: 3941-3950.
14. [hvd.ens-lyon.fr/teams/AAV](http://hvd.ens-lyon.fr/teams/AAV) (2012). Adeno-associated viruses and rAAV vectors. (Department, V, Ed.). University of Lyon.
15. Schaffer, DV, Koerber, JT, and Lim, KI (2008). Molecular engineering of viral gene delivery vehicles. *Annu Rev Biomed Eng* **10**: 169-194.
16. Mueller, C, and Flotte, TR (2008). Clinical gene therapy using recombinant adeno-associated virus vectors. *Gene Ther* **15**: 858-863.
17. Russell, DW, and Kay, M (1999). Adeno-Associated Virus Vectors and Hematology. *Blood* **94**: 864-874.
18. Hendrie, PC, Hirata, RK, and Russell, DW (2003). Chromosomal integration and homologous gene targeting by replication-incompetent

- vectors based on the autonomous parvovirus minute virus of mice. *J Virol* **77**: 13136-13145.
19. Donsante, A, *et al.* (2007). AAV vector integration sites in mouse hepatocellular carcinoma. *Science* **317**: 477.
  20. Thomas, KR, and Capecchi, MR (1987). Site-directed mutagenesis by gene targeting in mouse embryo-derived stem cells. *Cell* **51**: 503-512.
  21. Russell, DW, and Hirata, RK (1998). Human gene targeting by viral vectors. *Nat Genet* **18**: 325-330.
  22. Inoue, N, Dong, R, Hirata, RK, and Russell, DW (2001). Introduction of single base substitutions at homologous chromosomal sequences by adeno-associated virus vectors. *Mol Ther* **3**: 526-530.
  23. Inoue, N, Hirata, RK, and Russell, DW (1999). High-fidelity correction of mutations at multiple chromosomal positions by adeno-associated virus vectors. *J Virol* **73**: 7376-7380.
  24. Parekh-Olmedo, H, Ferrara, L, Brachman, E, and Kmiec, EB (2005). Gene therapy progress and prospects: targeted gene repair. *Gene Ther* **12**: 639-646.
  25. Miller, DG, Wang, PR, Petek, LM, Hirata, RK, Sands, MS, and Russell, DW (2006). Gene targeting in vivo by adeno-associated virus vectors. *Nat Biotechnol* **24**: 1022-1026.
  26. Hendrie, PC, and Russell, DW (2005). Gene targeting with viral vectors. *Mol Ther* **12**: 9-17.

27. Bergeron, B (2004). *Case studies in genes and disease.*, American College of Physicians Press.
28. Vasileva, A, and Jessberger, R (2005). Precise hit: adeno-associated virus in gene targeting. *Nat Rev Microbiol* **3**: 837-847.
29. Boyer, TD, Wright, TL, and Manns, MP (2006). *Zakim & Boyer's Hepatology: A textbook of liver disease*, Saunders.
30. Frevert, U, *et al.* (2005). Intravital observation of Plasmodium berghei sporozoite infection of the liver. *PLoS Biol* **3**: e192.
31. Burke, ZD, and Tosh, D (2006). The Wnt/beta-catenin pathway: master regulator of liver zonation? *Bioessays* **28**: 1072-1077.
32. Mitchell, GA, Grompe, M, Lambert, M, and Tanguay, R (2001). *Hypertyrosinemia. The Metabolic and Molecular Basis of Inherited Disease.*, McGraw-Hill.
33. Mahuran, DJ, Angus, RH, Braun, CV, Sim, SS, and Schmidt, DE, Jr. (1977). Characterization and substrate specificity of fumarylacetoacetate fumarylhydrolase. *Can J Biochem* **55**: 1-8.
34. Timm, DE, Mueller, HA, Bhanumoorthy, P, Harp, JM, and Bunick, GJ (1999). Crystal structure and mechanism of a carbon-carbon bond hydrolase. *Structure* **7**: 1023-1033.
35. Grompe, M (2001). The pathophysiology and treatment of hereditary tyrosinemia type 1. *Semin Liver Dis* **21**: 563-571.

36. Al-Dhalimy, M, Overturf, K, Finegold, M, and Grompe, M (2002). Long-term therapy with NTBC and tyrosine-restricted diet in a murine model of hereditary tyrosinemia type I. *Mol Genet Metab* **75**: 38-45.
37. Grompe, M, *et al.* (1993). Loss of fumarylacetoacetate hydrolase is responsible for the neonatal hepatic dysfunction phenotype of lethal albino mice. *Genes Dev* **7**: 2298-2307.
38. Aponte, JL, *et al.* (2001). Point mutations in the murine fumarylacetoacetate hydrolase gene: Animal models for the human genetic disorder hereditary tyrosinemia type 1. *Proc Natl Acad Sci U S A* **98**: 641-645.
39. Fernandez-Canon, JM, and Penalva, MA (1995). Fungal metabolic model for human type I hereditary tyrosinaemia. *Proc Natl Acad Sci U S A* **92**: 9132-9136.
40. Nebert, DW, Roe, AL, Dieter, MZ, Solis, WA, Yang, Y, and Dalton, TP (2000). Role of the aromatic hydrocarbon receptor and [Ah] gene battery in the oxidative stress response, cell cycle control, and apoptosis. *Biochem Pharmacol* **59**: 65-85.
41. Ruppert, S, Kelsey, G, Schedl, A, Schmid, E, Thies, E, and Schutz, G (1992). Deficiency of an enzyme of tyrosine metabolism underlies altered gene expression in newborn liver of lethal albino mice. *Genes Dev* **6**: 1430-1443.

42. Grompe, M, *et al.* (1995). Pharmacological correction of neonatal lethal hepatic dysfunction in a murine model of hereditary tyrosinaemia type I. *Nat Genet* **10**: 453-460.
43. Schmid, W, Muller, G, Schutz, G, and Gluecksohn-Waelsch, S (1985). Deletions near the albino locus on chromosome 7 of the mouse affect the level of tyrosine aminotransferase mRNA. *Proc Natl Acad Sci U S A* **82**: 2866-2869.
44. Loose, DS, *et al.* (1986). Trans regulation of the phosphoenolpyruvate carboxykinase (GTP) gene, identified by deletions in chromosome 7 of the mouse. *Proc Natl Acad Sci U S A* **83**: 5184-5188.
45. Kubo, S, *et al.* (1998). Hepatocyte injury in tyrosinemia type 1 is induced by fumarylacetoacetate and is inhibited by caspase inhibitors. *Proc Natl Acad Sci U S A* **95**: 9552-9557.
46. Sun, MS, Hattori, S, Kubo, S, Awata, H, Matsuda, I, and Endo, F (2000). A mouse model of renal tubular injury of tyrosinemia type 1: development of de Toni Fanconi syndrome and apoptosis of renal tubular cells in Fah/Hpd double mutant mice. *J Am Soc Nephrol* **11**: 291-300.
47. Jorquera, R, and Tanguay, RM (1999). Cyclin B-dependent kinase and caspase-1 activation precedes mitochondrial dysfunction in fumarylacetoacetate-induced apoptosis. *FASEB J* **13**: 2284-2298.
48. Vogel, A, *et al.* (2004). Chronic liver disease in murine hereditary tyrosinemia type 1 induces resistance to cell death. *Hepatology* **39**: 433-443.

49. Mitchell, G, Grompe, M, Lambert, M, and Tanguay, R (2001). Hypertyrosinemia. In: Scriver, C, A Beaudet, W Sly and D Valle eds). *The Metabolic and Molecular Basis of Inherited Disease*, 9 ed. MacGraw-Hill: New York. p 1777.
50. Luijck, MC, *et al.* (2004). Renal proximal tubular cells acquire resistance to cell death stimuli in mice with hereditary tyrosinemia type 1. *Kidney Int* **66**: 990-1000.
51. Spencer, PD, Medow, MS, Moses, LC, and Roth, KS (1988). Effects of succinylacetone on the uptake of sugars and amino acids by brush border vesicles. *Kidney Int* **34**: 671-677.
52. Holme, E, and Lindstedt, S (2000). Nontransplant treatment of tyrosinemia. *Clin Liver Dis* **4**: 805-814.
53. Jorquera, R, and Tanguay, RM (1997). The mutagenicity of the tyrosine metabolite, fumarylacetoacetate, is enhanced by glutathione depletion. *Biochem Biophys Res Commun* **232**: 42-48.
54. Manning, K, Al-Dhalimy, M, Finegold, M, and Grompe, M (1999). In vivo suppressor mutations correct a murine model of hereditary tyrosinemia type I. *Proc Natl Acad Sci U S A* **96**: 11928-11933.
55. Bain, MD, Purkiss, P, Jones, M, Bingham, P, Stacey, TE, and Chalmers, RA (1990). Dietary treatment eliminates succinylacetone from the urine of a patient with tyrosinaemia type 1. *Eur J Pediatr* **149**: 637-639.
56. Mohan, N, *et al.* (1999). Indications and outcome of liver transplantation in tyrosinaemia type 1. *Eur J Pediatr* **158 Suppl 2**: S49-54.

57. Perez-Cerda, C, *et al.* (1995). Liver transplantation in nine Spanish patients with tyrosinaemia type I. *J Inherit Metab Dis* **18**: 119-122.
58. Sokal, EM, Bustos, R, Van Hoof, F, and Otte, JB (1992). Liver transplantation for hereditary tyrosinemia--early transplantation following the patient's stabilization. *Transplantation* **54**: 937-939.
59. Mieles, LA, *et al.* (1990). Liver transplantation for tyrosinemia. A review of 10 cases from the University of Pittsburgh. *Dig Dis Sci* **35**: 153-157.
60. Busuttil, R, and Klintman, G (1996). *Transplantation of the liver*, W.B. Saunders: Philadelphia.
61. Schwetz, BA (2002). From the Food and Drug Administration. *JAMA* **287**: 1103.
62. Lindstedt, S, Holme, E, Lock, EA, Hjalmarson, O, and Strandvik, B (1992). Treatment of hereditary tyrosinaemia type I by inhibition of 4-hydroxyphenylpyruvate dioxygenase. *Lancet* **340**: 813-817.
63. Overturf, K, *et al.* (1996). Hepatocytes corrected by gene therapy are selected in vivo in a murine model of hereditary tyrosinaemia type I. *Nat Genet* **12**: 266-273.
64. Kvittingen, EA, Rootwelt, H, Brandtzaeg, P, Bergan, A, and Berger, R (1993). Hereditary tyrosinemia type I. Self-induced correction of the fumarylacetoacetase defect. *J Clin Invest* **91**: 1816-1821.
65. Overturf, K, al-Dhalimy, M, Ou, CN, Finegold, M, and Grompe, M (1997). Serial transplantation reveals the stem-cell-like regenerative potential of adult mouse hepatocytes. *Am J Pathol* **151**: 1273-1280.

66. Erker, L, *et al.* (2010). Therapeutic liver reconstitution with murine cells isolated long after death. *Gastroenterology* **139**: 1019-1029.
67. Azuma, H, *et al.* (2007). Robust expansion of human hepatocytes in Fah<sup>-/-</sup>/Rag2<sup>-/-</sup>/Il2rg<sup>-/-</sup> mice. *Nat Biotechnol* **25**: 903-910.
68. Wang, X, Montini, E, Al-Dhalimy, M, Lagasse, E, Finegold, M, and Grompe, M (2002). Kinetics of liver repopulation after bone marrow transplantation. *Am J Pathol* **161**: 565-574.
69. Paulk, NK, Wursthorn, K, Wang, Z, Finegold, MJ, Kay, MA, and Grompe, M (2010). Adeno-associated virus gene repair corrects a mouse model of hereditary tyrosinemia in vivo. *Hepatology* **51**: 1200-1208.
70. Overturf, K, *et al.* (1997). Adenovirus-mediated gene therapy in a mouse model of hereditary tyrosinemia type I. *Hum Gene Ther* **8**: 513-521.
71. Overturf, K, Al-Dhalimy, M, Manning, K, Ou, CN, Finegold, M, and Grompe, M (1998). Ex vivo hepatic gene therapy of a mouse model of Hereditary Tyrosinemia Type I. *Hum Gene Ther* **9**: 295-304.
72. Held, PK, Olivares, EC, Aguilar, CP, Finegold, M, Calos, MP, and Grompe, M (2005). In vivo correction of murine hereditary tyrosinemia type I by phiC31 integrase-mediated gene delivery. *Mol Ther* **11**: 399-408.
73. Montini, E, *et al.* (2002). In vivo correction of murine tyrosinemia type I by DNA-mediated transposition. *Mol Ther* **6**: 759-769.
74. Culiati, CT, *et al.* (2005). Identification of mutations from phenotype-driven ENU mutagenesis in mouse chromosome 7. *Mamm Genome* **16**: 555-566.

75. Fox, IJ, *et al.* (1998). Treatment of the Crigler-Najjar syndrome type I with hepatocyte transplantation. *N Engl J Med* **338**: 1422-1426.
76. Kay, MA, and High, K (1999). Gene therapy for the hemophilias. *Proc Natl Acad Sci U S A* **96**: 9973-9975.
77. Wang, L, Takabe, K, Bidlingmaier, SM, III, CR, and Verma, IM (1999). Sustained correction of bleeding disorder in hemophilia B mice by gene therapy. *Proc Natl Acad Sci U S A* **96**: 3906-3910.
78. Mian, A, *et al.* (2004). Long-term correction of ornithine transcarbamylase deficiency by WPRE-mediated overexpression using a helper-dependent adenovirus. *Mol Ther* **10**: 492-499.
79. Battaile, KP, *et al.* (1999). In vivo selection of wild-type hematopoietic stem cells in a murine model of Fanconi anemia. *Blood* **94**: 2151-2158.
80. Allen, KJ, *et al.* (2004). Liver cell transplantation leads to repopulation and functional correction in a mouse model of Wilson's disease. *J Gastroenterol Hepatol* **19**: 1283-1290.
81. Hirschhorn, R, Yang, DR, Israni, A, Huie, ML, and Ownby, DR (1994). Somatic mosaicism for a newly identified splice-site mutation in a patient with adenosine deaminase-deficient immunodeficiency and spontaneous clinical recovery. *Am J Hum Genet* **55**: 59-68.
82. De Vree, JM, Ottenhoff, R, Bosma, PJ, Smith, AJ, Aten, J, and Oude Elferink, RP (2000). Correction of liver disease by hepatocyte transplantation in a mouse model of progressive familial intrahepatic cholestasis. *Gastroenterology* **119**: 1720-1730.

83. Ellis, NA, Lennon, DJ, Proytcheva, M, Alhadeff, B, Henderson, EE, and German, J (1995). Somatic intragenic recombination within the mutated locus BLM can correct the high sister-chromatid exchange phenotype of Bloom syndrome cells. *Am J Hum Genet* **57**: 1019-1027.
84. Ortiz-Urda, S, Lin, Q, Yant, SR, Keene, D, Kay, MA, and Khavari, PA (2003). Sustainable correction of junctional epidermolysis bullosa via transposon-mediated nonviral gene transfer. *Gene Ther* **10**: 1099-1104.
85. Russell, DW, and Kay, MA (1999). Adeno-associated virus vectors and hematology. *Blood* **94**: 864-874.
86. Garrick, D, Firing, S, Martin, DI, and Whitelaw, E (1998). Repeat-induced gene silencing in mammals. *Nat Genet* **18**: 56-59.
87. Verma, IM, and Somia, N (1997). Gene therapy -- promises, problems and prospects. *Nature* **389**: 239-242.
88. Andrieu-Soler, C, *et al.* (2007). Single-stranded oligonucleotide-mediated in vivo gene repair in the rd1 retina. *Mol Vis* **13**: 692-706.
89. Huen, MS, Lu, LY, Liu, DP, and Huang, JD (2007). Active transcription promotes single-stranded oligonucleotide mediated gene repair. *Biochem Biophys Res Commun* **353**: 33-39.
90. Wu, XS, *et al.* (2005). Increased efficiency of oligonucleotide-mediated gene repair through slowing replication fork progression. *Proc Natl Acad Sci U S A* **102**: 2508-2513.
91. Vasquez, KM, Narayanan, L, and Glazer, PM (2000). Specific mutations induced by triplex-forming oligonucleotides in mice. *Science* **290**: 530-533.

92. Kren, BT, Bandyopadhyay, P, and Steer, CJ (1998). In vivo site-directed mutagenesis of the factor IX gene by chimeric RNA/DNA oligonucleotides. *Nat Med* **4**: 285-290.
93. Kren, BT, Parashar, B, Bandyopadhyay, P, Chowdhury, NR, Chowdhury, JR, and Steer, CJ (1999). Correction of the UDP-glucuronosyltransferase gene defect in the gunn rat model of crigler-najjar syndrome type I with a chimeric oligonucleotide. *Proc Natl Acad Sci U S A* **96**: 10349-10354.
94. Nakai, H, *et al.* (2003). Helper-independent and AAV-ITR-independent chromosomal integration of double-stranded linear DNA vectors in mice. *Mol Ther* **7**: 101-111.
95. Chen, ZY, Yant, SR, He, CY, Meuse, L, Shen, S, and Kay, MA (2001). Linear DNAs concatemerize in vivo and result in sustained transgene expression in mouse liver. *Mol Ther* **3**: 403-410.
96. Sands, MS, and Barker, JE (2000). Percutaneous intravenous injection in neonatal mice. *Comp Med* **50**: 107.
97. Grimm, D, Pandey, K, Nakai, H, Storm, TA, and Kay, MA (2006). Liver transduction with recombinant adeno-associated virus is primarily restricted by capsid serotype not vector genotype. *J Virol* **80**: 426-439.
98. Mitchell, C, and Willenbring, H (2008). A reproducible and well-tolerated method for 2/3 partial hepatectomy in mice. *Nat Protoc* **3**: 1167-1170.
99. Grimm, D (2002). Production methods for gene transfer vectors based on adeno-associated virus serotypes. *Methods* **28**: 146-157.

100. Choi, VW, Asokan, A, Haberman, RA, and Samulski, RJ (2007). Production of recombinant adeno-associated viral vectors for in vitro and in vivo use. *Curr Protoc Mol Biol* **Chapter 16**: Unit 16 25.
101. Grimm, D, Kay, MA, and Kleinschmidt, JA (2003). Helper virus-free, optically controllable, and two-plasmid-based production of adeno-associated virus vectors of serotypes 1 to 6. *Mol Ther* **7**: 839-850.
102. Grompe, M, Jones, SN, Loulseged, H, and Caskey, CT (1992). Retroviral-mediated gene transfer of human ornithine transcarbamylase into primary hepatocytes of spf and spf-ash mice. *Hum Gene Ther* **3**: 35-44.
103. Ponder, KP, *et al.* (1991). Mouse hepatocytes migrate to liver parenchyma and function indefinitely after intrasplenic transplantation. *Proc Natl Acad Sci U S A* **88**: 1217-1221.
104. Thomas, CE, Storm, TA, Huang, Z, and Kay, MA (2004). Rapid uncoating of vector genomes is the key to efficient liver transduction with pseudotyped adeno-associated virus vectors. *J Virol* **78**: 3110-3122.
105. Vasileva, A, Linden, RM, and Jessberger, R (2006). Homologous recombination is required for AAV-mediated gene targeting. *Nucleic Acids Res* **34**: 3345-3360.
106. Nickerson, HD, and Colledge, WH (2004). A LacZ-based transgenic mouse for detection of somatic gene repair events in vivo. *Gene Ther* **11**: 1351-1357.

107. Vijg, J, Dolle, ME, Martus, HJ, and Boerrigter, ME (1997). Transgenic mouse models for studying mutations in vivo: applications in aging research. *Mech Ageing Dev* **99**: 257-271.
108. Buning, H, Nicklin, SA, Perabo, L, Hallek, M, and Baker, AH (2003). AAV-based gene transfer. *Curr Opin Mol Ther* **5**: 367-375.
109. van Gent, DC, Hoeijmakers, JH, and Kanaar, R (2001). Chromosomal stability and the DNA double-stranded break connection. *Nat Rev Genet* **2**: 196-206.
110. Durant, S, and Karran, P (2003). Vanillins--a novel family of DNA-PK inhibitors. *Nucleic Acids Res* **31**: 5501-5512.
111. Beaudry, F, Ross, A, Lema, PP, and Vachon, P (2010). Pharmacokinetics of vanillin and its effects on mechanical hypersensitivity in a rat model of neuropathic pain. *Phytother Res* **24**: 525-530.
112. Johnson, JS, and Samulski, RJ (2009). Enhancement of adeno-associated virus infection by mobilizing capsids into and out of the nucleolus. *J Virol* **83**: 2632-2644.
113. Monahan, PE, *et al.* (2010). Proteasome inhibitors enhance gene delivery by AAV virus vectors expressing large genomes in hemophilia mouse and dog models: a strategy for broad clinical application. *Mol Ther* **18**: 1907-1916.
114. Finn, JD, *et al.* Proteasome inhibitors decrease AAV2 capsid derived peptide epitope presentation on MHC class I following transduction. *Mol Ther* **18**: 135-142.

115. Gu, Y, *et al.* (1997). Growth retardation and leaky SCID phenotype of Ku70-deficient mice. *Immunity* **7**: 653-665.
116. Finn, JD, *et al.* (2010). Proteasome inhibitors decrease AAV2 capsid derived peptide epitope presentation on MHC class I following transduction. *Mol Ther* **18**: 135-142.
117. Song, S, *et al.* (2004). DNA-dependent PK inhibits adeno-associated virus DNA integration. *Proc Natl Acad Sci U S A* **101**: 2112-2116.
118. Fattah, FJ, Lichter, NF, Fattah, KR, Oh, S, and Hendrickson, EA (2008). Ku70, an essential gene, modulates the frequency of rAAV-mediated gene targeting in human somatic cells. *Proc Natl Acad Sci U S A* **105**: 8703-8708.
119. Porteus, MH, Cathomen, T, Weitzman, MD, and Baltimore, D (2003). Efficient gene targeting mediated by adeno-associated virus and DNA double-strand breaks. *Mol Cell Biol* **23**: 3558-3565.
120. Nakai, H, *et al.* (2005). Large-scale molecular characterization of adeno-associated virus vector integration in mouse liver. *J Virol* **79**: 3606-3614.
121. Akagi, K, Hirose, M, Hoshiya, T, Mizoguchi, Y, Ito, N, and Shirai, T (1995). Modulating effects of ellagic acid, vanillin and quercetin in a rat medium term multi-organ carcinogenesis model. *Cancer Lett* **94**: 113-121.
122. Burri, J, Graf, M, Lambelet, P, and Loliger, J (1989). Vanillin: More than a flavouring agent--a potent antioxidant. *J Sci Food Agric* **48**: 49-56.

123. Sasaki, YF, *et al.* (1990). Suppressing effects of vanillin, cinnamaldehyde, and anisaldehyde on chromosome aberrations induced by X-rays in mice. *Mutat Res* **243**: 299-302.
124. Keshava, C, Keshava, N, Ong, TM, and Nath, J (1998). Protective effect of vanillin on radiation-induced micronuclei and chromosomal aberrations in V79 cells. *Mutat Res* **397**: 149-159.
125. Davidson, PM, and Naidu, AS (2000). Phyto-phenols. In: Naidu, AS (ed). *Natural Food Antimicrobial Systems*. CRC Press: Washington, DC. pp 265-294.
126. McCann, MJ, *et al.* (2007). Anti-cancer properties of phenolics from apple waste on colon carcinogenesis in vitro. *Food Chem Toxicol* **45**: 1224-1230.
127. Richardson, PG, *et al.* (2005). Bortezomib or high-dose dexamethasone for relapsed multiple myeloma. *N Engl J Med* **352**: 2487-2498.
128. Davidoff, AM, Ng, CY, Zhou, J, Spence, Y, and Nathwani, AC (2003). Sex significantly influences transduction of murine liver by recombinant adeno-associated viral vectors through an androgen-dependent pathway. *Blood* **102**: 480-488.
129. Ogura, T, *et al.* (2006). Utility of intraperitoneal administration as a route of AAV serotype 5 vector-mediated neonatal gene transfer. *J Gene Med* **8**: 990-997.
130. Ho, KJ, Bass, CE, Kroemer, AH, Ma, C, Terwilliger, E, and Karp, SJ (2008). Optimized adeno-associated virus 8 produces hepatocyte-specific

- Cre-mediated recombination without toxicity or affecting liver regeneration. *Am J Physiol Gastrointest Liver Physiol* **295**: G412-419.
131. Rebuffat, A, Harding, CO, Ding, Z, and Thony, B (2010). Comparison of adeno-associated virus pseudotype 1, 2, and 8 vectors administered by intramuscular injection in the treatment of murine phenylketonuria. *Hum Gene Ther* **21**: 463-477.
  132. Rinn, JL, and Snyder, M (2005). Sexual dimorphism in mammalian gene expression. *Trends Genet* **21**: 298-305.
  133. Clodfelter, KH, Holloway, MG, Hodor, P, Park, SH, Ray, WJ, and Waxman, DJ (2006). Sex-dependent liver gene expression is extensive and largely dependent upon signal transducer and activator of transcription 5b (STAT5b): STAT5b-dependent activation of male genes and repression of female genes revealed by microarray analysis. *Mol Endocrinol* **20**: 1333-1351.
  134. Fang, B, *et al.* (1994). Gene therapy for phenylketonuria: phenotypic correction in a genetically deficient mouse model by adenovirus-mediated hepatic gene transfer. *Gene Ther* **1**: 247-254.
  135. Shneider, BL (2002). Pediatric liver transplantation in metabolic disease: clinical decision making. *Pediatr Transplant* **6**: 25-29.
  136. Grompe, M (2001). Liver repopulation for the treatment of metabolic diseases. *J Inherit Metab Dis* **24**: 231-244.
  137. Grompe, M (2006). Principles of therapeutic liver repopulation. *J Inherit Metab Dis* **29**: 421-425.

138. Bateman, RL, *et al.* (2007). Slow-onset inhibition of fumarylacetoacetate hydrolase by phosphinate mimics of the tetrahedral intermediate: kinetics, crystal structure and pharmacokinetics. *Biochem J* **402**: 251-260.
139. Bateman, RL, Bhanumoorthy, P, Witte, JF, McClard, RW, Grompe, M, and Timm, DE (2001). Mechanistic inferences from the crystal structure of fumarylacetoacetate hydrolase with a bound phosphorus-based inhibitor. *J Biol Chem* **276**: 15284-15291.
140. Montagutelli, X, Lalouette, A, Coude, M, Kamoun, P, Forest, M, and Guenet, JL (1994). aku, a mutation of the mouse homologous to human alkaptonuria, maps to chromosome 16. *Genomics* **19**: 9-11.
141. Eckert, JW, Buerkle, CJ, Major, AM, Finegold, MJ, and Brandt, ML (1995). In situ hybridization utilizing a Y chromosome DNA probe. Use as a cell marker for hepatocellular transplantation. *Transplantation* **59**: 109-111.
142. Slocum, RH, and Cummings, JG (1991). *Techniques in Diagnostic Human Biochemical Genetics: A Laboratory Manual*, Wiley-Liss: New York.
143. Hoffmann, G, Aramaki, S, Blum-Hoffmann, E, Nyhan, WL, and Sweetman, L (1989). Quantitative analysis for organic acids in biological samples: batch isolation followed by gas chromatographic-mass spectrometric analysis. *Clin Chem* **35**: 587-595.
144. Gautier, L, Cope, L, Bolstad, BM, and Irizarry, RA (2004). affy--analysis of Affymetrix GeneChip data at the probe level. *Bioinformatics* **20**: 307-315.

145. Irizarry, RA, *et al.* (2003). Exploration, normalization, and summaries of high density oligonucleotide array probe level data. *Biostatistics* **4**: 249-264.
146. Gentleman, RC, *et al.* (2004). Bioconductor: open software development for computational biology and bioinformatics. *Genome Biol* **5**: R80.
147. Storey, JD (2002). A direct approach to false discovery rates. *J Roy Statist Soc B* **64**: 479-498.
148. Smyth, GK (2004). Linear models and empirical bayes methods for assessing differential expression in microarray experiments. *Stat Appl Genet Mol Biol* **3**: Article3.
149. McCarthy, DJ, and Smyth, GK (2009). Testing significance relative to a fold-change threshold is a TREAT. *Bioinformatics* **25**: 765-771.
150. Willenbring, H, *et al.* (2008). Loss of p21 permits carcinogenesis from chronically damaged liver and kidney epithelial cells despite unchecked apoptosis. *Cancer Cell* **14**: 59-67.
151. Tunon, MJ, Alvarez, M, Culebras, JM, and Gonzalez-Gallego, J (2009). An overview of animal models for investigating the pathogenesis and therapeutic strategies in acute hepatic failure. *World J Gastroenterol* **15**: 3086-3098.
152. Muller, L, Kasper, P, and Kaufmann, G (1992). The clastogenic potential in vitro of pyrrolizidine alkaloids employing hepatocyte metabolism. *Mutat Res* **282**: 169-176.

153. Sorrentino, BP (2002). Gene therapy to protect haematopoietic cells from cytotoxic cancer drugs. *Nat Rev Cancer* **2**: 431-441.
154. Koc, ON, Reese, JS, Davis, BM, Liu, L, Majczenko, KJ, and Gerson, SL (1999). DeltaMGMT-transduced bone marrow infusion increases tolerance to O6-benzylguanine and 1,3-bis(2-chloroethyl)-1-nitrosourea and allows intensive therapy of 1,3-bis(2-chloroethyl)-1-nitrosourea-resistant human colon cancer xenografts. *Hum Gene Ther* **10**: 1021-1030.
155. Endo, F, *et al.* (1997). Complete rescue of lethal albino c14CoS mice by null mutation of 4-hydroxyphenylpyruvate dioxygenase and induction of apoptosis of hepatocytes in these mice by in vivo retrieval of the tyrosine catabolic pathway. *J Biol Chem* **272**: 24426-24432.
156. Duan, D, Yue, Y, Yan, Z, Yang, J, and Engelhardt, JF (2000). Endosomal processing limits gene transfer to polarized airway epithelia by adeno-associated virus. *J Clin Invest* **105**: 1573-1587.
157. Miao, CH, *et al.* (2000). Nonrandom transduction of recombinant adeno-associated virus vectors in mouse hepatocytes in vivo: cell cycling does not influence hepatocyte transduction. *J Virol* **74**: 3793-3803.
158. Nakai, H, Fuess, S, Storm, TA, Muramatsu, S, Nara, Y, and Kay, MA (2005). Unrestricted hepatocyte transduction with adeno-associated virus serotype 8 vectors in mice. *J Virol* **79**: 214-224.
159. Nakai, H, *et al.* (2002). A limited number of transducible hepatocytes restricts a wide-range linear vector dose response in recombinant adeno-associated virus-mediated liver transduction. *J Virol* **76**: 11343-11349.

160. Davidoff, AM, *et al.* (2005). Comparison of the ability of adeno-associated viral vectors pseudotyped with serotype 2, 5, and 8 capsid proteins to mediate efficient transduction of the liver in murine and nonhuman primate models. *Mol Ther* **11**: 875-888.
161. Nonnenmacher, M, and Weber, T (2012). Intracellular transport of recombinant adeno-associated virus vectors. *Gene Ther.*
162. Halbert, CL, Rutledge, EA, Allen, JM, Russell, DW, and Miller, AD (2000). Repeat transduction in the mouse lung by using adeno-associated virus vectors with different serotypes. *J Virol* **74**: 1524-1532.
163. Manno, CS, *et al.* (2006). Successful transduction of liver in hemophilia by AAV-Factor IX and limitations imposed by the host immune response. *Nat Med* **12**: 342-347.
164. Mingozzi, F, and High, KA (2007). Immune responses to AAV in clinical trials. *Curr Gene Ther* **7**: 316-324.
165. Mingozzi, F, *et al.* (2007). CD8(+) T-cell responses to adeno-associated virus capsid in humans. *Nat Med* **13**: 419-422.
166. Nathwani, AC, *et al.* (2011). Adenovirus-associated virus vector-mediated gene transfer in hemophilia B. *N Engl J Med* **365**: 2357-2365.
167. Engelhardt, JF (2006). AAV hits the genomic bull's-eye. *Nat Biotechnol* **24**: 949-950.
168. Wright, JF (2008). Manufacturing and characterizing AAV-based vectors for use in clinical studies. *Gene Ther* **15**: 840-848.

169. Lock, M, *et al.* (2010). Characterization of a recombinant adeno-associated virus type 2 reference standard material. *Hum Gene Ther* **21**: 1273-1285.

## BIOGRAPHY

### Education

2007-12                      *Oregon Health & Science University*                      *Portland, OR*

Doctor of Philosophy, Cell and Developmental Biology

2002-06                      *Central Washington University*                      *Ellensburg, WA*

Bachelor of Science, Biology, Microbiology specialization, Chemistry minor

2001-02                      *Western Washington University*                      *Bellingham, WA*

### Research Experience

2006-12                      *Oregon Health & Science University*                      *Portland, OR*

*Department: Oregon Stem Cell Center*                      *Mentor: Dr. Markus Grompe, MD*

-Utilizing mouse models to develop gene repair therapies for metabolic disease.

2004-06                      *Central Washington University*                      *Ellensburg, WA*

*Department: Chemistry*                      *Mentor: Dr. Anne Johansen, PhD*

-Photochemical studies of atmospheric sulfinic acids and iron oxyhydroxides.

2003                      *United States Department of Agriculture*                      *Wapato, WA*

*Department: Pest Research*                      *Mentor: Dr. Lisa Neven, PhD*

-Nonchemical treatment of deciduous tree fruit with controlled atmosphere.

-Developed alternatives to methyl bromide fumigation for codling moth pests.

2002-04

Central Washington University

Ellensburg, WA

Department: Biology

Mentor: Dr. Steven Wagner, PhD

-Effects of malathion and glyphosate on the development of NW tadpoles.

### **Publications**

**NK Paulk**, L Marquez-Loza, MJ Finegold, *et al.* 2012. AAV-mediated gene repair is significantly enhanced by transient inhibition of NHEJ or the proteasome *in vivo*. (Accepted—*Human Gene Therapy*).

AM Taylor, A Preston, **NK Paulk**, *et al.* Ochronosis in a murine model of Alkaptonuria is analogous to the human condition (Accepted—*Osteoarthritis & Cartilage*).

**NK Paulk**, K Wursthorn, Z Wang, *et al.* 2010. AAV gene repair corrects a mouse model of hereditary tyrosinemia *in vivo*. *Hepatology* 51(4): 1200-1207.

A Duncan, R Hickey, **NK Paulk**, *et al.* 2009. Ploidy reductions in murine fusion-derived hepatocytes. *PLoS Genetics* 5(2): 1-11.

H Azuma, **N Paulk**, A Ranade, *et al.* 2007. A robust system for the *in vivo* expansion of human hepatocytes. *Nature Biotechnology* 25(8): 903-10.

JM Key, **N Paulk** and AM Johansen. 2008. Effects of DMSO oxidation products on iron speciation in photochemical simulation experiments. *Environmental Science & Technology* 42:133-139.

### **Pending Publications**

**NK Paulk**, A Haft, K Wursthorn, *et al.* The fumarylacetoacetate hydrolase inhibitor CEHPOBA allows for functional selection of transplanted hepatocytes *in vivo*. (In Preparation—*Nature Molecular Therapy*).

### **Academic & Professional Presentations**

2011            *American Society of Gene & Cell Therapy*            *Seattle, WA*  
-*In vivo* AAV-mediated gene repair is enhanced by the DNA-PK inhibitor vanillin.

2011            *Keystone: Genomic Instability & DNA Repair*            *Keystone, CO*  
-Transient vanillin administration inhibits DNA-PK and promotes HR during gene repair *in vivo*.

2010            *Northwest Genome Engineering Consortium*            *Seattle, WA*  
-Use for non-cleaving homing endonucleases in improving AAV gene repair.

2010            *American Society of Gene & Cell Therapy*            *Washington, DC*  
-Single-polarity rAAV may enhance hepatic gene targeting *in vivo*.

2009 Northwest Genome Engineering Consortium Seattle, WA

-Increasing targeted DSBs to improve AAV-mediated gene repair *in vivo*.

2008 American Society of Gene Therapy Boston, MA

-AAV8-mediated correction of a metabolic renal disease via gene repair *in vivo*.

2008-11 OHSU Annual Student Research Forum Portland, OR

-*In vivo* AAV-mediated gene repair is enhanced by the DNA-PK inhibitor vanillin.

-Single-polarity rAAV may enhance hepatic gene repair *in vivo*.

-AAV8-mediated correction of a metabolic renal disease via gene repair *in vivo*.

### **Graduate Awards**

NIH F31 NRSA Ruth Kirschstein Predoctoral Fellowship \$330,000 (2007-12)

Travel award from American Society for Gene & Cell Therapy \$500 (2012)

Travel award from American Society for Gene & Cell Therapy \$500 (2011)

Oregon Graduate Scholarship Fund \$2,000 (2010-11)

Travel award from NW Genome Engineering Consortium \$500 (2010)

USA Funds Access to Education Academic Scholarship \$12,000 (2007-10)

Leslie S. Parker Memorial Scholarship \$1,000 (2009-10)

Travel award from NW Genome Engineering Consortium \$500 (2009)

Mary Horstkotte Memorial Scholarship \$2,000 (2008-09)

Travel award from American Society for Gene Therapy \$500 (2008)

Mildred and CK Dart Memorial Scholarship \$2,000 (2007-08)